UNIVERSITÀ DI PISA

DIPARTIMENTO DI INGEGNERIA CIVILE E INDUSTRIALE
Corso di laurea magistrale in Ingegneria Aerospaziale

MASTER THESIS

DYNAMIC INVERSION CONTROL FOR A SMALL-SCALE HELICOPTER

Supervisors:
Ing. Francesco Schettini
Prof. Ing. Eugenio Denti
Prof. Ing. Roberto Galatolo
Ing. Gianpietro Di Rito

Author:
Vito Grasso

ACADEMIC YEAR 2015–2016

Ai miei genitori

Abstract

University of Pisa is performing a research finalized to develop Rotary Unmanned Aerial Vehicles (RUAV), starting from small commercial Radio Commanded helicopters, capable to perform autonomous or automatic flight. The aim of this thesis is to develop a non-linear control laws system, based on feedback linearization method, in order to allow the machine to perform automatic missions. This work has been carried out starting from an existing non-linear open-loop model of the helicopter, whose parameters have been identified in a previous thesis. In the first part of this work the non-linear system was analyzed in terms of trim condition. After the simplification of the commands chain, the system was linearized and both the non-linear and linear system have been excited by collective and cyclic command signals and their responses have been compared. In the second part of the thesis the control laws for automatic flight mode have been developed. Since the attempt to use the input-output exact feedback linearization procedure was ineffective, a cascade linearization method, called dynamic inversion linearization, was used in order to develop the controller. Finally, the controller was implemented and tested in order to validate it.

Contents

List of Figures

Notation

A_1	Lateral cyclic pitch
A_{1corr}	Lateral cyclic pitch corrected by the effect of the flybar
a_0	coning angle
a_1	Longitudinal flapping coefficients
a_{1fb}	Longitudinal flapping coefficients of flybar
a_{bl}	Lift coefficient of the blade
a_{fb}	Lift coefficient of the flybar
a_{1s}	Longitudinal flapping coefficients referred to the shaft
B	Main rotor blade flapping inertia
B_1	Longitudinal cyclic pitch
B_{1corr}	Longitudinal cyclic pitch corrected by the effect of the Flybar
B_{fb}	Flybar rotor blade flapping inertia
b_1	Lateral flapping coefficients
b_{1fb}	Lateral flapping coefficients of flybar
b_{1s}	Lateral flapping coefficients referred to the shaft
c	Main rotor chord
c_{fb}	Flybar rotor chord
c_t	Tail rotor chord
D	Fusolage drag
e	Nondimensional main rotor offset
e_{fb}	Nondimensional flybar rotor offset
f	Main rotor distance in x direction from c.g.
H_d	Disk drag
h	Main rotor height above c.g., nondimensional
h_c	Drag coefficient
h_t	Tail rotor distance in z direction from c.g.
I_{xx}, I_{yy}, I_{zz}	Helicopter moments of inertia
I_{xy}, I_{xz}, I_{yz}	Helicopter centrifugal moments of inertia
K_{iv}	Induced velocity ratio

K_β	Blade stiffness index
L, M, N	Moments in body axes
l	Main rotor distance in y direction from c.g.
l_t	Tail rotor distance in x direction from c.g.
M_f	Pitching moment of fuselage
M_s	Pitching moment per unit tilt of all the blades due to hinge offset
m	Helicopter mass
m_{bl}	Blade mass
n_{es}	Gear ratio of engine shaft to main rotor
n_t	Gear ratio of tail rotor to main rotor
P_x,P_y,P_z	Weight components in body axes
p,q,r	Angular rates in body axes
Q	Rotor torque
q_c	Torque coefficient
R	Main rotor radius
R_{fb}	Flybar rotor radius
R_t	Tail rotor radius
S_x^{fus}	Frontal fuselage drag area
S_y^{fus}	Side fuselage drag area
S_z^{fus}	Vertical fuselage drag area
s	Main rotor solidity
T_d	Rotor thrust
T_t	Tail thrust
t_c	Thrust coefficient
U, V, W	Velocities in body axes
v_i	General induced velocity at rotor
v_{i0}	Mean induced velocity
w_c	Weight coefficient
X, Y, Z	Forces in body axes
x_B, y_B, z_B	Axes of the body reference system
x_g	Blade c.g. position
α_d	Disk incidence

β	Blade flapping angle
$\overline{\beta}$	$\partial\beta/\partial\psi$
γ_{bl}	Blade Lock number
γ_{fb}	Paddle Lock number
δ	Main rotor mean lift drag coefficient
θ	Fuselage pitch attitude
θ_0	Collective pitch angle
θ_t	Tail collective pitch angle
λ, λ_D	Inflow ratio
λ_i	$v_i/\Omega R$
μ	Advance ratio
ϕ	Fuselage roll attitude
ψ	Azimuthal angular position of blade
ψ	Fuselage yaw attitude
Ω	Main rotor angular velocity
Ω_t	Tail rotor angular velocity

Introduction

Among the Unmanned Aerial Vehicles (UAVs), there is a growing interest in developing unmanned autonomous helicopters. The helicopter has unique capabilities, such as takeoff and land vertically, maintain hovering for an extended period of time, broad envelope of flight and high maneuverability. These abilities result in a wide range of application, both in civil and in military field. In particular, the University of Pisa (Department of Ingegneria Civile e Industriale - Aerospace Section) has available a T-Rex 500 ESP radio commanded helicopter T-Rex 500 ESP.

In a previous work, a non-linear model of the helicopter's dynamics has been developed using Matlab-Simulink and its parameters have been identified by using flight tests data.

The aim of this thesis is to enable T-Rex 500 to the automatic flight mode by equipping it with appropriate sensors and PC unit and developing flight control laws.

The term automatic flight mode concerns the fact that the pilot assigns the three velocity components (longitudinal, lateral and vertical) and the yaw angle, rather than commanding the swash plate and the tail collective pitch through the rotation of the servo-actuators.

As first step, a linear model has been obtained, starting from hovering condition, by applying an automatic tool of Matlab-Simulink on the non-linear model. The results of this activity has been used to understand the dynamic behavior of the helicopter following the application of pilot open-loop commands. Consequently a feedback linearization procedure has been chosen in order to synthesize the controller for the automatic flight mode.

Finally the controller was implemented and tested in order to check its capability and to evaluate the performance

In Chapter 1, a generic description of the RUAV is provided, with particular attention to the specific model T-REX 500 ESP. Moreover, the identified non-linear model developed for this small scale helicopter is described in detail through its flapping equations, forces and moments equations and equations of motion. Finally the command chain was strongly simplified.

Chapter 2 shows the analysis of the trim conditions in the operative helicopter speed range. In particular, the spatial orientation of the swash plate and rotor plane, as well as the attitude angles of the helicopter, for the different forward flight coefficient value, are plotted.

In Chapter 3 some simplifications to the helicopter model are introduced in order to acquire a model for controller design.

In Chapter 4 the procedure of feedback linearization is described. The math-

ematical concepts of Lie derivative, relative degree of the system, zero dynamics etc. are introduced and applied for the linearization of the system.

In Chapter 5 a cascade linearization method, called dynamic inversion linearization is used in order to develop the controller. Starting with the control laws for the angular velocity and, passing through the control of the attitude angles, the controller is synthesized for the automatic flight, having as input the longitudinal, lateral and vertical speed and the yaw angle ψ. After this the controller is tested in order to validate it.

Furthermore a controller for the hovering is synthesized and tested.

Finally conclusion and future works are presented.

Part I

Non-Linear Model

Chapter 1

Background and model simplification

Figure 1.1: T-REX 500 ESP.

In this chapter the dynamic model of T-REX 500 ESP (Fig. 1.1), developed by our team in previous works of thesis [1], will be introduced.

Furthermore some simplifications will be made in order to make easier the development of controller.

1.1 T-REX 500 ESP

The helicopter model available in the department is the T-REX 500 ESP (Fig. 1.1), suitable for aerobatics and high performance flight.

The T-REX 500 is a small rotorcraft popular among hobby pilots for aerobatics: it is highly manoeuvrable, with inverted flight capabilities, so it is suited for studies on guidance algorithms and high-frequency dynamics.

The helicopter is made of plastic material and carbon fibres, that ensure the structural strength and the low weight; the vertical and horizontal stabilizer surfaces of this helicopter are small and perforated, they only ensure the protection of the tail rotor, and therefore will be neglected in subsequent calculations.

The main characteristic is the rigid hingeless rotor head with carbon fibres blades. The flapping motion is allowed only by the blade elasticity and by the damper rubber O-ring of the feathering shaft (Fig. 1.2).

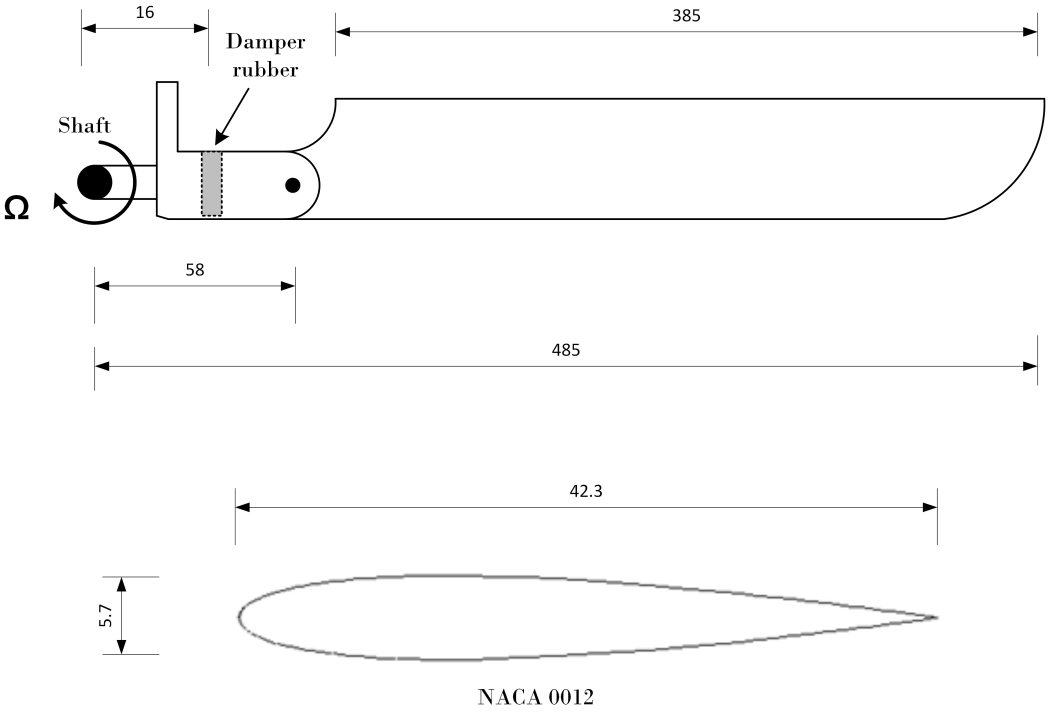

Figure 1.2: Blade schematic representation.

The rotorcraft is equipped with a stabilizer bar, also known as flybar. The stabilizer bar (Fig. 1.3) is a secondary rotor consisting in two paddles connected to the main rotor shaft by an unrestrained teetering hinge. It receives only cyclic input from the swashplate, and its flapping motion influences the main rotor blades pitch via the Bell-Hiller mixer bar. The flybar is used to generate a control augmentation to the main rotor cyclic input and realizes a "mechanical feedback" in angular rates p and q.

The tail rotor (Fig. 1.4) generates a thrust to counter the main rotor torque. Its tip speed is nearly equal to that of the main rotor.

In Tab. 1.1 the main inertial and aero-mechanical characteristics of the helicopter, found through identification in [1], are reported

Inertial data	
$m = 2.14\,\mathrm{kg}$	Helicopter mass
$I_{xx} = 0.02\,\mathrm{kg\,m^2}$	Helicopter rolling moment of inertia
$I_{yy} = 0.065\,\mathrm{kg\,m^2}$	Helicopter pitching moment of inertia
$I_{zz} = 0.066\,\mathrm{kg\,m^2}$	Helicopter yawing moment of inertia

$I_{xy} = -0.0007\,\mathrm{kg\,m^2}$	Helicopter centrifugal moment of inertia - XY
$I_{xz} = -0.0009\,\mathrm{kg\,m^2}$	Helicopter centrifugal moment of inertia - XZ
$I_{yz} \approx 0\,\mathrm{kg\,m^2}$	Helicopter centrifugal moment of inertia - YZ
	Main rotor data
$m_{bl} = 0.2\,\mathrm{kg}$	Blade mass
$B = 6.7 \times 10^{-3}\,\mathrm{kg\,m^2}$	Main rotor blade flapping inertia
$K_\beta = 22\,\mathrm{kg\,m^2}$	Blade stiffness index
$\Omega = 240.7\,\mathrm{rad\,s^{-1}}$	Main rotor velocity
$R = 0.485\,\mathrm{m}$	Main rotor radius
$c = 0.0423\,\mathrm{m}$	Main rotor chord
$e = 0.04$	Nondimensional main rotor hinge offset
$x_g = 0.194\,\mathrm{m}$	Blade c.g. position
$s = 0.056$	Main rotor solidity
$n_{es} = 12.46$	Gear ratio of engine shaft to main rotor
$a_{bl} = 5.12\,\mathrm{rad^{-1}}$	Lift coefficient of the blade
$\gamma_{bl} = 2.35$	Blade Lock number
$\delta = 0.025$	Main rotor mean lift drag coefficient
	Flybar data
$B_{fb} = 7.8 \times 10^{-4}\,\mathrm{kg\,m^2}$	Flybar rotor blade flapping inertia
$R_{fb} = 0.235\,\mathrm{m}$	Flybar rotor radius
$c_{fb} = 0.039\,\mathrm{m}$	Flybar rotor chord
$e_{fb} = 0.7$	Nondimensional flybar rotor offset
$a_{fb} = 2\,\mathrm{rad^{-1}}$	Lift coefficient of the flybar
$\gamma_{fb} = 0.2447$	Paddle Lock number
	Tail rotor data
$\Omega_t = 1126.5\,\mathrm{rad\,s^{-1}}$	Tail rotor velocity
$R_t = 0.105\,\mathrm{m}$	Tail rotor radius
$c_t = 0.017\,\mathrm{m}$	Tail rotor chord
$n_t = 4.68$	Gear ratio of tail rotor to main rotor
$h_t = 0.0505$	Tail rotor distance in z direction from c.g.
$l_t = 1.2$	Tail rotor distance in x direction from c.g.
	General data
$P_{eng}^{id} = 0\,\mathrm{W}$	Engine idle power
$P_{eng}^{max} = 1890\,\mathrm{W}$	Engine max power
$t_c^{max} = 0.076$	Maximum thrust coefficient
$S_x^{fus} = 0.0382\,\mathrm{m^2}$	Frontal fuselage drag area
$S_y^{fus} = 0.0705\,\mathrm{m^2}$	Side fuselage drag area
$S_z^{fus} = 0.0625\,\mathrm{m^2}$	Vertical fuselage drag area
$h = 0.289$	Main rotor height above c.g., nondimensional
$f = -0.028$	Main rotor distance in x direction from c.g.
$l = 0.0036$	Main rotor distance in y direction from c.g.

Table 1.1: Parameters of T-REX 500 helicopter.

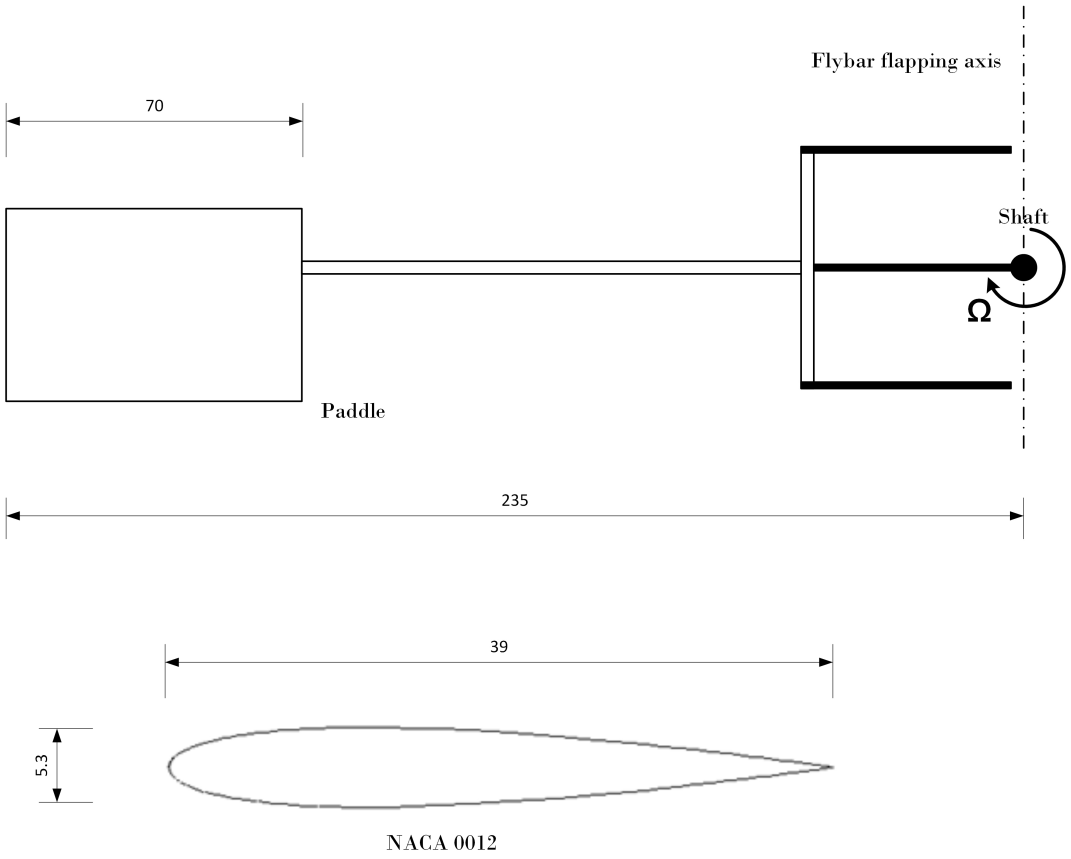

Figure 1.3: Flybar schematic representation.

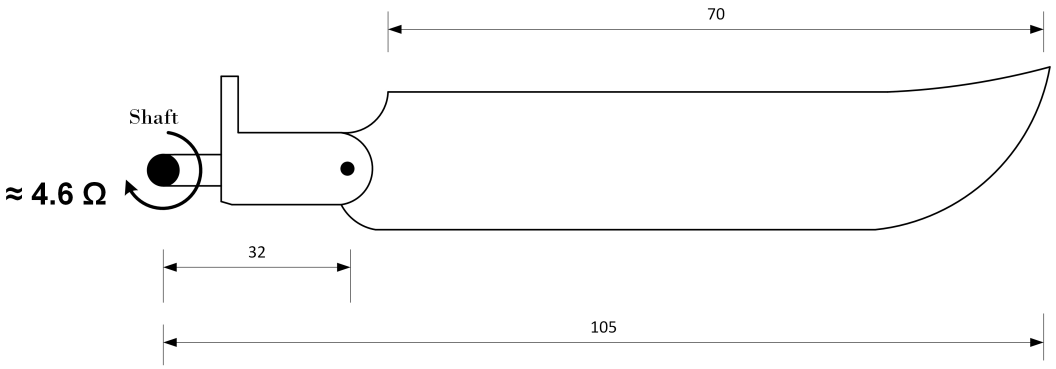

Figure 1.4: Tail schematic representation.

1.2 Non-linear system

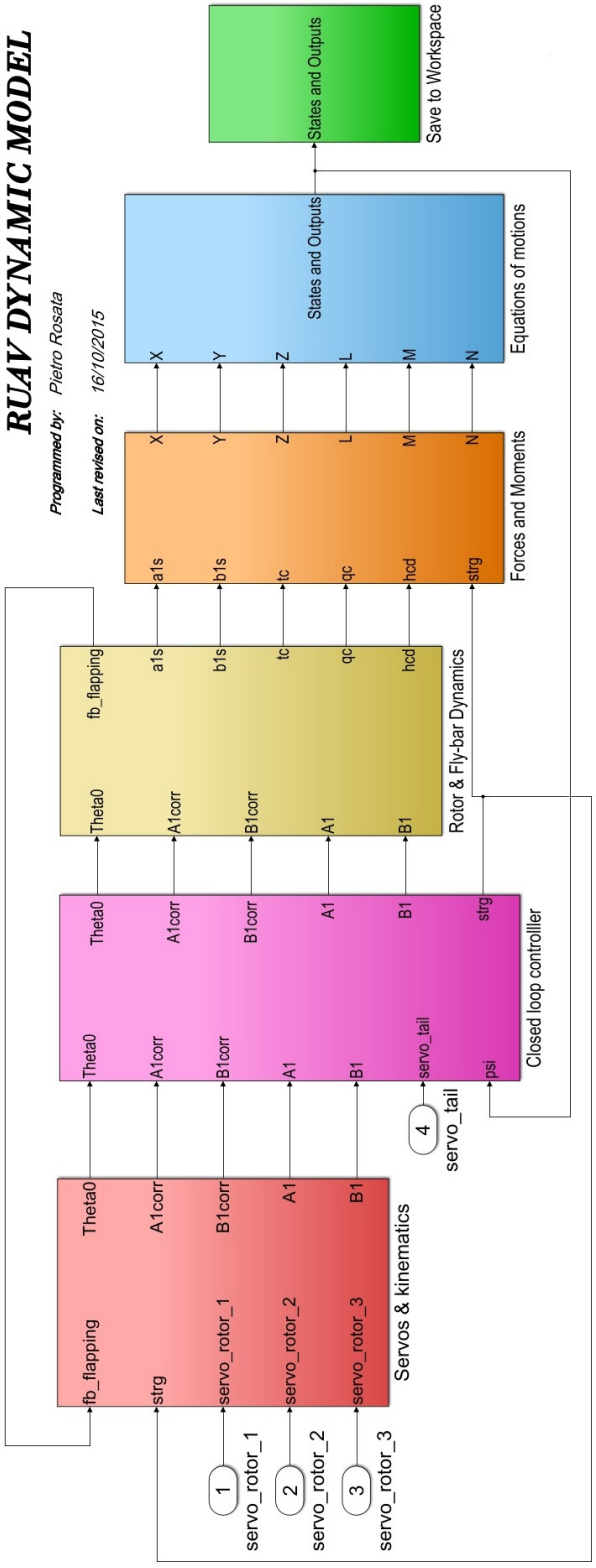

Figure 1.5: Simulink complete model of RUAV.

In Fig. 1.5 it is shown the Simulink complete model derived in [1]. This model is the starting point for the development of the controller. Each block of the model will be described in the next sections.

1.2.1 Servos and kinematics

In the "Servos & kinematics" the electric commands, coming from the radio controller, are converted into θ_0, A_1, B_1; they are corrected by the dynamic of the flybar and converted in A_{1corr}, B_{1corr}.

1.2.2 Closed loop control

In "Closed loop controller" the controller will be located. The tail command controller will be developed in this thesis but the helicopter has its own gyro-control system that guarantees the heading-lock without any commands from the pilot to the tail.

1.2.3 Rotor and Flybar Dynamics

In "Rotor & Flybar Dynamics" are calculated the orientation of the rotor and flybar compared to the shaft, even the thrust, the torque and the drag of the rotor are calculated on the basis of the input signals and the helicopter flight conditions. The entity of the swashplate command is:

$$\theta = \theta_0 - A_{1corr} \cos\psi - B_{1corr} \sin\psi \tag{1.1}$$

As shown in Appendix A, flapping motion is a periodic function. Expressing it as a Fourier series with no harmonics greater than one, the flapping equation can be rewritten as a second-order matrix differential equation:

$$\ddot{\boldsymbol{a}} + \Omega\, \boldsymbol{D}\, \dot{\boldsymbol{a}} + \Omega^2\, \boldsymbol{K}\, \boldsymbol{a} = \boldsymbol{f} \tag{1.2}$$

where $\boldsymbol{a}$ is the blade flapping state matrix, $\boldsymbol{D}$ is the damping matrix , $\boldsymbol{K}$ is the stiffness matrix and $\boldsymbol{f}$ are the forcing terms; the explicit expression is reported in section A.3.1.

For the flybar a similar second order differential equation in matrix form can be obtained with the same approach:

$$\ddot{\boldsymbol{a}}_{\boldsymbol{fb}} + \Omega\, \boldsymbol{D}_{\boldsymbol{fb}}\, \dot{\boldsymbol{a}}_{\boldsymbol{fb}} + \Omega^2\, \boldsymbol{K}_{\boldsymbol{fb}}\, \boldsymbol{a}_{\boldsymbol{fb}} = \boldsymbol{f}_{\boldsymbol{fb}}, \tag{1.3}$$

where $\boldsymbol{a}_{\boldsymbol{fb}}$ is the flybar flapping state matrix , $\boldsymbol{D}_{\boldsymbol{fb}}$ is the damping matrix , $\boldsymbol{K}_{\boldsymbol{fb}}$ is the stiffness matrix and $\boldsymbol{f}_{\boldsymbol{fb}}$ are the forcing terms; the explicit expression is reported in section A.4.

1.2.4 Force and Moments

In "Forces and Moments" the rotor's forces and moments are transformed in the axes body forces and moments (X, Y, Z, L, M and N). No elastic modes and vibrations will be considered: the tip-path plane simplified model will be used.

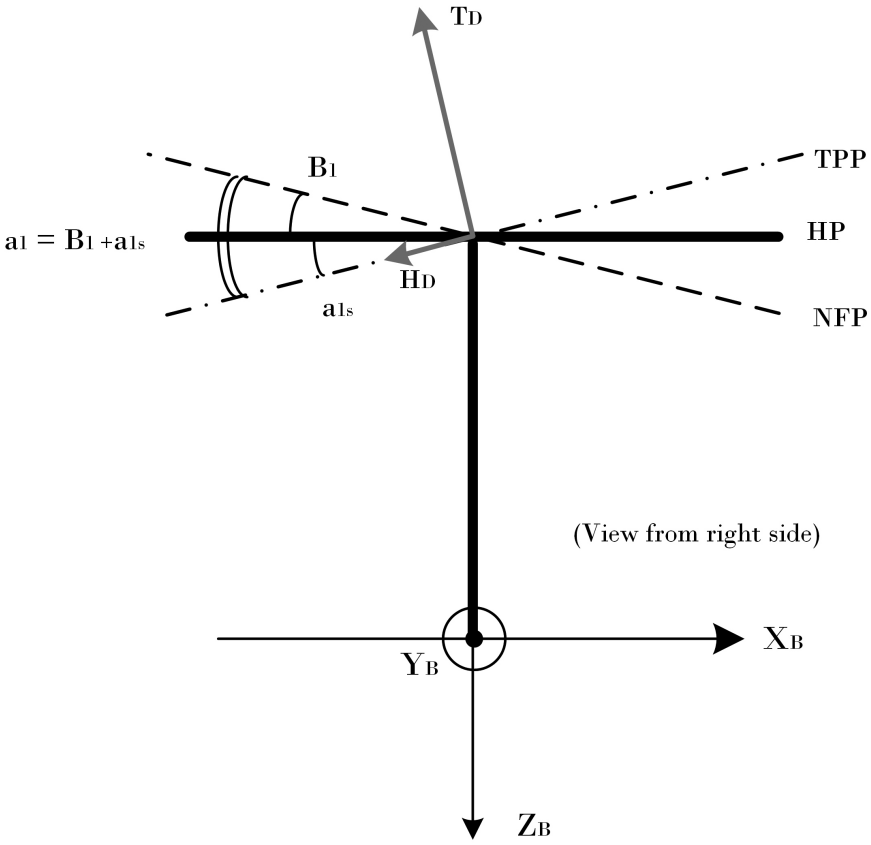

Figure 1.6: Interpretation of flapping and feathering coefficients in the longitudinal plane.

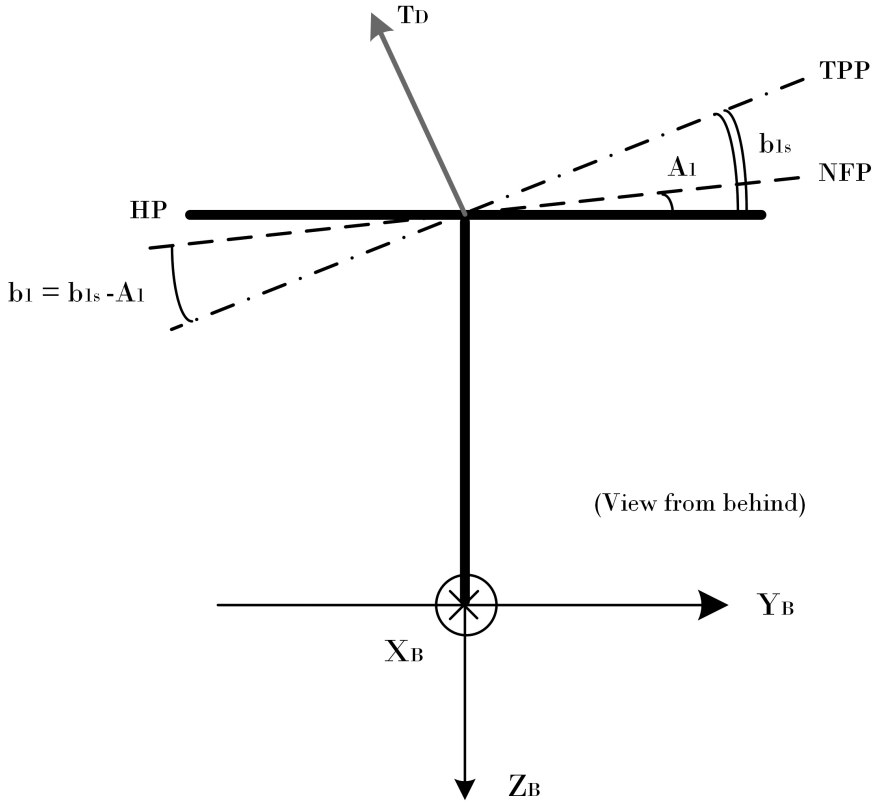

Figure 1.7: Interpretation of flapping and feathering coefficients in the lateral plane.

Referring to Fig. 1.6 and 1.7, the resultant of forces along x_B, y_B and z_B axes are, respectively:

$$X = P_x - T_d a_{1s} - H_d - D\cos(\theta - \tau_c) \tag{1.4}$$

$$Y = P_y - T_d b_{1s} + T_t \tag{1.5}$$

$$Z = P_z - T_d + H_d a_{1s} - D\sin(\theta - \tau_c) \tag{1.6}$$

The weight components can be written as:

$$\begin{bmatrix} P_x \\ P_y \\ P_z \end{bmatrix} = \left[R_{hz2hb}\right] \cdot \begin{bmatrix} 0 \\ 0 \\ mg \end{bmatrix} \tag{1.7}$$

where:

$$\left[R_{hz2hb}\right] = \begin{bmatrix} c\psi c\theta & s\psi c\theta & -s\theta \\ c\psi s\theta s\phi - s\psi c\phi & s\psi s\theta s\phi + c\psi c\phi & c\theta s\phi \\ c\psi s\theta c\phi + s\psi s\phi & s\psi s\theta c\phi - c\psi s\phi & c\theta c\phi \end{bmatrix} \tag{1.8}$$

where, for the sake of simplicity, s indicates the sine function and c the cosine function. We obtain:

$$\begin{bmatrix} P_x \\ P_y \\ P_z \end{bmatrix} = \begin{bmatrix} -mg\sin\theta \\ mg\cos\theta\sin\phi \\ mg\cos\theta\cos\phi \end{bmatrix} \tag{1.9}$$

Finally, we have:

$$\begin{cases} X = -mg\sin\theta - T_d a_{1s} - H_d - D\cos(\theta - \tau_c) \\ Y = mg\cos\theta\sin\phi - T_d b_{1s} + T_t \\ Z = mg\cos\theta\cos\phi - T_d + H_d a_{1s} - D\sin(\theta - \tau_c) \end{cases} \tag{1.10}$$

The moment acting on the fuselage consists of the moment produced by the tilting of the thrust vector due to the blade flapping and the moment produced by inertial forces and hinge restraint.

Developing every term (cf. [1]), the obtained expressions are:

$$\begin{cases} L = -m_{bl} e x_g \Omega^2 R b_{1s} - T_D b_{1s} h R + T_t h_t R + T_D l R - K_\beta b_{1s} \\ M = m_{bl} e x_g \Omega^2 R a_{1s} + T_d a_{1s} h R + H_d h R + M_f - (T_d - H_d a_{1s}) f R + K_\beta a_{1s} \\ N = -T_t l_t R - Q \end{cases} \tag{1.11}$$

Note that, in trim conditions, T_t is negative, i.e. towards the negative y-axis. In other words, the tail rotor pitch is normally negative. For the symbols used in the text one can refer to [1].

1.2.5 Equations of motion

In "Equations of motion" the forces and moments are used in the equations of rigid body dynamic and, due their integration, the linear velocities, the angular rates and the attitude angles in body axes are calculated.

For a first analysis of the dynamics, the assumption of rigid structure is reasonable and sufficient for linear dynamics simulation.

The first and second Newton-Euler's equations have been used for the rigid body dynamics

$$\boldsymbol{F} = \frac{\mathrm{d}\boldsymbol{Q}}{\mathrm{d}t} \tag{1.12}$$

$$\dot{\boldsymbol{K}}_{\boldsymbol{O}} = \boldsymbol{M}_{\boldsymbol{O}} + \boldsymbol{\Psi}_{\boldsymbol{O}} - \boldsymbol{v}_{\boldsymbol{O}} \times \boldsymbol{Q} \tag{1.13}$$

where:

$$\boldsymbol{K}_{\boldsymbol{O}} = \boldsymbol{K}_{\boldsymbol{\omega}} + m\, \boldsymbol{OG} \times \boldsymbol{v}_{\boldsymbol{O}} \tag{1.14}$$

In this case, assuming that the pole O is coincident with the helicopter center of gravity G, Eq. (1.14) becomes:

$$\boldsymbol{K}_{\boldsymbol{\omega}} = \boldsymbol{I} \cdot \boldsymbol{\Omega} = \begin{bmatrix} I_{xx} & -I_{xy} & -I_{xz} \\ -I_{xy} & I_{yy} & -I_{yz} \\ -I_{xz} & -I_{yz} & I_{zz} \end{bmatrix} \begin{bmatrix} p \\ q \\ r \end{bmatrix} = \begin{bmatrix} I_{xx}p - I_{xy}q - I_{xz}r \\ -I_{xy}p + I_{yy}q - I_{yz}r \\ -I_{xz}p - I_{yz}q + I_{zz}r \end{bmatrix} \tag{1.15}$$

where $\boldsymbol{I}$ is the helicopter matrix of inertia.

The centrifugal moment I_{yz} is approximately zero (the plane x-z is approximately a plane of symmetry).

Using Eq. (1.15), and supposing $I_{yz} \approx 0$, the second Euler's, Eq. (1.13), becomes:

$$\dot{\boldsymbol{K}}_{\boldsymbol{G}} = \begin{bmatrix} I_{xx}\dot{p} - I_{xy}\dot{q} - I_{xz}\dot{r} + q(I_{zz}r - I_{xz}p) - r(I_{yy}q - I_{xz}p) \\ I_{yy}\dot{q} - I_{xy}\dot{p} + r(I_{xx}p - I_{xz}q - I_{xz}r) - p(I_{zz}r - I_{xz}p) \\ I_{zz}\dot{r} - I_{xz}\dot{p} + p(I_{yy}q - I_{xy}p) - q(I_{xx}p - I_{xy}q - I_{xz}r) \end{bmatrix} = \boldsymbol{M_O} \tag{1.16}$$

where $\boldsymbol{M_O}$ is the moment with pole in O of the aerodynamic forces.

The velocity of helicopter centroid G is:

$$\boldsymbol{v_G} = u\ \boldsymbol{i_B} + v\ \boldsymbol{j_B} + w\ \boldsymbol{k_B} \tag{1.17}$$

So, the translational momentum $\boldsymbol{Q}$ is:

$$\boldsymbol{F} = \dot{\boldsymbol{Q}} = m\dot{\boldsymbol{v}}_{\boldsymbol{G}} = m \begin{bmatrix} \dot{u} + qw - vr \\ \dot{v} + ur - pw \\ \dot{w} + pv - uq \end{bmatrix} \tag{1.18}$$

Writing Eqs. (1.16) and (1.18) in extended version, we obtain the following set of equations for helicopter dynamics:

$$X = m(\dot{u} + qw - vr) \tag{1.19a}$$
$$Y = m(\dot{v} + ur - pw) \tag{1.19b}$$
$$Z = m(\dot{w} + pv - uq) \tag{1.19c}$$
$$I_{xx}\dot{p} + I_{xy}(pr - \dot{q}) - I_{xz}(\dot{r} + pq) - qr(I_{yy} - I_{zz}) = L \tag{1.19d}$$
$$I_{yy}\dot{q} - I_{xy}(\dot{p} + qr) - (I_{zz} - I_{xx})pr + I_{xz}(p^2 - r^2) = M \tag{1.19e}$$
$$I_{zz}\dot{r} - (I_{xx} - I_{yy})pq + I_{xy}(q^2 - p^2) + I_{xz}(qr - \dot{p}) = N \tag{1.19f}$$

where X, Y and Z are the resultants according the x-axis, y-axis and z-axis of aerodynamic and gravitational forces and L, M and N are the moments of aerodynamic forces, with centroid as pole (Fig. 1.9).

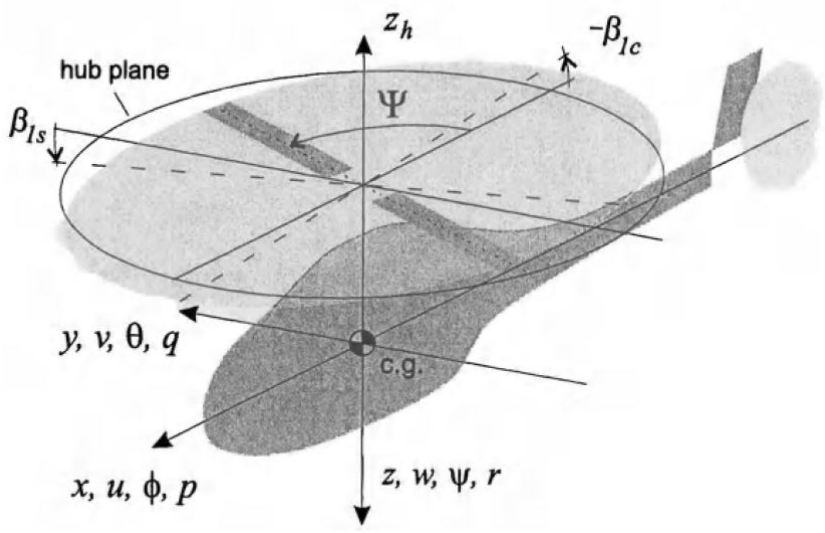

Figure 1.8: Helicopter with its body-fixed reference frame.

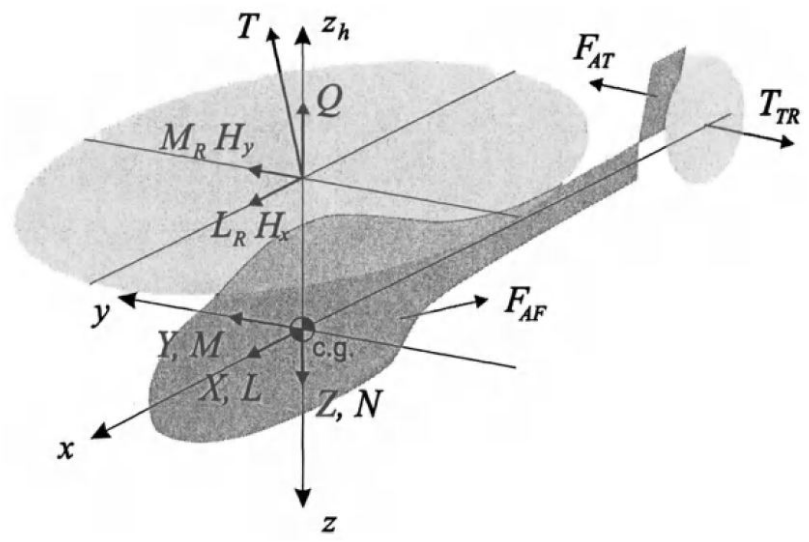

Figure 1.9: Forces and moments acting on the helicopter.

1.2.6 Data storage

In the last block "Data storage" all the results from the simulation tests are transformed in inertial axes and saved to plot the simulation results.

1.3 Model simplifications

As synthetically illustrated in section 1.2.1, the "Servos & kinematics" Simulink block includes the command chain from the rotation of the servo-actuators to the rotation of the swash plate. This link is described by a set of 21 highly coupled kinematic equations, which considers even the coupling between the blade and the flybar rotation.

The entire kinematic command chain will be neglected in order to make easier the development of the controller. To do this, it is necessary to understand how flybar acts on the blade equations and find a simplified way to express mathematically this relation.

$$\theta = \theta_0 - A_{1corr} \cos\psi - B_{1corr} \sin\psi \quad \text{for the blade} \tag{1.20}$$

To provide a "mechanical" feedback in pitch and roll rate on T-Rex 500 it has been used a Bell-Hiller stabilizer bar.

As with the rotor:

$$\theta = -A_1 \sin\psi + B_1 \cos\psi \quad \text{for the flybar} \tag{1.21}$$

An idea about how the flybar acts on the principal dynamic, is given by the scheme of Fig. 1.10.

The rotor receives commands which are the sum of two contributes: a part coming from the servo-actuators and another one coming from the flybar feedback (every contribute is scaled by convenient coefficients).

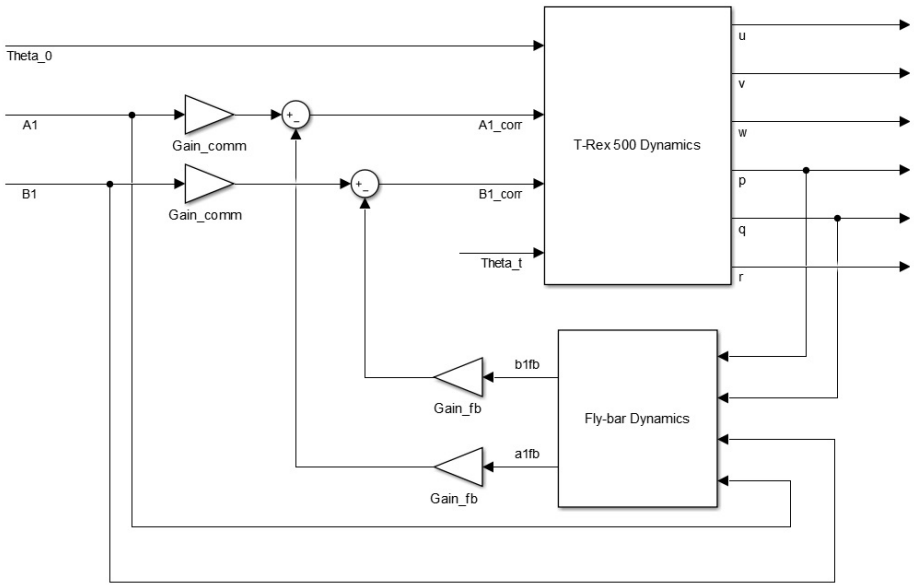

Figure 1.10: Flybar feedback.

In mathematical terms it means:

$$A_{1corr} = gain_{comm} A_1 - gain_{fb} a_{1fb} \tag{1.22}$$

$$B_{1corr} = gain_{comm} B_1 - gain_{fb} b_{1fb} \tag{1.23}$$

where:

$$\begin{cases} gain_{comm} = 0.44 \\ gain_{fb} = 0.5 \end{cases} \tag{1.24}$$

The values of $gain_{comm}$ and $gain_{fb}$ has been found by a fitting procedure, using data coming from flight tests [1]. The results of this procedure are shown in Fig. 1.11.

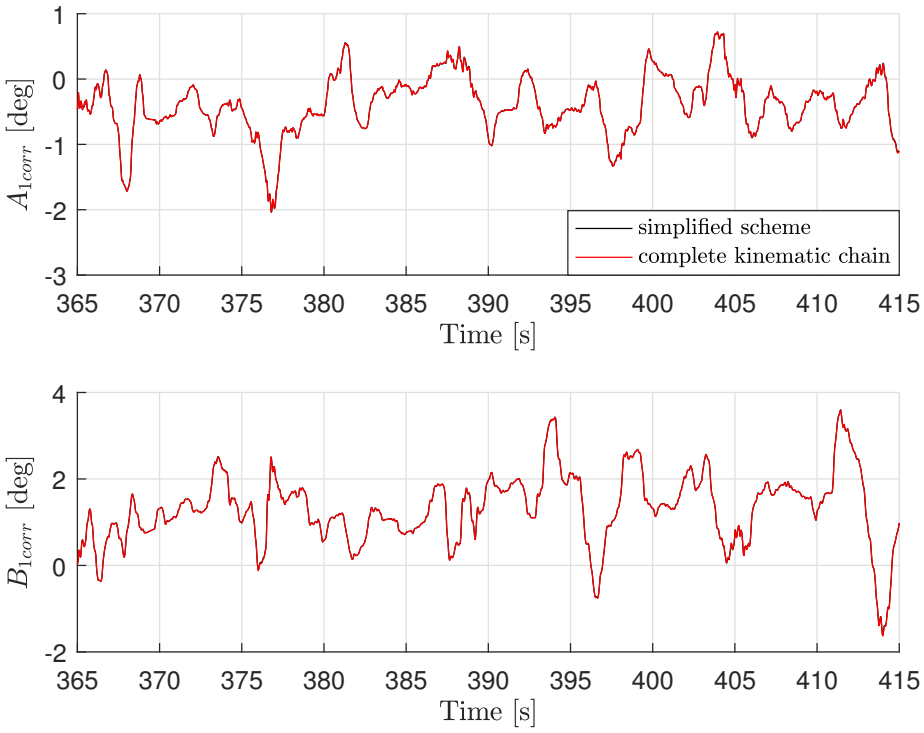

Figure 1.11: Fitting procedure results.

Chapter 2

Trim and Linearization

The aim of this chapter is to evaluate the main parameters of the T-Rex 500 in various conditions of trim. This procedure will be carried on in parallel with another study made on the model of the same helicopter based on literature [2].

Starting from trim condition, the dynamic model will be linearized and studied in terms of transfer functions and responses, in the time domain, to the commands.

2.1 Trim

2.1.1 Trim procedure (literature)

In this section, the helicopter trim equations will be solved.

Simplifying hypothesis

The main simplifying hypotheses are:

- rotor blade and stabilizer bar are rigid in bending and torsion, with no twist;
- command chain and blade elasticity are neglected;
- drag coefficient δ and lift coefficient a of airfoil independent of local blade angle of attack (mean values have been considered);
- both the flapping angle and the inflow angle were assumed to be small (i.e. low ratio T/A and high blade aspect ratio) and this analysis uses simple Glauert theory;
- the effects of the helicopter dynamic on the blade flapping were limited to those due to the angular accelerations $\dot{p}$ and $\dot{q}$, the angular rates p and q, z-axis acceleration $\dot{w}$ and translation velocities u and v;
- the reversed flow region was ignored, as the compressibility and stall effects;
- the inflow was assumed to vary according the Glauert theory:

$$v_i = v_{i0} \cdot (1 + K_{iv} x \cos\psi) \tag{2.1}$$

- the *tip loss factor* was assumed to be 1; *root-cutout effect* is neglected.

Trim equations

Because of the asymmetry of the helicopter, the longitudinal and lateral plane should be solve simultaneously. In [3], an analysis demonstrates that flight parameters are related through no less than fourteen equation: however this is not necessary in practice. The longitudinal and lateral plane equation will therefore be solve independently of one another.

Referring to Fig. 2.1 and 2.2, resolving forces vertically and horizontally ([2], [4]):

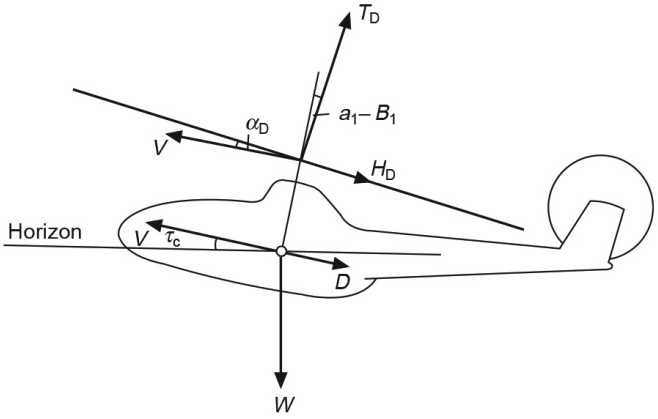

Figure 2.1: Forces and moments in longitudinal plane.

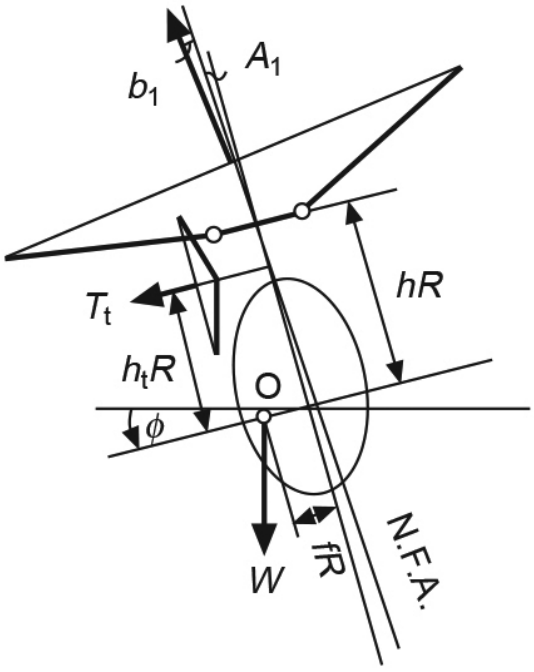

Figure 2.2: Forces and moments in lateral plane.

$$T_D \cos(\alpha_D + \tau_c) - H_D \sin(\alpha_D + \tau_c) = W + D \sin\tau \tag{2.2a}$$
$$T_D \sin(\alpha_D + \tau_c) + H_D \cos(\alpha_D + \tau_c) = D \cos\tau \tag{2.2b}$$

Making small angles assumption and neglecting term $H_D \sin(\alpha_D + \tau_c)$, Eq. (2.2) can be solved iteratively, knowing the correlation between t_c and h_D and aero-mechanical parameters. Taking moments about O and making the small angles assumption, it gives:

$$-WfR - T_D hRB_1 + (H_D + T_D a_1)hR + M_f - M_s(B_1 - a_1) = 0 \tag{2.3}$$

Solving for B_1:

$$B_1 = a_1 + \frac{M_f + H_D hR - WfR}{WhR + M_s} \tag{2.4}$$

Referring now to the lateral plane (Fig. 2.2 and 2.4), taking moments about O:

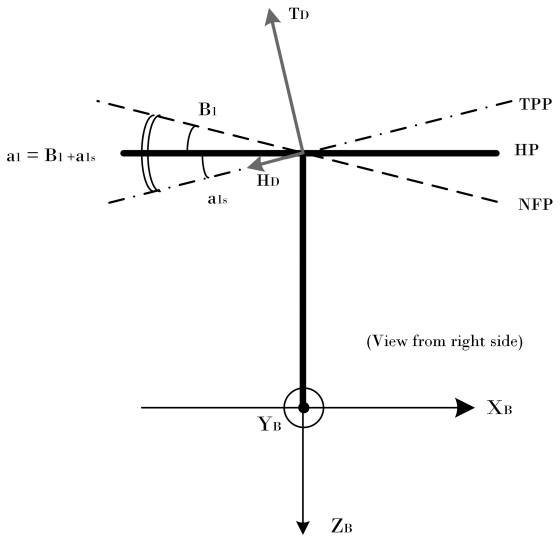

Figure 2.3: Interpretation of flapping and feathering coefficients in the longitudinal plane.

$$WlR - Whr(A_1 + b_1) + T_t h_t R - M_s(A_1 + b_1) = 0 \tag{2.5}$$

Solving for A_1:

$$A_1 = -b_1 + \frac{WfR + T_t h_t R}{WhR + M_S} \tag{2.6}$$

in non-dimensional form:

$$A_1 = -b_1 + \frac{w_c f + (T_t/W)t_c h_t}{t_c h + C_{ms}} \tag{2.7}$$

Solving forces according the y-direction, it gives:

$$W(A_1 + b_1 + \phi) + T_t = 0 \tag{2.8}$$

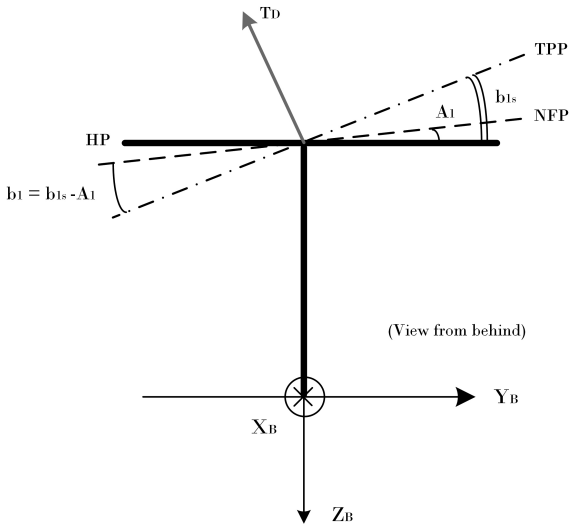

Figure 2.4: Interpretation of flapping and feathering coefficients in the lateral plane.

that gives:

$$\phi = -(T_t/W) + b_1 + A_1 = -(T_t/W) + b_{1s} \tag{2.9}$$

In the Fig. 2.6-2.13, the following helicopter trim parameters for the T-REX 500 will be shown as a function of μ:

- longitudinal and lateral control to trim θ_0, A_1 and B_1;
- blade flapping coefficients a_0, a_1 and b_1;
- attitude θ and ϕ.

For the exact meaning of every single term used in the expressions above see [2].

2.1.2 Trim procedure (Simulink)

To find the trim conditions on the non-linear model (see Fig. 2.5) described in the previous Chapter, it has been used an automatic Simulink tool of linearization. The aim of this analysis is to evaluate the differences between the non-linear identified model and the model coming from literature [2] in term of attitude angles, flapping coefficients and command coefficients.

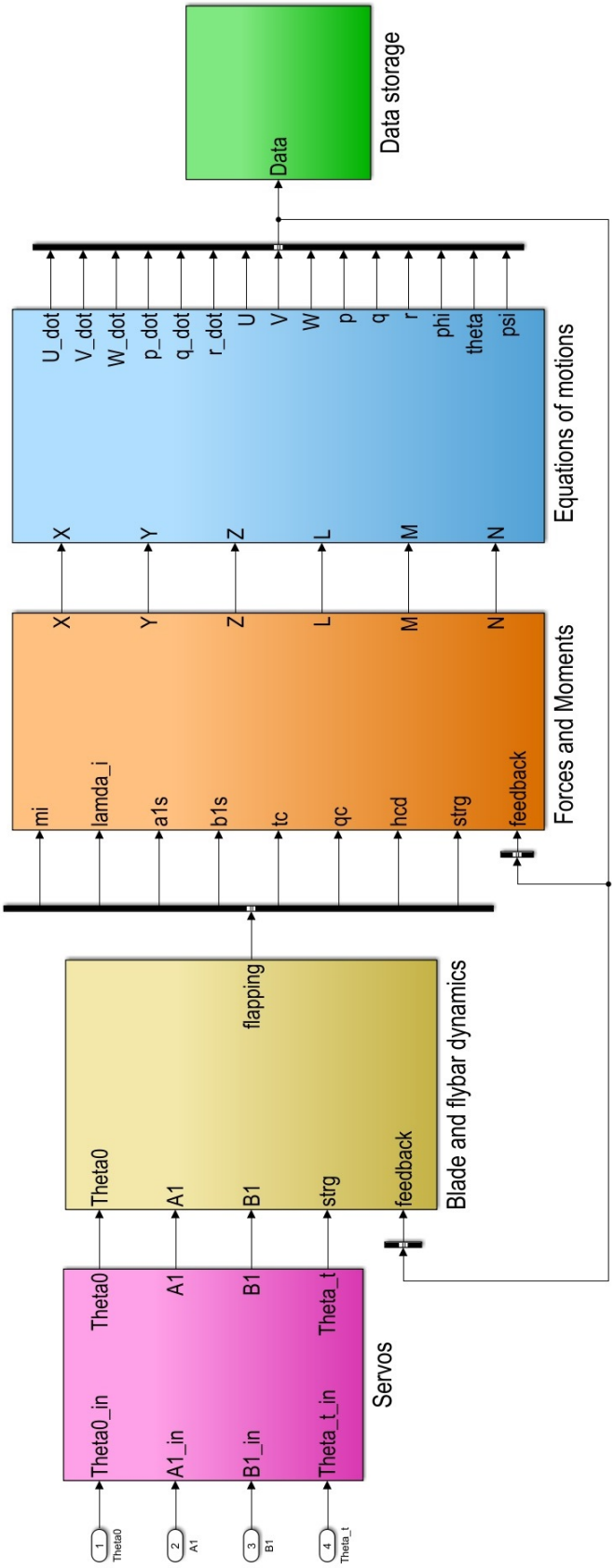

Figure 2.5: Simulink trim scheme.

2.1.3 Results

The two procedures have been tested in an interval of the advance ratio $0 \leq \mu \leq 0.175$. The obtained results are shown in Fig. 2.6-2.13.

It can be observed that the two procedures give congruent results in the interested interval of the advance ratio (μ).

The literature model from [2] is valid for big helicopter (generally with flapping hinge on the hub) in which the longitudinal and lateral dynamics are enough decoupled. The Simulink model instead was developed for our small-scale helicopter.

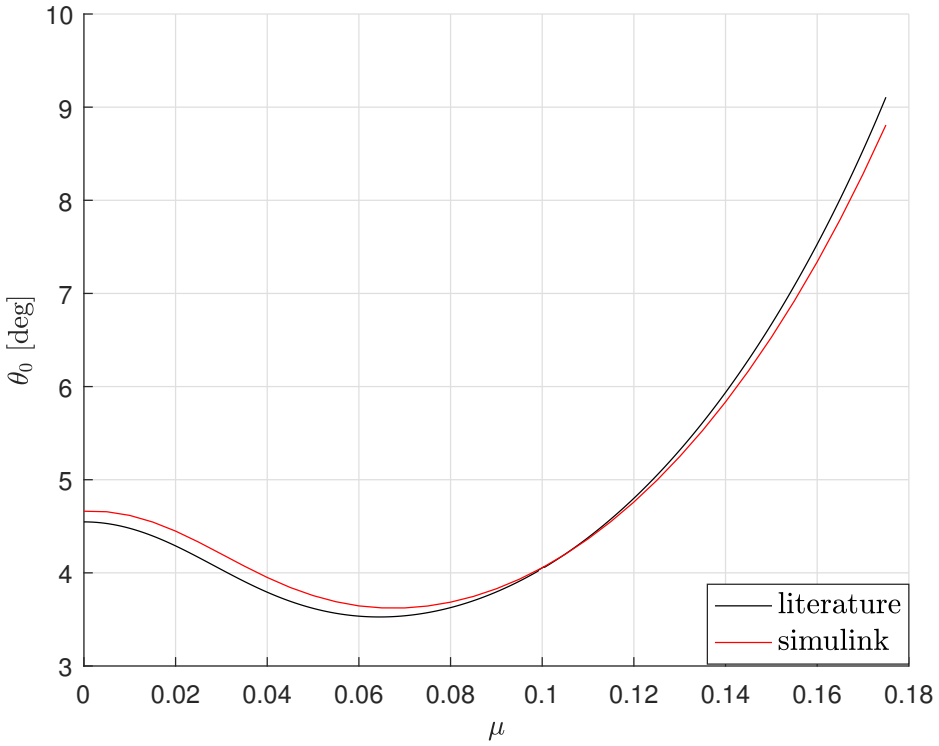

Figure 2.6: Comparison of θ_0.

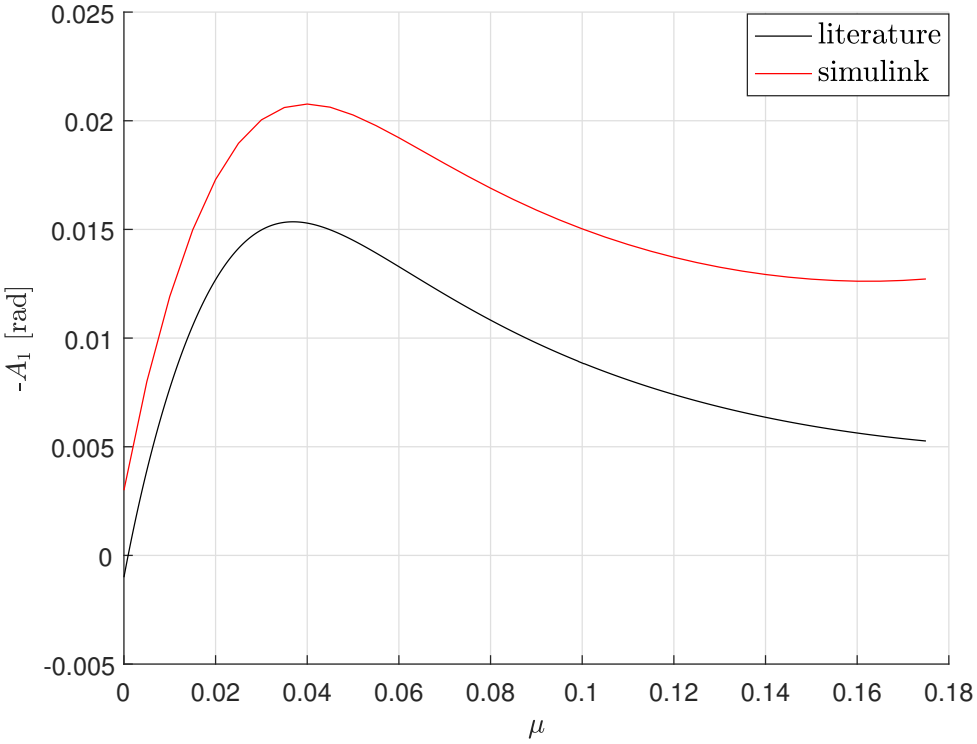

Figure 2.7: Comparison of A_1.

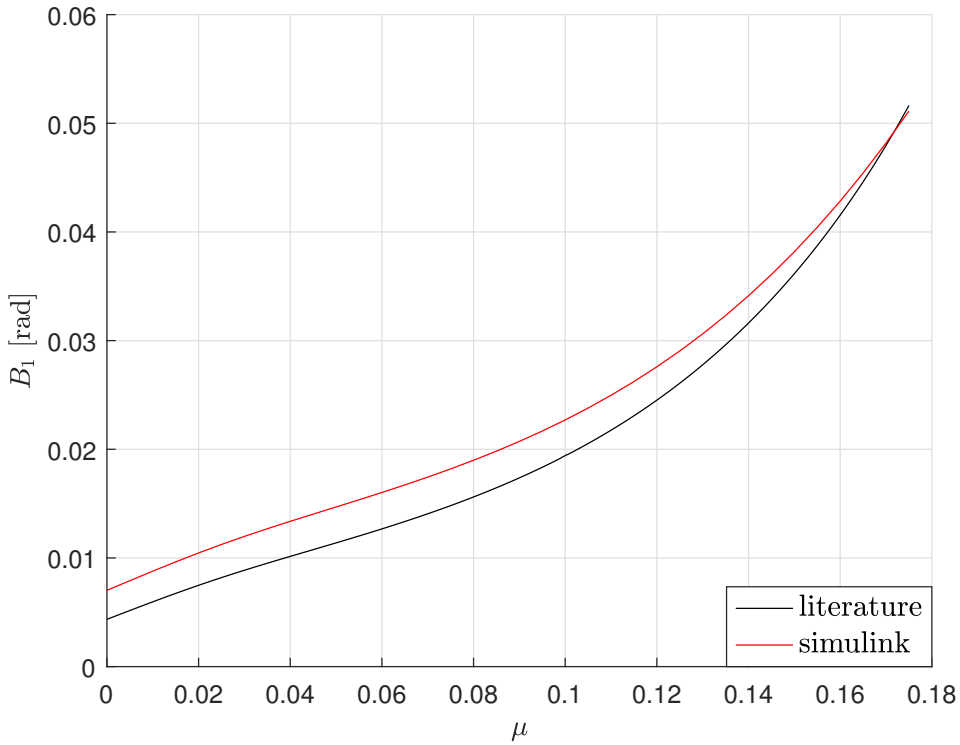

Figure 2.8: Comparison of B_1.

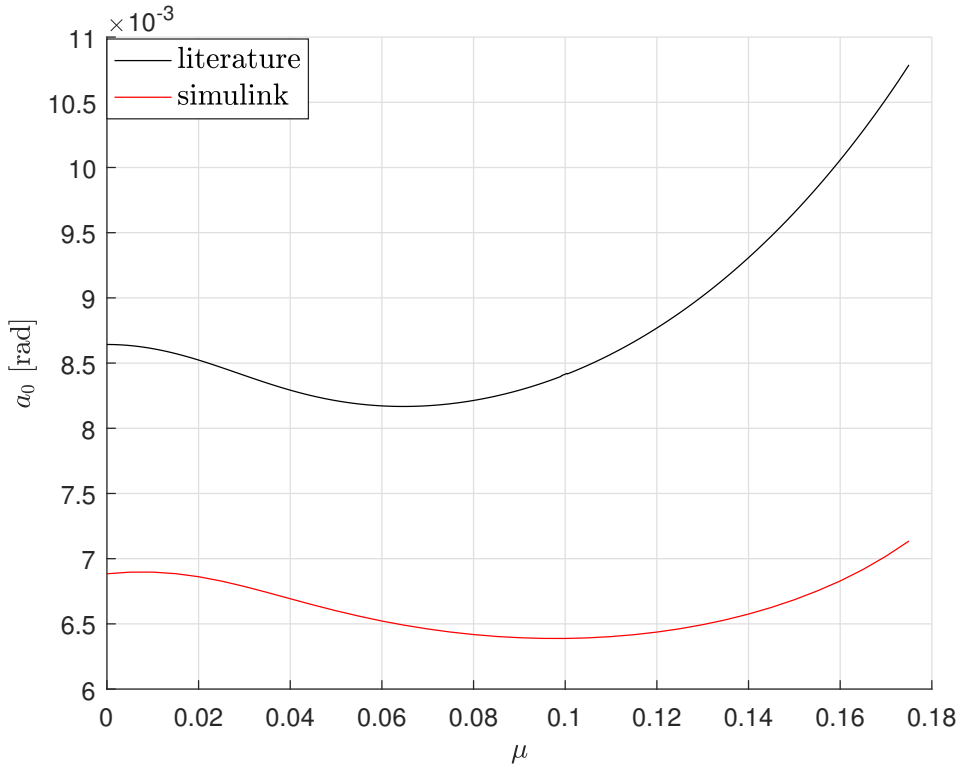

Figure 2.9: Comparison of a_0.

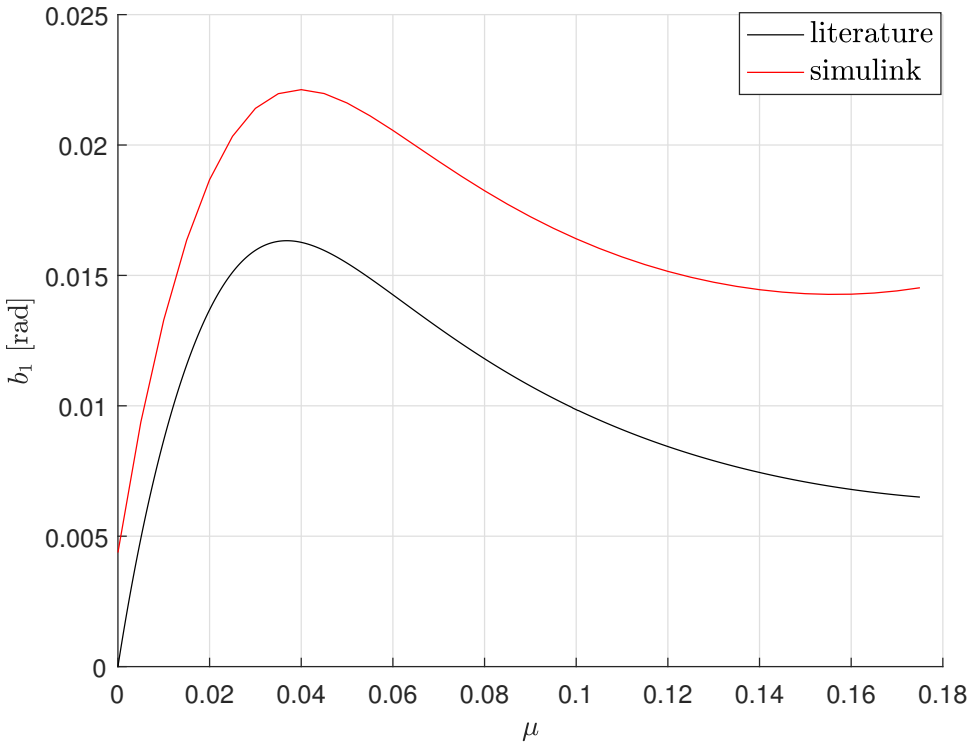

Figure 2.10: Comparison of b_1.

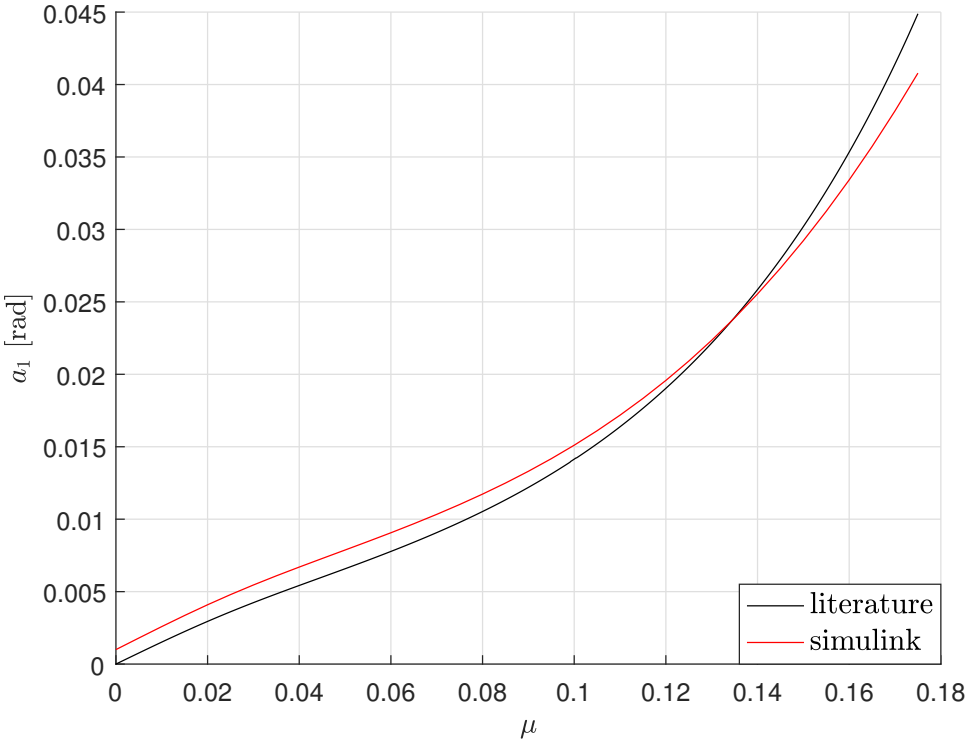

Figure 2.11: Comparison of a_1.

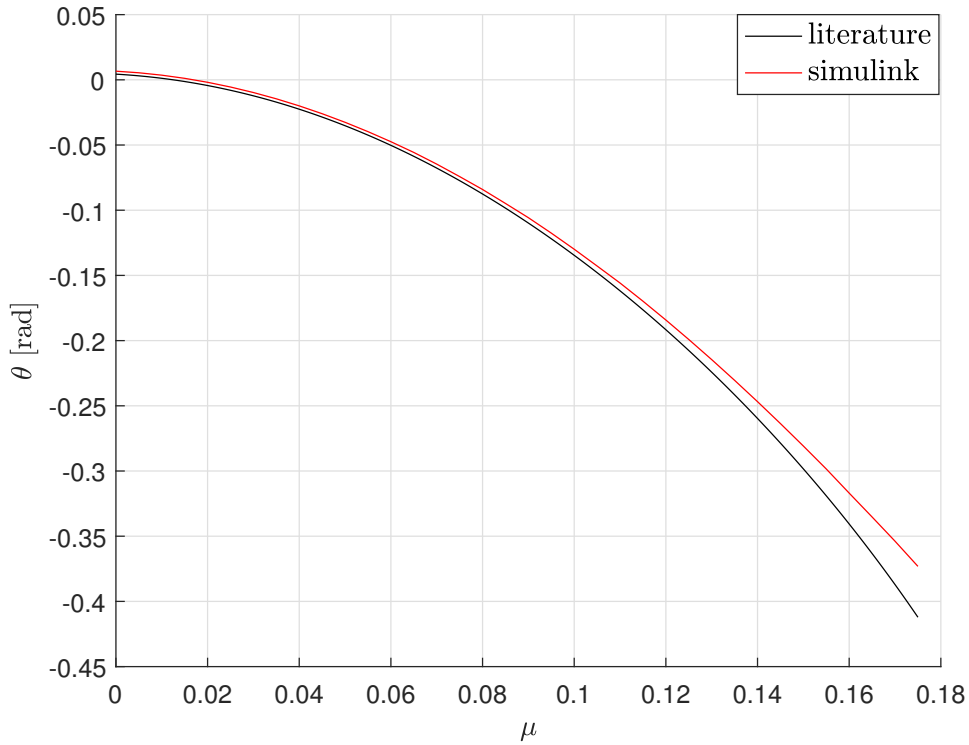

Figure 2.12: Comparison of θ.

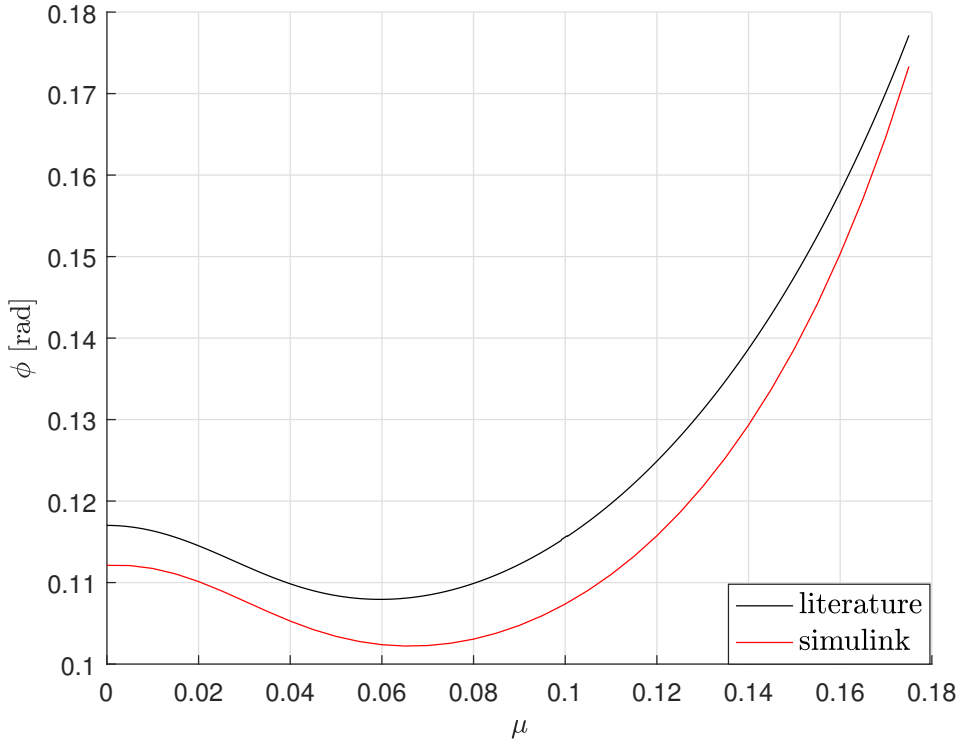

Figure 2.13: Comparison of ϕ.

2.2 Linearization

Starting from hovering condition the dynamic model was linearized, using an automatic Simulink tool, in order to obtain a system with the following structure:

$$\begin{cases} \dot{\boldsymbol{x}}(t) = \boldsymbol{A}\boldsymbol{x}(t) + \boldsymbol{B}\boldsymbol{u}(t) \\ \boldsymbol{y}(t) = \boldsymbol{C}\boldsymbol{x}(t) + \boldsymbol{D}\boldsymbol{u}(t) \end{cases} \tag{2.10}$$

2.2.1 Transfer functions

The main transfer functions, coming from the linearization procedure, are:

$$\frac{p}{A_1} = \frac{-4.8476e06(s+4.597e04)(s+23.18)(s+18.28)(s+0.0004296)(s^2-1.947s+2.315e05)}{(s+33.33)(s-0.00307)(s^2+43.44s+477.8)(s^2+18.81s+2780)(s^2+17.13s+2.317e05)(s^2+55.82s+2.5e05)} \tag{2.11}$$

$$\frac{q}{B_1} = \frac{-429.02(s+421.6)(s+21.69)(s+18.26)(s-0.003892)(s^2-2.834s+2.311e05)(s^2-326.9s+3.796e05)}{(s+33.33)(s-0.00307)(s^2+43.44s+477.8)(s^2+10.44s+642.7)(s^2+17.13s+2.317e05)(s^2+55.82s+2.5e05)} \tag{2.12}$$

$$\frac{r}{\theta_t} = \frac{6645.6}{(s+6.425)(s^2+43.09s+1027)} \tag{2.13}$$

$$\frac{W}{\theta_0} = \frac{-5532.6(s+0.01883)(s-0.01495)}{s(s-0.00307)(s+1.076)(s+33.33)} \tag{2.14}$$

In Eqs. 2.11-2.14 various dynamics can be observed:

- the real pole $(s+33.33)$ expresses the servo-actuator high frequency dynamic;
- the four imaginary poles $(s^2+17.13s+2.317e05)$ and $(s^2+55.82s+2.5e05)$ express the second order flapping dynamics of the blade and the flybar. These dynamics are completely decoupled from the rest of the model;
- the controller in r acts as a first order with frequencies $\omega = 6.425\,\text{rad/s}$, completely decoupled from the rest of the model. Even the vertical velocity response is enough decoupled from the rest of the model; in the short period it acts like a first order with frequency $\omega = 1.076\,\text{rad/s}$, in long period it is affected by the general instability of the helicopter;
- the two imaginary poles $(s^2+43.44s+477.8)$ express an higher dynamic coupling between the longitudinal and the lateral dynamic responses;
- the poles $(s^2+18.81s+2780)$ and $(s^2+10.44s+642.7)$ express an higher dynamic coupling between the flapping dynamic and the rigid body pitching and rolling dynamics;
- the zeros in RHP, that make difficult the stabilization of the closed loop system in the long period, are due to the position of the c.g. behind the shaft.

2.2.2 Response in the time domain

In order to test the difference between the responses in the time domain of the linearized dynamic model and the non-linear model, they were excited by the same signals.For each simulation test only one input channel at time was excited by a non-zero step sygnal. The values of the input step signals are shown in Eq. (2.15).

$$\begin{aligned} \theta_0 &= 10^{-2}\,\text{rad} \\ A_1 &= 10^{-2}\,\text{rad} \\ B_1 &= 10^{-2}\,\text{rad} \\ \theta_t &= 10^{-1}\,\text{rad} \end{aligned} \tag{2.15}$$

In Fig. 2.14-2.16 the response to B_1 are shown while the responses to A_1, θ_0 and θ_t are not represented for brevity.

From the responses in the time domain we can deduce the presence of a time-scale separation between the response in angular velocity (fast), attitude variation (slow) and velocity variation (slower).

Furthermore we can note a quick separation between the behaviour of the non-linear model and the linearized model. For this reason, we have decided to synthesize a non-linear controller.

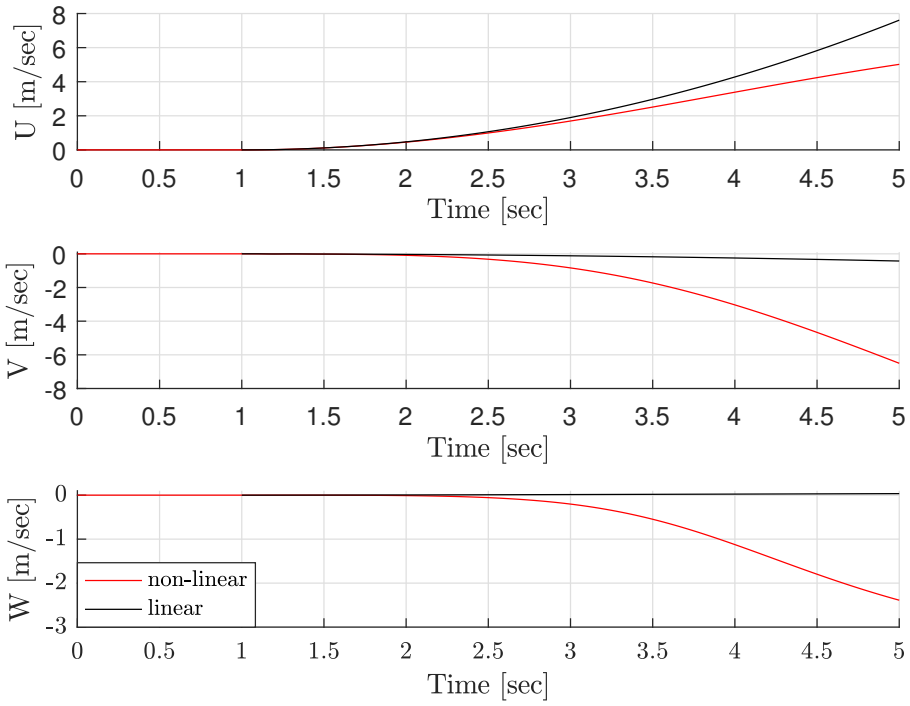

Figure 2.14: Velocity response to B_1.

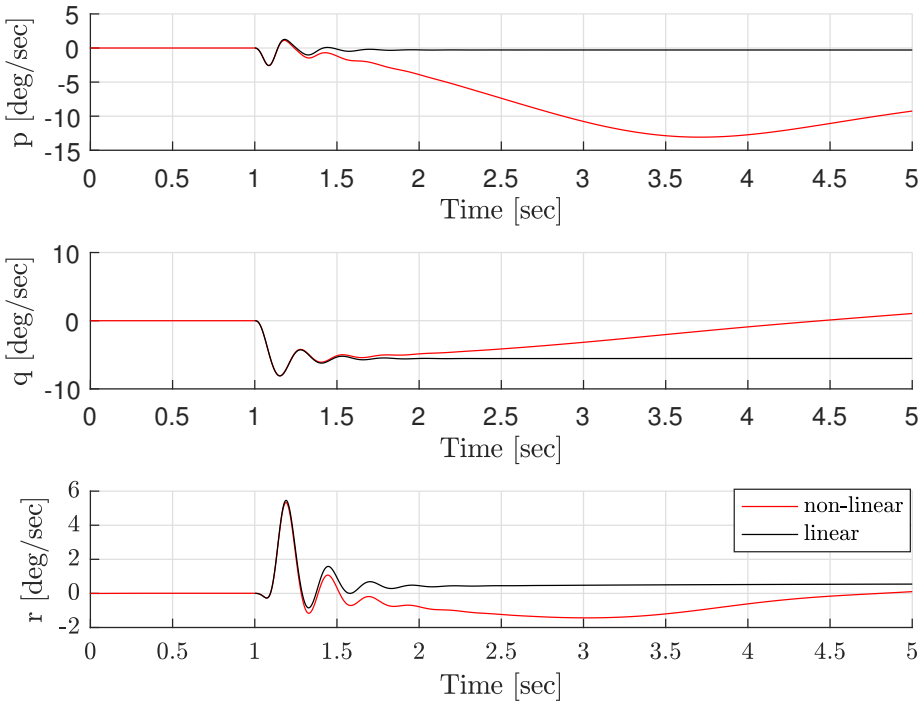

Figure 2.15: Angular velocity response to B_1.

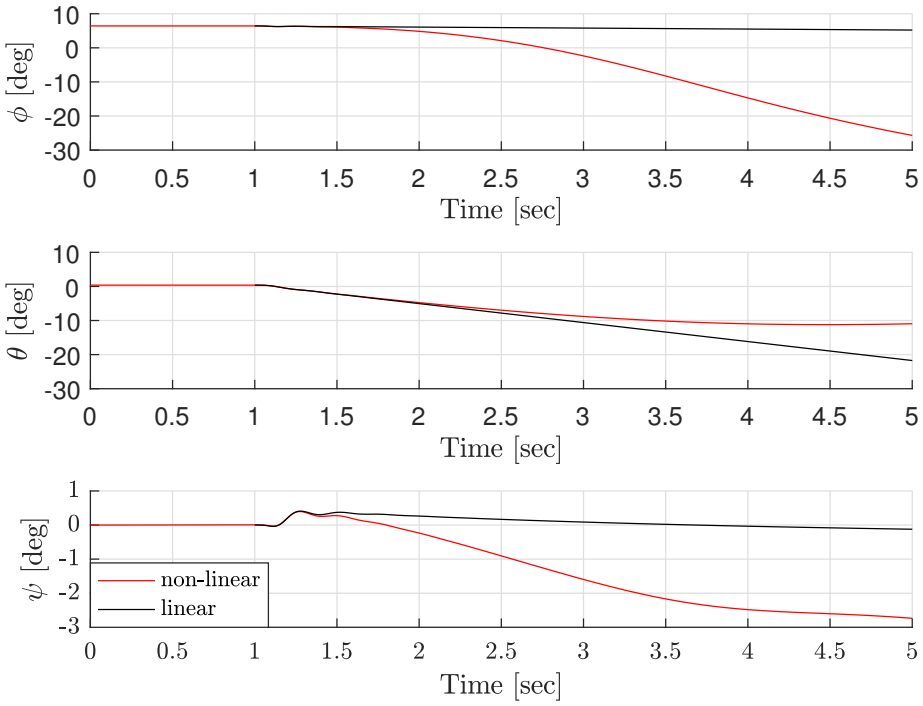

Figure 2.16: Attitude response to B_1.

Part II

Controller

Chapter 3

Controller introduction and simplifications

In this chapter, some simplification to the helicopter model, derived in Chapter 1, will be introduced in order to acquire a model for controller design.

A particular reference system will be defined in order to develop a controller for the longitudinal, lateral, vertical velocity and the yaw angle ψ.

3.1 Model simplification

The helicopter model derived in this thesis is a highly complex non-linear model with 26 states. The main purpose of this thesis is to use a non-linear control approach, based on feedback linearization theory, to cancel out non-linearities. The main point of this form of control is to identify the non-linearities of the system and, using feedback, to cancel them out. As it can be anticipated, this control design approach relies heavily on the accuracy of the model, in order to identify the non-linearities, thus effectively restricting the simplifications that can be applied to the full order model. Therefore the full order model is simplified as much as possible.

After the control design application, and the model complexity degree evaluation, if the control results prove unsatisfactory, due to the reduced model complexity, the neglected dynamics are added iteratively, until the satisfactory results are obtained.

A schematic representation of the helicopter dynamic model is shown in Fig. 3.1

The simplifications that can be applied to the full order model are:

- neglecting the servo-actuator's dynamics;
- decoupling the rotor and flybar dynamics from the rigid body dynamics.

Using these approximations it's possible to divide the model into two effectively decoupled parts, an input dynamics part containing the actuator dynamics and rotor and flybar dynamics, and a rigid body part containing the force and moment generation and rigid body dynamics.

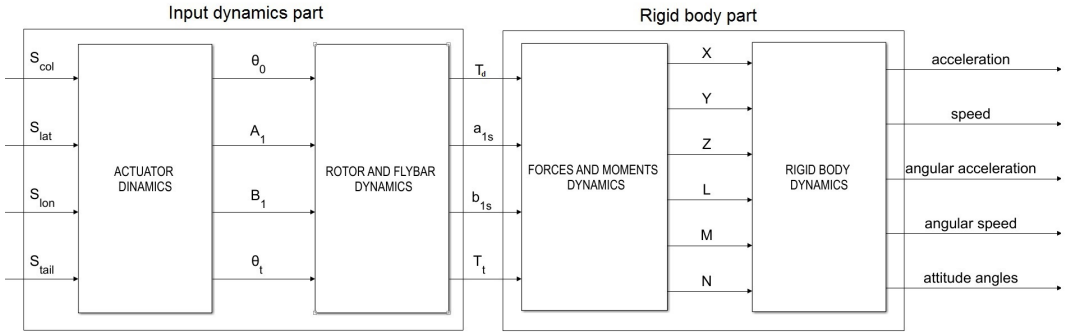

Figure 3.1: Non-linear Model.

The model for the first attempt of non-linear control design is thus chosen to contain only rigid body dynamics and force and moment dynamics.

Neglecting the input dynamics part the new input of our model become T_d, a_{1s}, b_{1s} and T_t, as shown in Fig. 3.2.

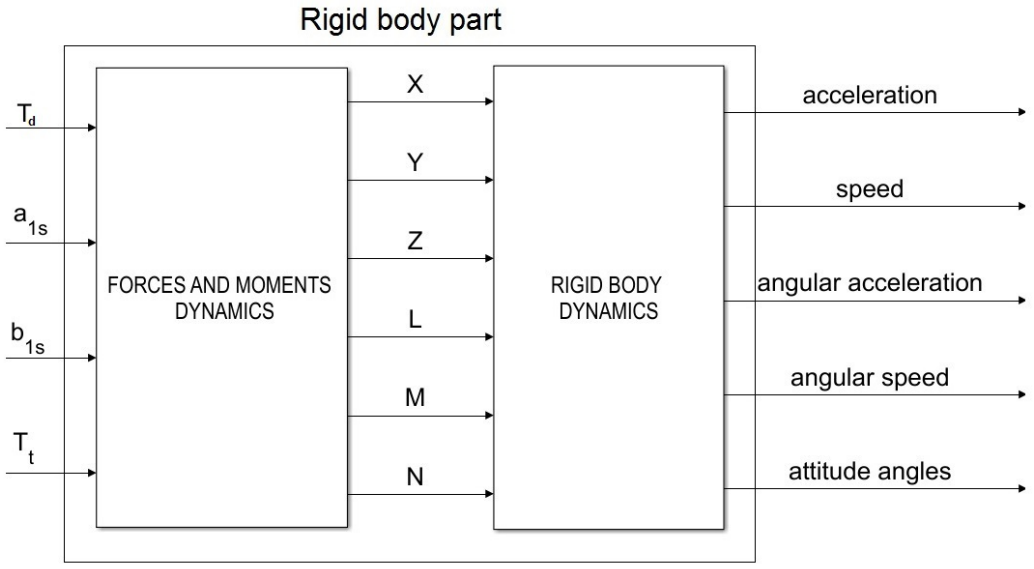

Figure 3.2: Simplified Non-linear Model.

3.2 Reference System for the Controller

It's necessary to define a particular reference system (for ease of reference called horizontal-body) which differs from the vertical for a positive eastward rotation of the yaw angle ψ. This particular reference system is used to set the tracking signals as V_{lon}, V_{cross}, V_z and ψ.

The transformation matrix from body axes to horizontal-body axes it's explic-

itly described by Eq. (3.1)

$$\begin{bmatrix} V_{lon} \\ V_{cross} \\ V_z \end{bmatrix} = \boldsymbol{R}_{B2HB} \begin{bmatrix} U \\ V \\ W \end{bmatrix} \tag{3.1}$$

where:

$$\boldsymbol{R}_{B2HB} = \begin{bmatrix} \cos\theta & \sin\phi\sin\theta & \cos\phi\sin\theta \\ 0 & \cos\phi & -\sin\phi \\ -\sin\theta & \sin\phi\cos\theta & \cos\phi\cos\theta \end{bmatrix} \tag{3.2}$$

Chapter 4

Feedback Linearization Control

The aim of this chapter is to study the stability of the helicopter and develop control laws.

Classic linear system control method is very difficult to ensure system stability, and non-linear control methods are general approaches.

Non-linear control methods are generally based on feedback linearization theory [5], that has successful applications in aircraft and rotorcraft control.

4.1 Feedback linearization

Considering a non-linear multiple input multiple output (MIMO) system with m inputs and outputs, of the following form:

$$\begin{cases} \dot{\boldsymbol{x}} = \boldsymbol{f}(x) + \sum_{i=1}^{m} \boldsymbol{g}_i(x) u_i \\ \boldsymbol{y} = \boldsymbol{h}(x) \end{cases} \tag{4.1}$$

where $\boldsymbol{x} \in \mathbb{R}^n$, $\boldsymbol{f}(x)$, $\boldsymbol{g}_1(x)$, $\boldsymbol{g}_m(x)$ and $\boldsymbol{h}(x)$ are smooth vector fields, and are defined as:

$$\boldsymbol{g} = \begin{bmatrix} \boldsymbol{g}_1 & \dots & \boldsymbol{g}_m \end{bmatrix} \tag{4.2}$$

$$\boldsymbol{h} = \begin{bmatrix} h_1 \\ \vdots \\ h_m \end{bmatrix} \tag{4.3}$$

$$\boldsymbol{u} = \begin{bmatrix} u_1 \\ \vdots \\ u_m \end{bmatrix} \tag{4.4}$$

If there exists a change of variables:

$$\dot{\boldsymbol{\xi}} = \boldsymbol{\Phi}(x) \tag{4.5}$$

such that the system is transformed in to:

$$\begin{cases} \dot{\boldsymbol{\xi}} = \boldsymbol{A_c}\boldsymbol{\xi} + \boldsymbol{B_c}\boldsymbol{v} \\ \boldsymbol{y} = \boldsymbol{C_c}\boldsymbol{\xi} \end{cases} \tag{4.6}$$

that results linear introducing the state feedback control [5]:

$$\boldsymbol{u} = \boldsymbol{\alpha} + \boldsymbol{\beta}\boldsymbol{v} \tag{4.7}$$

In order to apply this procedure, certain definitions and their application on the system are introduced.

4.1.1 Lie Derivative and relative degree

First we introduce the concept of relative degree, r_i, with respect to output y_i, as an integer such that:

$$L_{g_j} L_f^k h_i(x) = 0 \tag{4.8}$$

for all $1 \leq j \leq m$, for all $k < r_i - 1$, for all $1 \leq i \leq m$, and for all x in a proximity of equilibrium point x^o, and:

$$L_{g_j} L_f^{r_i - 1} h_i(x) \neq 0 \tag{4.9}$$

for at least one $1 \leq j \leq m$.

$$L_f h_i(x) = \frac{\partial h_i}{\partial \boldsymbol{x}} f(x) \tag{4.10}$$

is called the Lie Derivative of h_i with respect to f along f.

In other words, r_i is exactly the number of times one has to differentiate the i-th output, y_i, in order to have at least one component of the input vector u, explicitly appear.

Consider a non-linear system, of the form (4.1), evaluating all output functions and collecting the calculations, we can put the system in the form:

$$\begin{aligned} \begin{bmatrix} y_1^{r_1} \\ \vdots \\ y_m^{r_m} \end{bmatrix} &= \begin{bmatrix} L_f^{r_1} h_1 \\ \vdots \\ L_f^{r_m} h_m \end{bmatrix} + \begin{bmatrix} L_{g_1} L_f^{r_1 - 1} h_1 & \dots & L_{g_m} L_f^{r_1 - 1} h_1 \\ \vdots & \ddots & \vdots \\ L_{g_1} L_f^{r_m - 1} h_m & \dots & L_{g_m} L_f^{r_m - 1} h_m \end{bmatrix} \boldsymbol{u} \\ &= \boldsymbol{b}(x) + \boldsymbol{A}(x)\boldsymbol{u} \end{aligned} \tag{4.11}$$

Furthermore if the feedback is introduced in form of:

$$\begin{aligned} \boldsymbol{u} &= \boldsymbol{A}^{-1}[-\boldsymbol{b}(x) + \boldsymbol{v}] \\ &= -\boldsymbol{A}^{-1}(x)\boldsymbol{b}(x) + \boldsymbol{A}^{-1}\boldsymbol{v} \\ &= \boldsymbol{\alpha}(x) + \boldsymbol{\beta}(x)\boldsymbol{v} \end{aligned} \tag{4.12}$$

we acquire a linear closed loop system, that is decoupled from the input $\boldsymbol{v}$ to the output $\boldsymbol{y}$. This decoupled and input-output linearized system is given by:

$$\begin{bmatrix} y_1^{r_1} \\ \vdots \\ y_m^{r_m} \end{bmatrix} = \begin{bmatrix} v_1 \\ \vdots \\ v_m \end{bmatrix} \tag{4.13}$$

If the matrix $\boldsymbol{A}(x)$ is singular, we cannot use a static state feedback to linearized the non-linear system, and we have to look for a dynamic state feedback to achieve linearization by state feedback [5].

Having a particular tracking signal $y_d(t)$, it is possible to obtain an exponentially stable dynamic introducing the control law:

$$v_i = y_{d_i}^{r_i} - K_{i,0}e_i - K_{i,1}\dot{e}_i - \cdots - K_{i,(r_i-1)}e_i^{(r_i-1)} \tag{4.14}$$

with opportune value of $K_{i,j}$ and with:

$$e = y_i - y_d \tag{4.15}$$

the error to minimize.

4.1.2 Coordinate change function

Considering the Eq. (4.11), first input-output channel can be written as:

$$\begin{cases} y_1 = h_1(x) \\ y_1^{(1)} = L_f h_1(x) \\ y_1^{(r_i-1)} = L_f^{r_i-1} h_1(x) \\ y_1^{(r_i)} = L_f^{r_1} h_1(x) + L_{g_1} L_f^{r_1-1} h_1(x) u_1(x) + \cdots + L_{g_m} L_f^{r_1-1} h_1(x) u_m(x) \end{cases} \tag{4.16}$$

If we define transformation function as:

$$\boldsymbol{\xi} = \boldsymbol{\Phi}(x) = col(\Phi_1(x), \ldots, \Phi_{r_1}) = col(h(x), L_f h_1(x), \ldots, L_f^{r_1-1} h_1(x)) \tag{4.17}$$

and apply it to the above system we get:

$$\begin{cases} y_1 = \xi_1 \\ \dot{\xi}_1 = \xi_2 \\ \vdots \\ \dot{\xi}_{r_i-1} = \xi_{r_i} \\ \dot{\xi}_{r_i} = L_f^{r_1} h_1(x) + L_{g_1} L_f^{r_1-1} h_1(x) u_1(x), \ldots, L_{g_m} L_f^{r_1-1} h_1(x) u_m(x) \end{cases} \tag{4.18}$$

We extend the coordinate transformation equation to contain all input-output sets, therefore, the coordinate change function, that transforms the full system in to

$$f(\boldsymbol{\xi}) = f(\boldsymbol{\Phi}(x)) \tag{4.19}$$

has the following form:

$$\boldsymbol{\Phi} = col(\Phi_1^1(x), \ldots, \Phi_{r_1}^1(x), \ldots, \Phi_1^m(x), \ldots, \Phi_{r_m}^m(x)) \tag{4.20}$$

m denotes the number of outputs and

$$\begin{cases} \Phi_1^i(x) = h_i(x) \\ \Phi_2^i(x) = L_f h_i(x) \\ \vdots \\ \Phi_{r_i}^i = L_f^{r_i-1} h_i(x) \end{cases} \tag{4.21}$$

The transformation of this form does not always transform all the states of the system. We can have some unobservable states.

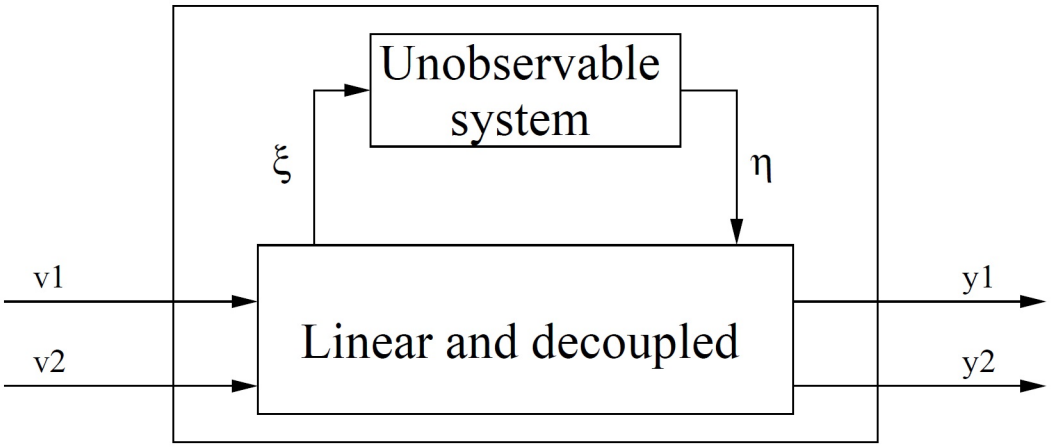

Figure 4.1: Sketch of the input-output feedback linearizing principle

4.1.3 Input-output Exact Feedback Linearization

If a system has relative degree $r = r_1 + r_2 + \cdots + r_m < n$, feedback linearization of a given system can still be achieved from the input-output point of view using the same algorithm of the Eq. (4.12). The consequences of this approach are that some states of the linearized system, zero dynamics states η, become unobservable, see Fig. 4.1.

These states can be identified by applying the coordinate change of the system states of the following form:

$$f(\xi, \eta) = f(\mathbf{\Phi}(x)) \tag{4.22}$$

where ξ are the states of the observable system and η are the states of the unobservable system. The coordinate transformation function is defined as:

$$\mathbf{\Phi} = col(\Phi_1^1(x), \ldots, \Phi_{r_1}^1(x), \ldots, \Phi_1^m(x), \ldots, \Phi_{r_m}^m(x), \Phi_{r+1}(x), \ldots, \Phi_n(x)) \tag{4.23}$$

where, m denotes the number of outputs, n denotes the order of the system, r denotes the sum of relative degree elements and:

$$\begin{cases} \Phi_1^i(x) = h_i(x) \\ \Phi_2^i(x) = L_f h_i(x) \\ \vdots \\ \Phi_{r_i}^i = L_f^{r_i - 1} h_i(x) \end{cases} \tag{4.24}$$

Furthermore, the extra functions, $\Phi_{r+1}(x), \ldots, \Phi_n(x)$, defining the zero dynamic states, can be chosen arbitrary as long as distribution,

$$\boldsymbol{G} = span\{g_1, \ldots, g_m\} \tag{4.25}$$

is involutive, and the chosen function satisfy:

$$L_{g_j} \Phi_i(x) = 0 \quad \text{for: } r + 1 \leq i \leq n, 1 \leq j \leq m \tag{4.26}$$

Zero dynamics of a input-output feedback linearized system might exhibit unstable behaviour, therefore, in order to guarantee the stability of the overall system, it is not sufficient to look at input-output stability, we have to make sure that the unobservable part of the system is stable as well [5].

4.2 Definition of the Model

Applying the approximation deduced in Chapter 3, the inputs of the dynamic model become T_d, a_{1s}, b_{1s}, T_t.

Using the results obtained in Chapter 1 it's possible to write the dynamic model as:

$$\dot{\boldsymbol{x}} = f(\boldsymbol{x}) + g(\boldsymbol{u}) \tag{4.27}$$

where:

$$\boldsymbol{x} = \begin{bmatrix} U \\ V \\ W \\ p \\ q \\ r \\ \phi \\ \theta \\ \psi \end{bmatrix} \tag{4.28}$$

and

$$\boldsymbol{u} = \begin{bmatrix} T_d \\ a_{1s} \\ b_{1s} \\ T_t \end{bmatrix} \tag{4.29}$$

It can be shown that the helicopter dynamic model, used in this thesis, is not of the structure (4.1), due to the fact that several states are exited with multiple inputs, or functions of inputs, that are multiplied with each other. Dynamic extension is used to transform the system equations, to the form described by (4.1). Dynamic extension "delays" a given input trough an integrator, thus extending the system state equation with one state, therefore, the dynamic extended system is:

$$\begin{bmatrix} \dot{U} \\ \dot{V} \\ \dot{W} \\ \dot{p} \\ \dot{q} \\ \dot{r} \\ \dot{\phi} \\ \dot{\theta} \\ \dot{\psi} \\ \dot{T}_d \\ \dot{a}_{1s} \\ \dot{b}_{1s} \end{bmatrix} = f(x) + \sum_{i=1}^{m} g_i(x) u_i \tag{4.30}$$

with:

$$\sum_{i=1}^{m} g_i(x)u_i = \boldsymbol{g}\boldsymbol{u} = \begin{bmatrix} g_1 & g_2 & g_3 & g_4 \end{bmatrix} \begin{bmatrix} \dot{T}_d \\ \dot{a}_{1s} \\ \dot{b}_{1s} \\ T_t \end{bmatrix} \tag{4.31}$$

4.3 Procedure of Linearization

To perform the input-output exact feedback linearization the chosen output functions are:

$$\boldsymbol{h} = \begin{bmatrix} U \\ V \\ W \\ \psi \end{bmatrix} \tag{4.32}$$

where the corresponding relative degree is $\{r_1, r_2, r_3, r_4\} = \{2, 2, 2, 2\}$. Using this set of output functions to linearize the system, there are 4 unobservarble states, p, q, ϕ and θ, that have to be tested for stability.

First it's necessary to calculate the matrix $\boldsymbol{A}$ used to define the control laws that linearize the model

$$\boldsymbol{A} = \begin{bmatrix} L_{g_1}L_f^{r_1-1}h_1 & L_{g_2}L_f^{r_1-1}h_1 & L_{g_3}L_f^{r_1-1}h_1 & L_{g_4}L_f^{r_1-1}h_1 \\ L_{g_1}L_f^{r_2-1}h_2 & L_{g_2}L_f^{r_2-1}h_2 & L_{g_3}L_f^{r_2-1}h_2 & L_{g_4}L_f^{r_2-1}h_2 \\ L_{g_1}L_f^{r_3-1}h_3 & L_{g_2}L_f^{r_3-1}h_3 & L_{g_3}L_f^{r_3-1}h_3 & L_{g_4}L_f^{r_3-1}h_3 \\ L_{g_1}L_f^{r_4-1}h_4 & L_{g_2}L_f^{r_4-1}h_4 & L_{g_3}L_f^{r_4-1}h_4 & L_{g_4}L_f^{r_4-1}h_4 \end{bmatrix} \tag{4.33}$$

The matrix has full rank, therefore the system is input-output linearizable using the control laws defined in Eq. (4.12).

According to Eq. (4.14):

$$\begin{cases} v_1 = \ddot{y}_{d_1} - K_{1,0}e_1 - K_{1,1}\dot{e}_1 \\ v_2 = \ddot{y}_{d_2} - K_{2,0}e_2 - K_{2,1}\dot{e}_2 \\ v_3 = \ddot{y}_{d_3} - K_{3,0}e_3 - K_{3,1}\dot{e}_3 \\ v_4 = \ddot{y}_{d_4} - K_{4,0}e_2 - K_{4,1}\dot{e}_4 \end{cases} \tag{4.34}$$

The feedback gains are determined using pole-placement method and the result is:

$$\begin{bmatrix} K_{1,0} \\ K_{1,1} \\ K_{2,0} \\ K_{2,1} \\ K_{3,0} \\ K_{3,1} \\ K_{4,0} \\ K_{4,1} \end{bmatrix} = \begin{bmatrix} 14 \\ 5 \\ 14 \\ 5 \\ 14 \\ 5 \\ 14 \\ 5 \end{bmatrix} \tag{4.35}$$

In order to test the stability of the feedback linearized system, a simulation test has been performed; the tracking signals y_{d_i} used for the test are the hovering condition. In Fig. 4.2 it is shown the scheme of the control.

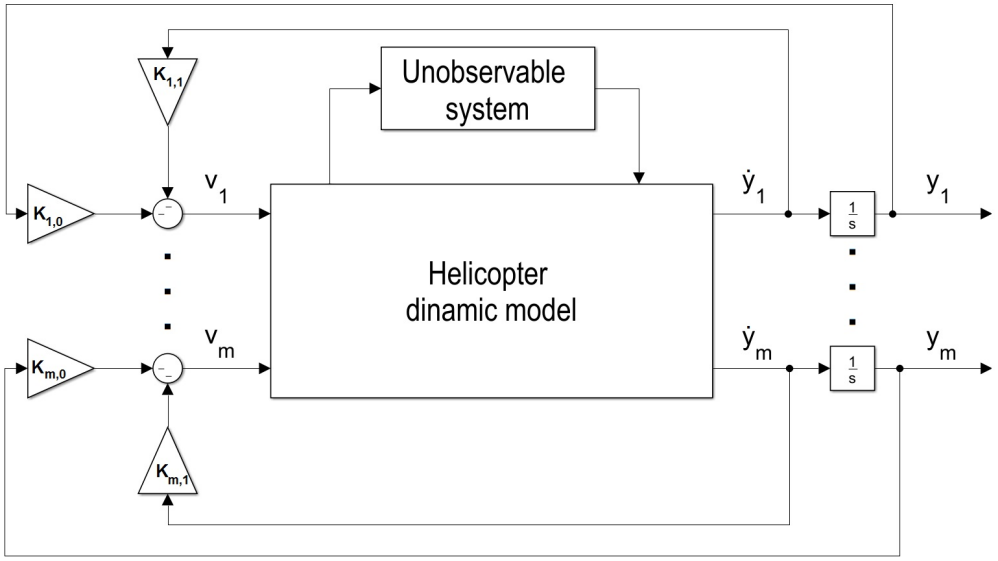

Figure 4.2: Sketch of the closed loop feedback linearized system

4.4 Simulation results

As shown in [6] [7] it is not possible to stabilize the system due the instability of the zero dynamics states p, q, ϕ and θ.

Initializing the system output states with the following values:

$$\boldsymbol{y} = \begin{bmatrix} U \\ V \\ W \\ \psi \end{bmatrix} = \begin{bmatrix} 0.5 \\ -0.5 \\ 0 \\ 0.1 \end{bmatrix} \tag{4.36}$$

where U, V and W are in m/s and ψ is in rad, the result of the simulation it is shown in Fig. 4.3-4.8.

At first glance of Fig. 4.6, the simulated outputs seem to have stabilized at the correct level, thus suggesting that the control task was successful. However taking a look at the zero dynamics states on Fig. 4.7-4.8 , it can be seen that the unobservable part of the system is far from stable. The reason for this behavior is the structure of the feedback linearizing procedure, where the linearizing feedback will use the observable states and the first inputs it encounters to control the given output.

In our case, due to the fact that pitch and roll angles and their respective rates are unobservable, the linearizing feedback attempts to stabilize the helicopter translatory velocity directly trough the decomposition of the thrust vector in longitudinal and lateral direction, instead of using pitch and roll Euler angles to turn the helicopter in the opposite direction of the flight path, and thus stabilize the system. Therefore we conclude that exact feedback linearization of a helicopter is not possible.

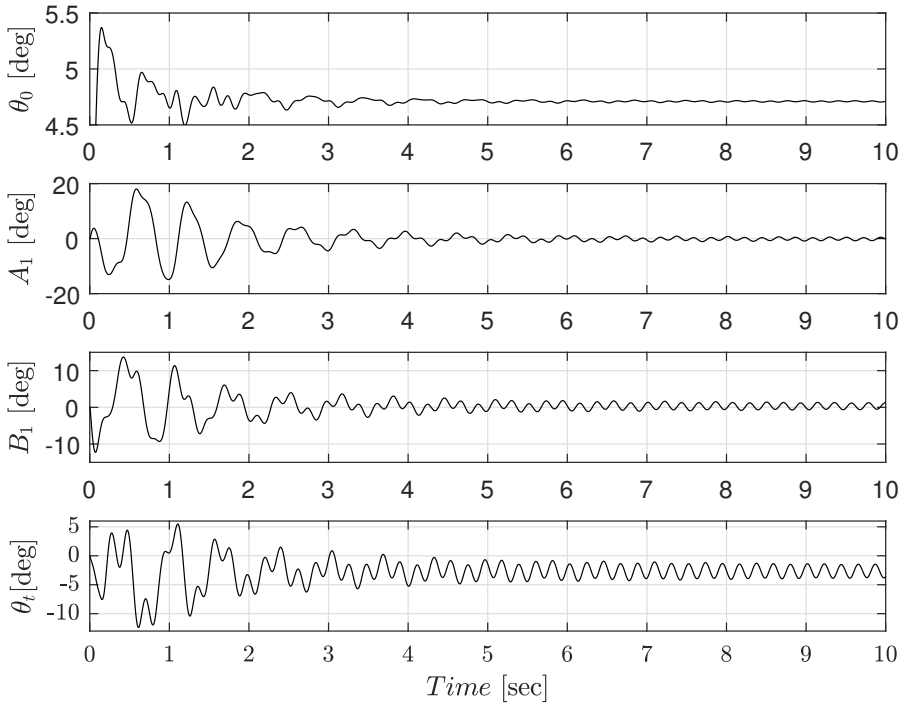

Figure 4.3: Effect of the control on the command angles.

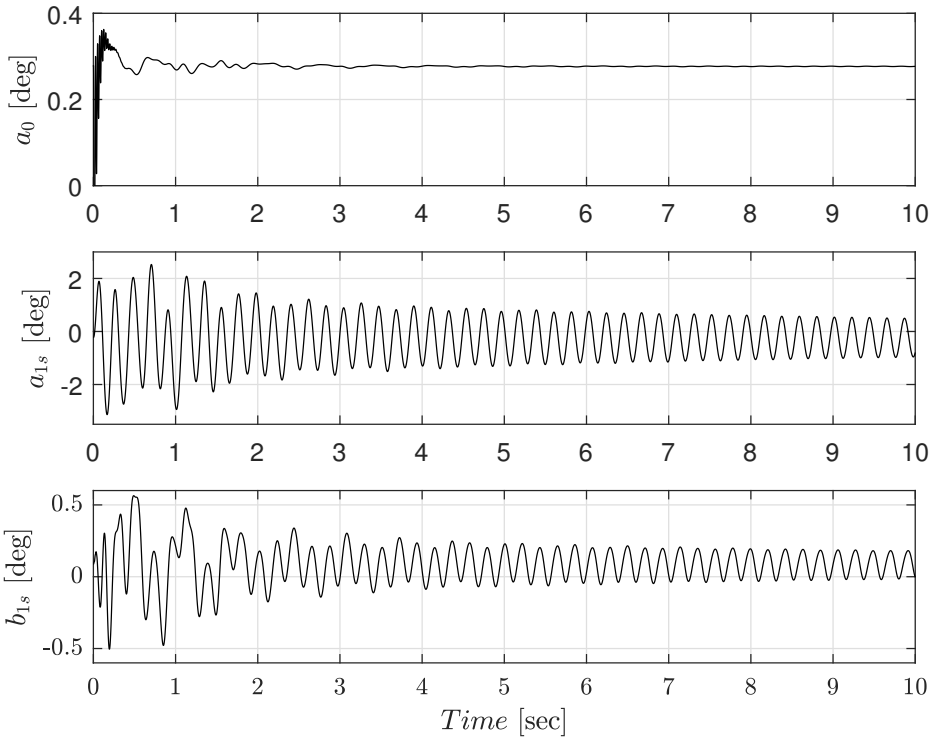

Figure 4.4: Effect of the control on the flapping angles.

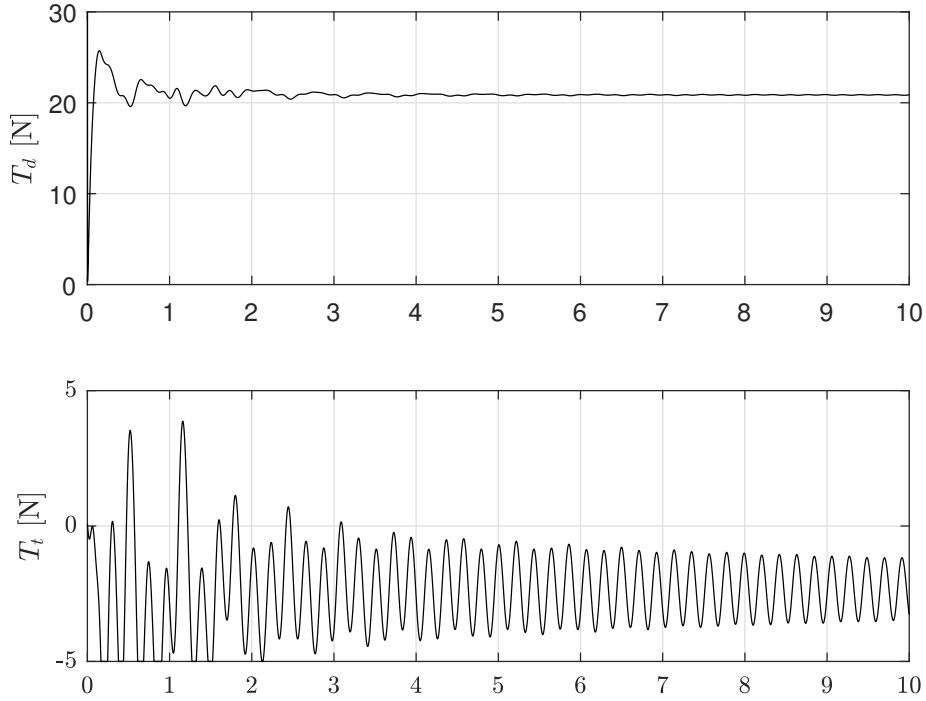

Figure 4.5: Effect of the control on Rotor and Tail Trust.

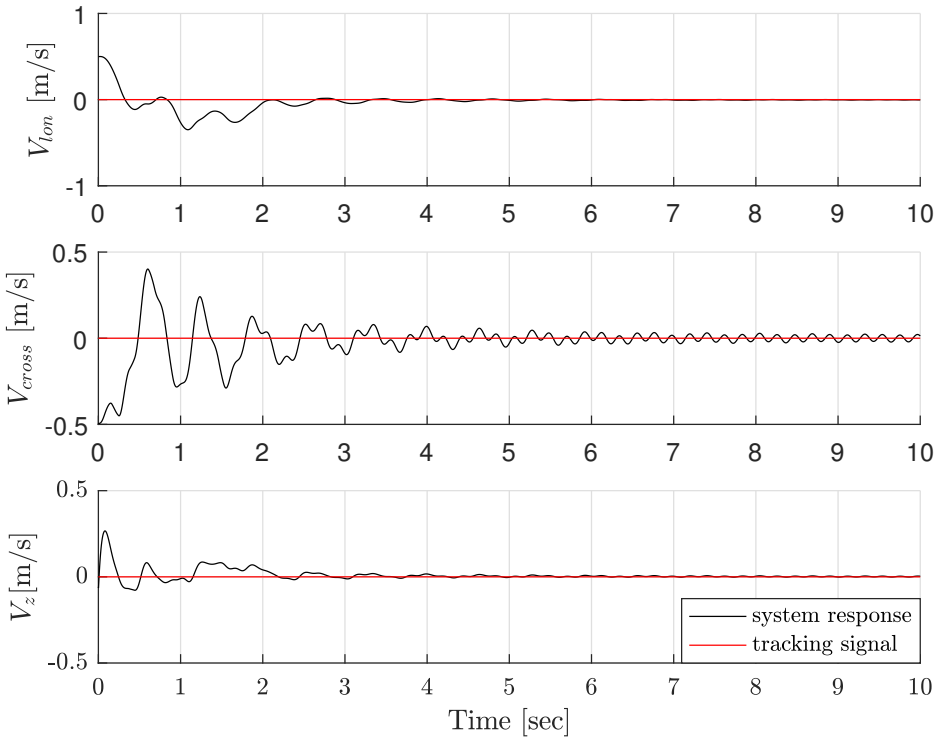

Figure 4.6: Comparison between effective and desire velocities.

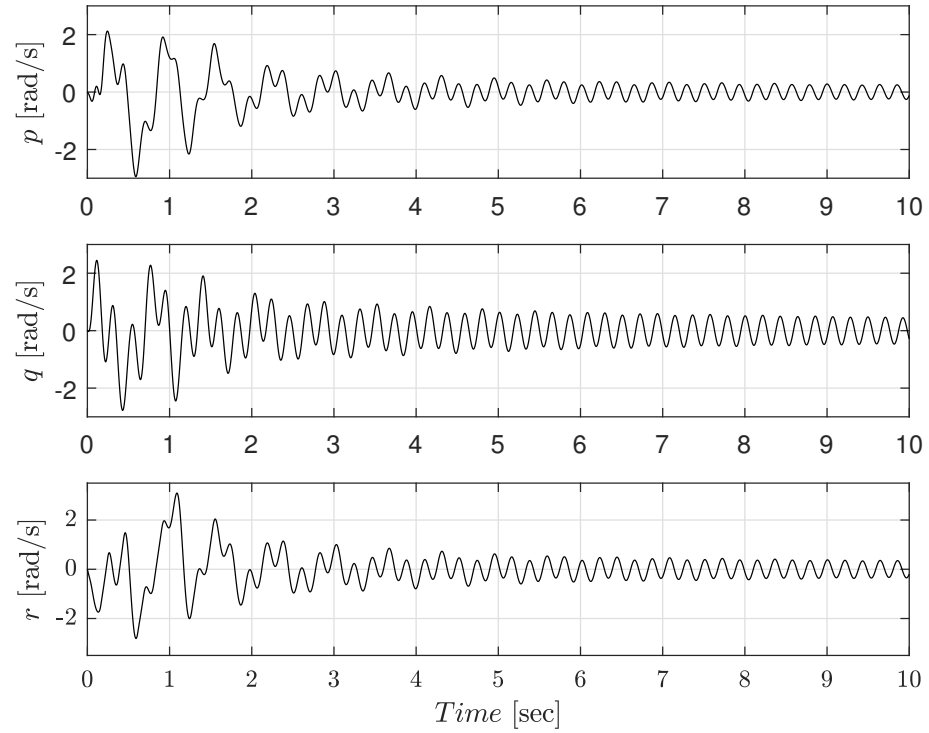

Figure 4.7: Effect of the control on angular velocity.

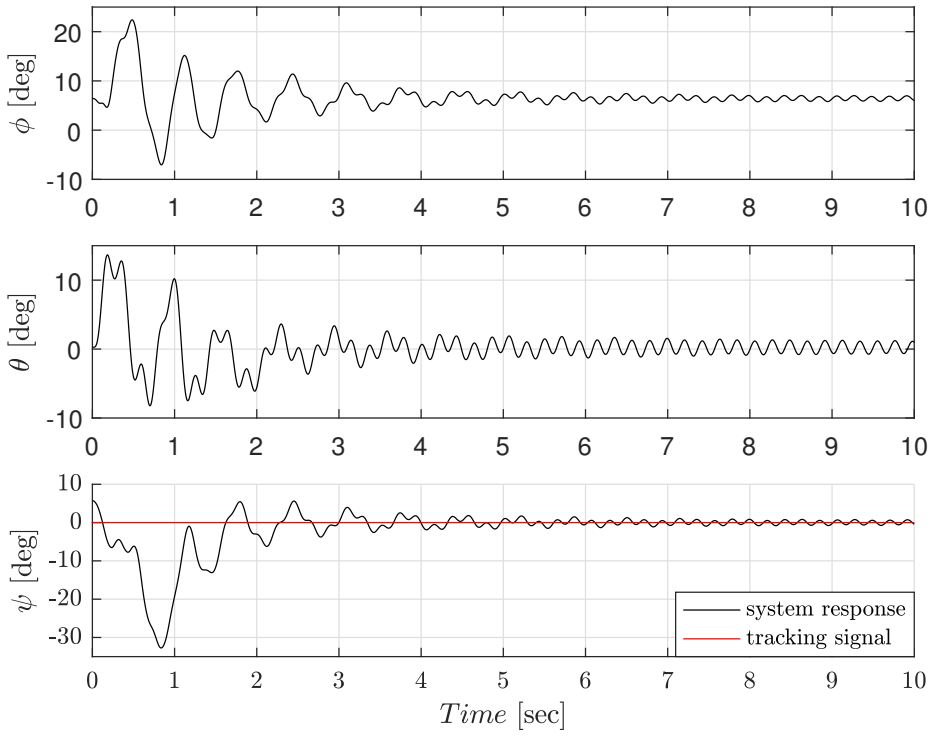

Figure 4.8: Effect of the control on attitude angles.

Chapter 5

Dynamic Inversion Controls

In this chapter dynamic inversion control method will be applied to the non-linear model in order to control the helicopter attitude angle ψ and thus the three velocity component V_{lon}, V_{cross} and V_z

5.1 Dynamic Inversion

Dynamic Inversion is a method based on feedback linearization with time scale separation approximation. According to "Partial Inversion" method, we can divide the system into several sub-circuits, which have different time scales [8], and control them in cascade.

Firstly, model state variables are divided into different groups, according to its response velocity. The principle for state variable grouping is: dynamic characteristics of inner circuit can be ignored in outer circuit design, when the response velocity of internal circuit is almost three times faster than the outer circuit. This division has the advantages that the inverse system can be very simple after the division and it is possible to avoid the generation of unobservable states.

According to the movement of the helicopter, giving a variation of the input T_d, a_{1s}, b_{1s} and T_t the helicopter changes its angular velocities p, q, r and its vertical velocity V_z. Due to the generation of these angular velocities there is a changing on the attitude angles ϕ, θ and ψ. Finally the variation of the Euler angles ϕ and θ is used to generate the desire velocities V_{lon} and V_{cross}.

According to this, helicopter state variables can be divided into three different groups:

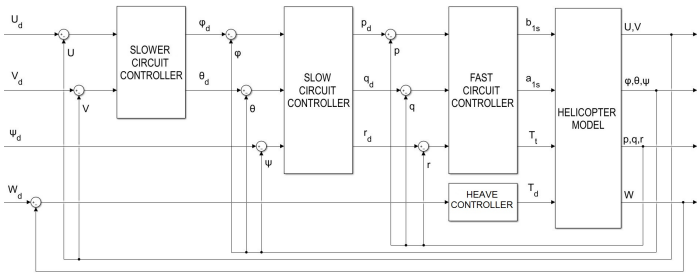

Figure 5.1: Sketch of the dynamic inversion controller.

- $[p, q, r, W]$ have fast response in system, called fast variables;
- $[\phi, \theta, \psi]$ have slow response in system, called slow variables;
- $[U, V]$ have slowest response in system, called slower variables;

The Fig. 5.1 show a schematic representation of the controller chain.

According to the approximation of time scale separation, when solving the inverse controller in fast circuit, the slow circuit variables can be considered as approximately constant, and vice versa, so every single circuit controller can be studied separately.

5.2 Linearization of the single circuit

Using the approximations introduced in Chapter 3 and the formulation of the dynamic equations as:

$$\begin{aligned}\begin{bmatrix} y_1^{r_1} \\ \vdots \\ y_m^{r_m} \end{bmatrix} &= \begin{bmatrix} L_f^{r_1} h_1 \\ \vdots \\ L_f^{r_m} h_m \end{bmatrix} + \begin{bmatrix} L_{g_1} L_f^{r_1-1} h_1 & \dots & L_{g_m} L_f^{r_1-1} h_1 \\ \vdots & \ddots & \vdots \\ L_{g_1} L_f^{r_1-1} h_m & \dots & L_{g_m} L_f^{r_1-1} h_m \end{bmatrix} \boldsymbol{u} \\ &= \boldsymbol{b}\big(x\big) + \boldsymbol{A}\big(x\big)\boldsymbol{u}\end{aligned} \tag{5.1}$$

as shown in Chapter 4 it is possible to linearize the model using the fictitious input:

$$\begin{bmatrix} v_1 \\ \vdots \\ v_i \end{bmatrix} = \begin{bmatrix} -K_{1,0} e_i - K_{1,1} \dot{e}_1 - \dots - K_{1,\left(r_1-1\right)} e_1^{\left(r_1-1\right)} \\ \vdots \\ -K_{i,0} e_i - K_{i,1} \dot{e}_i - \dots - K_{i,\left(r_i-1\right)} e_i^{\left(r_i-1\right)} \end{bmatrix} \tag{5.2}$$

and applying the transformation:

$$\boldsymbol{u} = \boldsymbol{A}^{-1}[-\boldsymbol{b}\big(x\big) + \boldsymbol{v}] \tag{5.3}$$

as schematically shown in Fig. 5.2

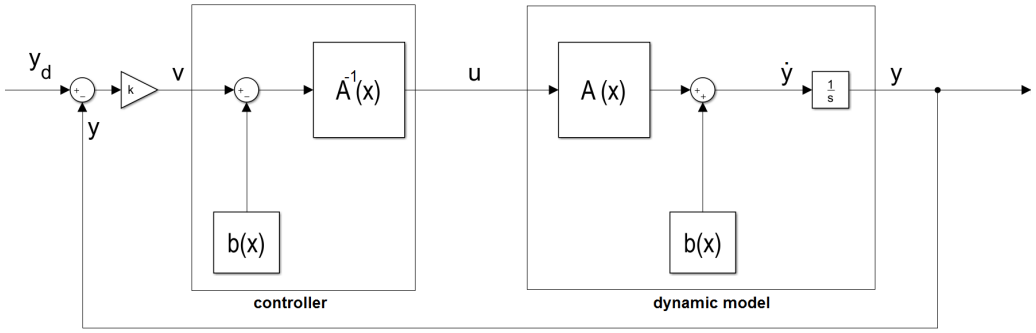

Figure 5.2: Sketch of a single circuit controller

We can now linearize the model.

5.3 Angular velocity and heave controller

The state equations of the fast circuit can be expressed as follows:

$$\begin{bmatrix} \dot{p} \\ \dot{q} \\ \dot{r} \end{bmatrix} = \begin{bmatrix} b_p \\ b_q \\ b_r \end{bmatrix} + \begin{bmatrix} A_{11} & A_{12} & A_{13} \\ A_{21} & A_{22} & A_{23} \\ A_{31} & A_{32} & A_{33} \end{bmatrix} \begin{bmatrix} a_{1s} \\ b_{1s} \\ T_t \end{bmatrix} \tag{5.4}$$

and

$$\dot{W} = b_W - \frac{1}{m} \cdot T_d \tag{5.5}$$

where:

$$\begin{aligned} b_p = &- \big(I_{yy} \cdot I_{xy} \cdot \big(- I_{xz} \cdot \big(p^2 - r^2\big) - p \cdot r \cdot \big(I_{xx} - I_{yy}\big) + I_{xy} \cdot q \cdot r + \\ &+ H_d \cdot h \cdot r - T_d \cdot R \cdot f\big) + I_{yy} \cdot I_{yy} \cdot \big(T_d \cdot R \cdot l + I_{xz} \cdot p \cdot q + \\ &+ q \cdot r \cdot \big(I_{yy} - I_{yy}\big) - I_{xy} \cdot p \cdot r\big) + I_{yy} \cdot I_{xz} \cdot \big(I_{xy} \cdot \big(p^2 - q^2\big) + \\ &+ p \cdot q \cdot \big(I_{xx} - I_{yy}\big) - I_{xz} \cdot q \cdot r - Q\big)\big) / \big(I_{yy} \cdot I_{xz}^2 + \\ &+ I_{yy} \cdot I_{xy}^2 - I_{xx} \cdot I_{yy} \cdot I_{yy}\big) \end{aligned}$$

$$\begin{aligned} b_q = &- \big(I_{yy} \cdot I_{xy} \cdot \big(- I_{xz} \cdot \big(p^2 - r^2\big) - p \cdot r \cdot \big(I_{xx} - I_{yy}\big) + I_{xy} \cdot q \cdot r + \\ &+ H_d \cdot h \cdot r - T_d \cdot R \cdot f\big) + I_{yy} \cdot I_{yy} \cdot \big(T_d \cdot R \cdot l + I_{xz} \cdot p \cdot q + \\ &+ q \cdot r \cdot \big(I_{yy} - I_{yy}\big) - I_{xy} \cdot p \cdot r\big) + \\ &+ I_{yy} \cdot I_{xz} \cdot \big(I_{xy} \cdot \big(p^2 - q^2\big) + p \cdot q \cdot \big(I_{xx} - I_{yy}\big) + \\ &- I_{xz} \cdot q \cdot r - Q\big)\big) / \big(I_{yy} \cdot I_{xz}^2 + I_{yy} \cdot I_{xy}^2 - I_{xx} \cdot I_{yy} \cdot I_{yy}\big) \end{aligned} \tag{5.6}$$

$$\begin{aligned} b_r = &- \big(I_{xz} \cdot I_{xy} \cdot \big(- I_{xz} \cdot \big(p^2 - r^2\big) - p \cdot r \cdot \big(I_{xx} - I_{yy}\big) + \\ &+ I_{xy} \cdot q \cdot r + H_d \cdot h \cdot R - T_d \cdot f \cdot R\big) - I_{xy}^2 \cdot \big(I_{xy} \cdot \big(p^2 - q^2\big) + \\ &+ p \cdot q \cdot \big(I_{xx} - I_{yy}\big) - I_{xz} \cdot q \cdot r - Q\big) + I_{yy} \cdot I_{xz} \cdot \big(T_d \cdot l \cdot R + \\ &+ I_{xz} \cdot p \cdot q + q \cdot r \cdot \big(I_{yy} - I_{yy}\big) - I_{xy} \cdot p \cdot r\big) + \\ &+ I_{xx} \cdot I_{yy} \cdot \big(I_{xy} \cdot \big(p^2 - q^2\big) + p \cdot q \cdot \big(I_{xx} - I_{yy}\big) - I_{xz} \cdot q \cdot r + \\ &- Q\big)\big) / \big(I_{yy} \cdot I_{xz}^2 + I_{yy} \cdot I_{xy}^2 - I_{xx} \cdot I_{yy} \cdot I_{yy}\big) \end{aligned}$$

$$A_{11} = \frac{-I_{xy} \cdot \left(K_\beta + \Omega^2 \cdot R \cdot e \cdot m_{bl} \cdot x_g + H_d \cdot f \cdot R + T_d \cdot h \cdot R\right)}{I_{yy} \cdot I_{xz}^2 + I_{yy} \cdot I_{xy}^2 - I_{xx} \cdot I_{yy} \cdot I_{yy}}$$

$$A_{12} = \frac{I_{yy} \cdot I_{yy} \cdot \left(T_d \cdot h \cdot R + e \cdot m_{bl} \cdot x_g \cdot \Omega^2 \cdot R + K_\beta\right)}{I_{yy} \cdot I_{xz}^2 + I_{yy} \cdot I_{xy}^2 - I_{xx} \cdot I_{yy} \cdot I_{yy}}$$

$$A_{13} = - \frac{I_{yy} \cdot I_{yy} \cdot R \cdot h_t - I_{yy} \cdot I_{xz} \cdot R \cdot lt}{I_{yy} \cdot I_{xz}^2 + I_{yy} \cdot I_{xy}^2 - I_{xx} \cdot I_{yy} \cdot I_{yy}}$$

$$A_{21} = \frac{\left(K_\beta + \Omega^2 \cdot R \cdot e \cdot m_{bl} \cdot x_g + H_d \cdot f \cdot R + T_d \cdot h \cdot R\right) \cdot \left(I_{xz}^2 - I_{xx} \cdot I_{yy}\right)}{I_{yy} \cdot I_{xz}^2 + I_{yy} \cdot I_{xy}^2 - I_{xx} \cdot I_{yy} \cdot I_{yy}}$$

$$A_{22} = \frac{I_{yy} \cdot I_{xy} \cdot \left(T_d \cdot h \cdot R + e \cdot m_{bl} \cdot x_g \cdot \Omega^2 \cdot R + K_\beta\right)}{I_{yy} \cdot I_{xz}^2 + I_{yy} \cdot I_{xy}^2 - I_{xx} \cdot I_{yy} \cdot I_{yy}} \tag{5.7}$$

$$A_{23} = - \frac{I_{yy} \cdot I_{xy} \cdot R \cdot h_t - I_{xz} \cdot I_{xy} \cdot R \cdot l_t}{I_{yy} \cdot I_{xz}^2 + I_{yy} \cdot I_{xy}^2 - I_{xx} \cdot I_{yy} \cdot I_{yy}}$$

$$A_{31} = - \frac{I_{xz} \cdot I_{xy} \cdot \left(K_\beta + \Omega^2 \cdot R \cdot e \cdot m_{bl} \cdot x_g + H_d \cdot f \cdot R + T_d \cdot h \cdot R\right)}{I_{yy} \cdot I_{xz}^2 + I_{yy} \cdot I_{xy}^2 - I_{xx} \cdot I_{yy} \cdot I_{yy}}$$

$$A_{32} = \frac{I_{yy} \cdot I_{xz} \cdot \left(T_d \cdot h \cdot R + e \cdot m_{bl} \cdot x_g \cdot \Omega^2 \cdot R + K_\beta\right)}{I_{yy} \cdot I_{xz}^2 + I_{yy} \cdot I_{xy}^2 - I_{xx} \cdot I_{yy} \cdot I_{yy}}$$

$$A_{33} = - \frac{R \cdot l_t \cdot I_{xy}^2 - I_{xx} \cdot I_{yy} \cdot R \cdot l_t + I_{yy} \cdot I_{xz} \cdot R \cdot h_t}{I_{yy} \cdot I_{xz}^2 + I_{yy} \cdot I_{xy}^2 - I_{xx} \cdot I_{yy} \cdot I_{yy}}$$

and:

$$b_W = - \frac{S_{Zfus} \cdot \rho \cdot \left(W + \Omega \cdot R \cdot \lambda_i\right) \cdot \sqrt{\left(U^2 + V^2 + W^2\right)}}{2 \cdot m} + \\ + U \cdot q - V \cdot p + g \cdot cos\phi \cdot cos\theta \tag{5.8}$$

Taking $\boldsymbol{h}$ as output to control:

$$\boldsymbol{h} = \begin{bmatrix} p \\ q \\ r \\ W \end{bmatrix} \tag{5.9}$$

the corresponding relative degree is $\{r_p, r_q, r_r, r_W\} = \{1, 1, 1, 1\}$.

The two fictitious input signal used to linearize the model are v_ω and v_w:

$$\boldsymbol{v_\omega} = \begin{bmatrix} v_p \\ v_q \\ v_r \end{bmatrix} = \begin{bmatrix} K_p e_p \\ K_q e_q \\ K_r e_r \end{bmatrix} = \begin{bmatrix} K_p \cdot (p_d - p) \\ K_q \cdot (q_d - q) \\ K_r \cdot (r_d - r) \end{bmatrix} \tag{5.10}$$

and:

$$v_W = K_W e_W = K_W \cdot (W_d - W) \tag{5.11}$$

The feedback gains, determined using pole-placement method, are:

$$\begin{bmatrix} K_p \\ K_q \\ K_r \\ K_W \end{bmatrix} = \begin{bmatrix} 25 \\ 25 \\ 25 \\ 15 \end{bmatrix} \tag{5.12}$$

A schematic representation of the controller is shown in Fig. 5.3.

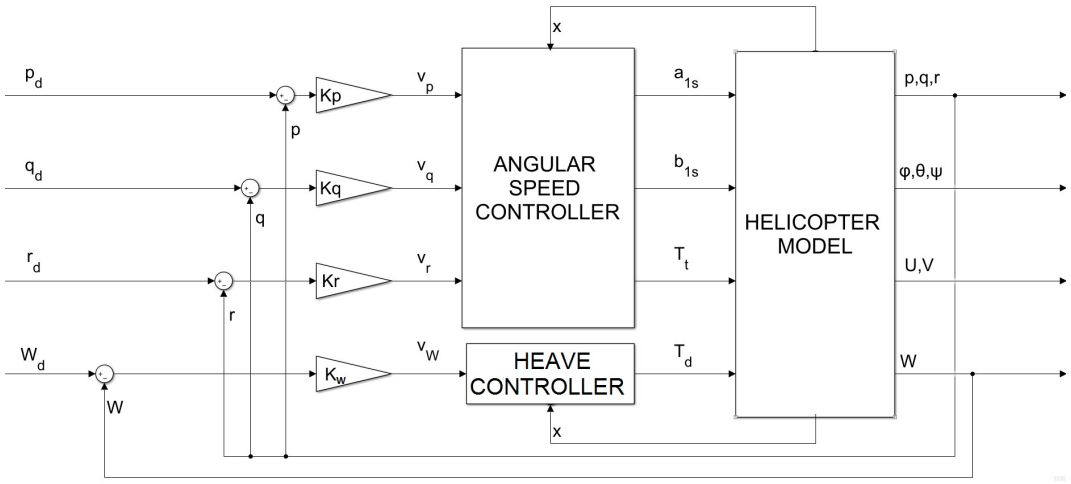

Figure 5.3: Sketch of fast controller.

5.3.1 Fast circuit simulation results

In order to test the stability of the controller, some simulation tests have been performed. The system was initialized in hovering condition and was exited by different tracking signals p_d, q_d and r_d.

For each simulation test only one input channel at a time was exited by a non-zero signal. The input signal was a square wave with amplitude 10 deg/s, mean-value 0 deg/s and frequency 0.25 Hz.

Time responses to a tracking signal p_d are shown in Fig. 5.4-5.6.

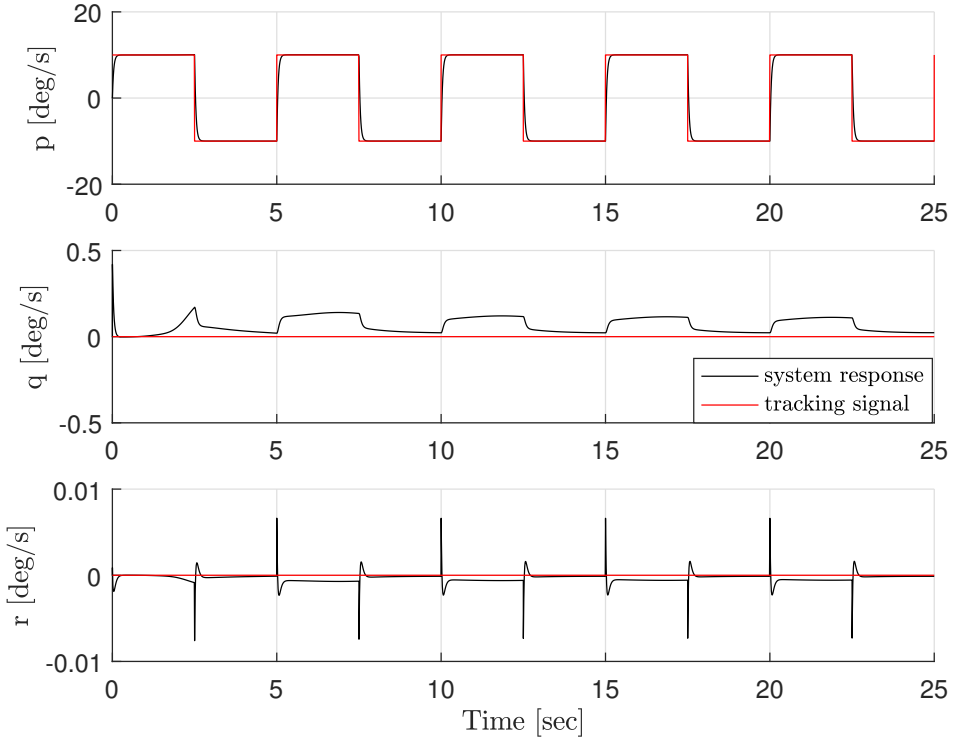

Figure 5.4: Angular velocity response to a tracking signal p_d.

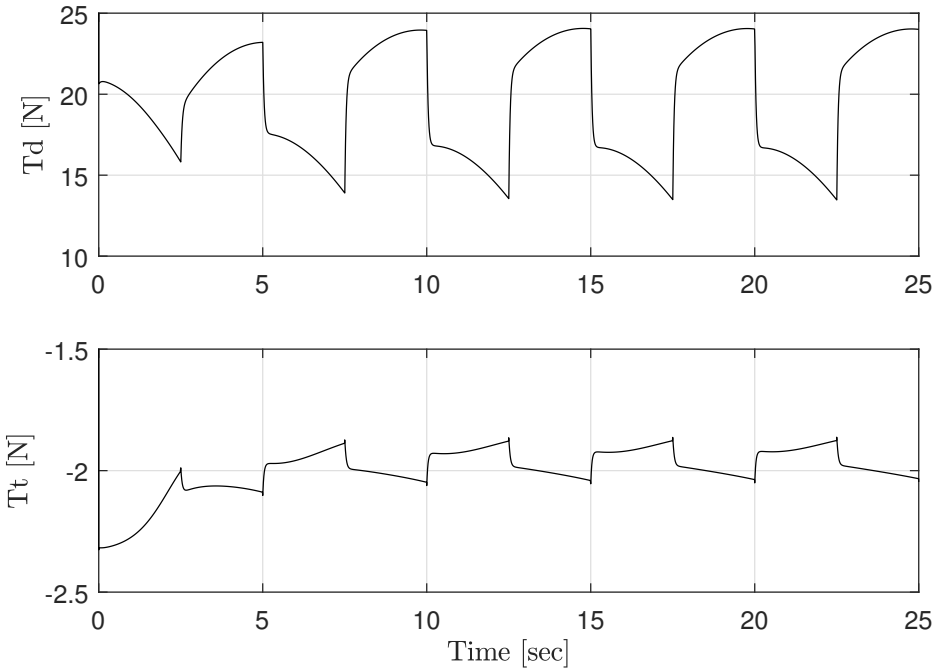

Figure 5.5: Thrust commands response to a tracking signal p_d.

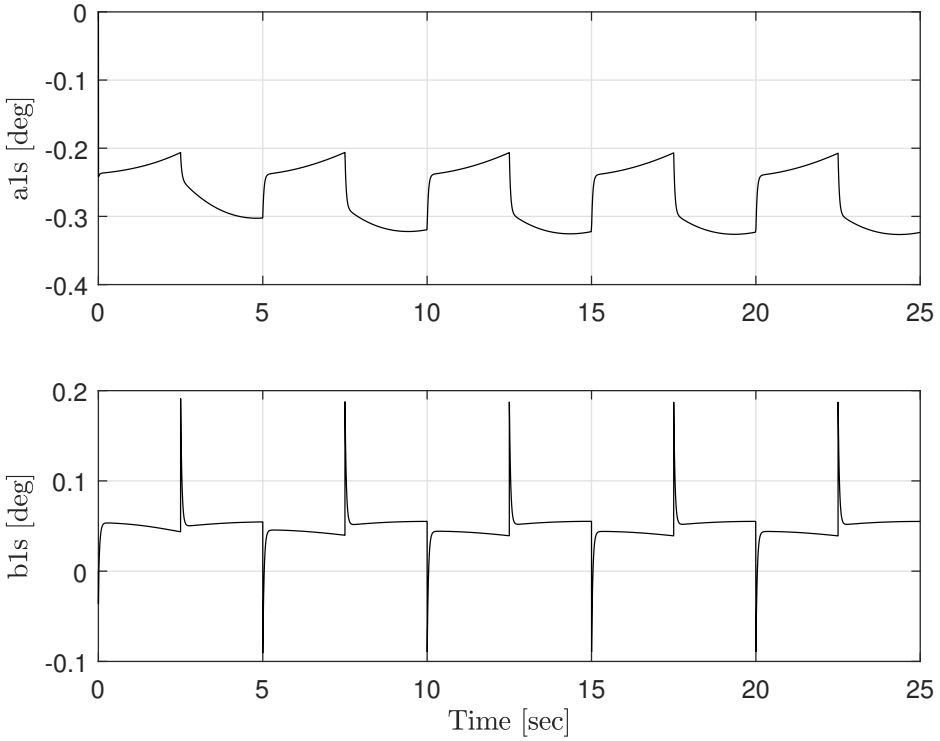

Figure 5.6: Flapping coefficients response to a tracking signal p_d.

The other simulation results are shown in Appendix B.1.

As can be seen, the system acts as a high frequency first order system and there are not saturations of the commands.

5.4 Attitude angles controller

The state equations of slow circuit can be expressed as follows:

$$\begin{bmatrix} \dot{\phi} \\ \dot{\theta} \\ \dot{\psi} \end{bmatrix} = \begin{bmatrix} 0 \\ 0 \\ 0 \end{bmatrix} + \begin{bmatrix} 1 & \sin\phi\tan\theta & \cos\phi\tan\theta \\ 0 & \cos\phi & -\sin\phi \\ 0 & \dfrac{\sin\phi}{\cos\theta} & \dfrac{\cos\phi}{\cos\theta} \end{bmatrix} \begin{bmatrix} p \\ q \\ r \end{bmatrix} \tag{5.13}$$

Taking $\boldsymbol{h}$ as output to control:

$$\boldsymbol{h} = \begin{bmatrix} \phi \\ \theta \\ \psi \end{bmatrix} \tag{5.14}$$

the corresponding relative degree is $\{r_\phi, r_\theta, r_{psi}\} = \{1, 1, 1\}$.

The fictitious input signal used to linearize the model is v_{ang}:

$$v_{ang} = \begin{bmatrix} v_\phi \\ v_\theta \\ v_\psi \end{bmatrix} = \begin{bmatrix} K_\phi e_\phi \\ K_\theta e_\theta \\ K_\psi e_\psi \end{bmatrix} = \begin{bmatrix} K_\phi \cdot (\phi_d - \phi) \\ K_\theta \cdot (\theta_d - \theta) \\ K_\psi \cdot (\psi_d - \psi) \end{bmatrix} \tag{5.15}$$

The feedback gains, determined using pole-placement method, are :

$$\begin{bmatrix} K_\phi \\ K_\theta \\ K_\psi \end{bmatrix} = \begin{bmatrix} 15 \\ 15 \\ 15 \end{bmatrix} \tag{5.16}$$

A schematic representation of the controller is shown in Fig. 5.7.

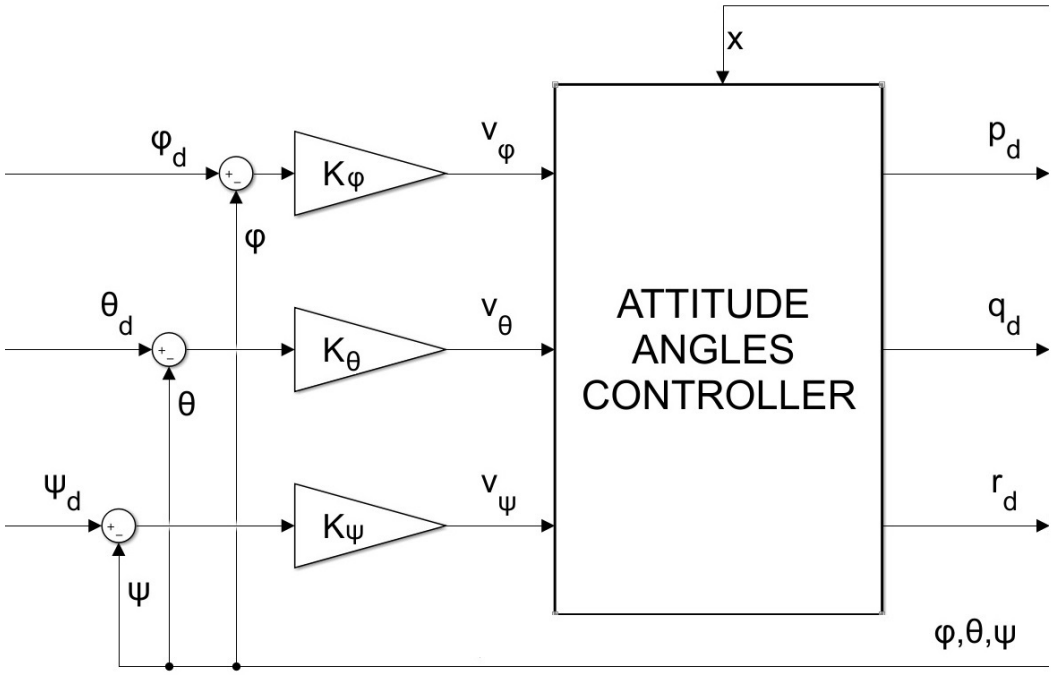

Figure 5.7: Sketch of slow controller.

5.4.1 Slow circuit simulation results

As has been done for the fast controller, some simulation tests have been performed even for the attitude angles controller.

The system was initialized in hovering condition and was exited by different tracking signals ϕ_d, θ_d and ψ_d.

For each simulation only one input channel at a time was excited by a non-zero signal. The input signal was a square wave with amplitude 40 deg, mean-value 0 deg and frequency 0.1 Hz. For each input channel, rate-limiters, with rising and falling rate of 0.35 rad/s, have been used to avoid instability problems.

Time responses to a tracking signal ϕ_d are shown in Fig. 5.8-5.10.

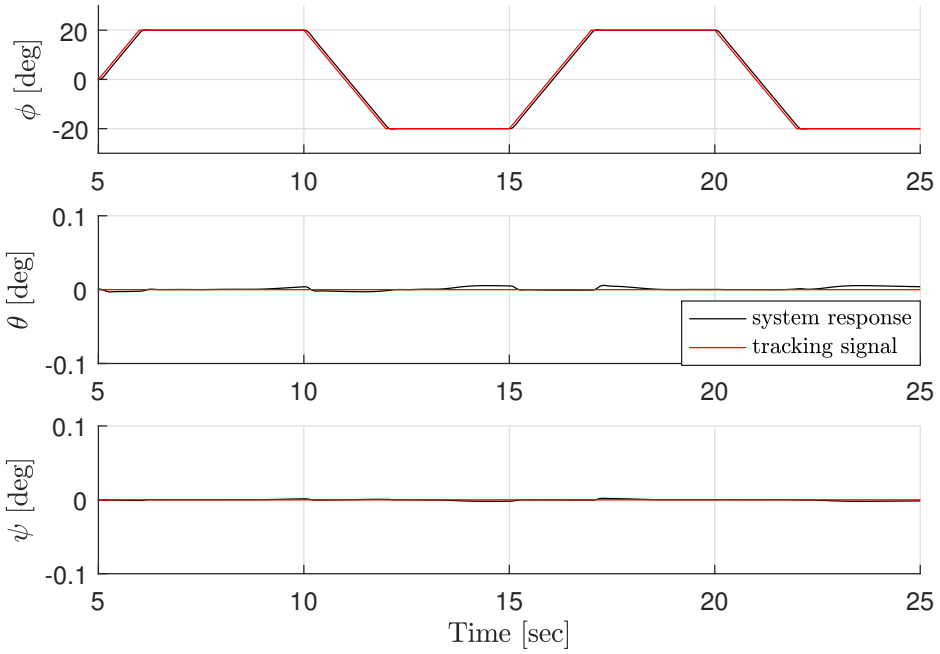

Figure 5.8: Angular response to a tracking signal ϕ_d.

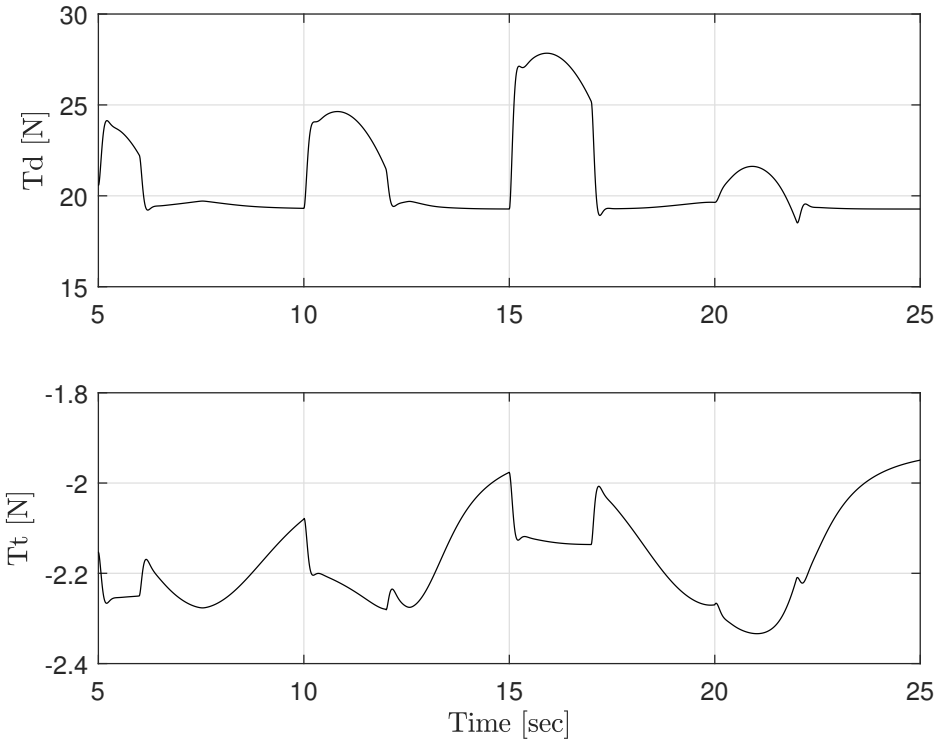

Figure 5.9: Thrust commands response to a tracking signal ϕ_d.

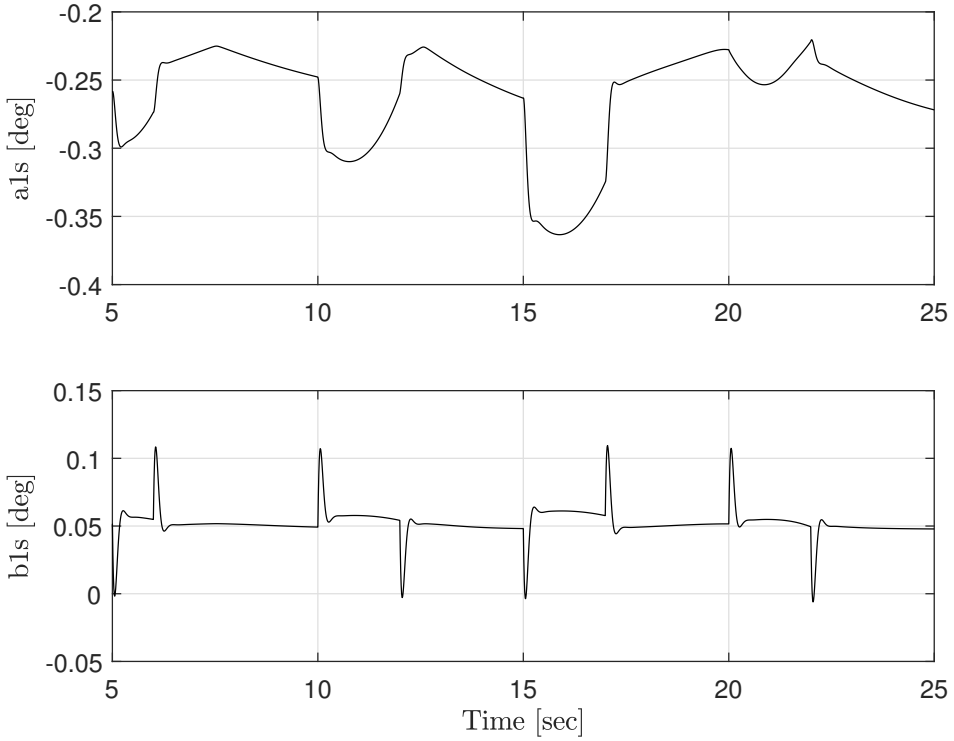

Figure 5.10: Flapping coefficients response to a tracking signal ϕ_d.

The other simulation results are shown in Appendix B.2.

5.5 Speed controller

The state equations of slower circuit can be expressed as follows:

$$\begin{bmatrix} \dot{U} \\ \dot{V} \end{bmatrix} = \begin{bmatrix} V \cdot r - W \cdot q - \dfrac{H_d}{m} - \dfrac{T_d \cdot a_1 s}{m} \\ \dfrac{T_t}{m} - \dfrac{T_d \cdot b_1 s}{m} + W \cdot p - U \cdot r \end{bmatrix} + \begin{bmatrix} g \cdot \sin\theta \\ g \cdot \cos\theta \sin\phi \end{bmatrix} \tag{5.17}$$

As can be seen, the Eq. (5.17) is not in the form of the Eq. (5.1). As shown above, in order to enable the dynamic inversion linearization, it is necessary to dynamically extend the model through the introduction of two integrator.

The state equation of the controller become:

$$\begin{bmatrix} \dot{U} \\ \dot{V} \\ \dot{\phi} \\ \dot{\theta} \end{bmatrix} = \begin{bmatrix} V \cdot r - W \cdot q - \dfrac{H_d}{m} - \dfrac{T_d \cdot a_1 s}{m} + g \cdot \sin\theta \\ W \cdot p - U \cdot r + \dfrac{T_t}{m} - \dfrac{T_d \cdot b_1 s}{m} + g \cdot \cos\theta \sin\phi \\ 0 \\ 0 \end{bmatrix} + \begin{bmatrix} 0 & 0 \\ 0 & 0 \\ 1 & 0 \\ 0 & 1 \end{bmatrix} \begin{bmatrix} \dot{\phi} \\ \dot{\theta} \end{bmatrix} \tag{5.18}$$

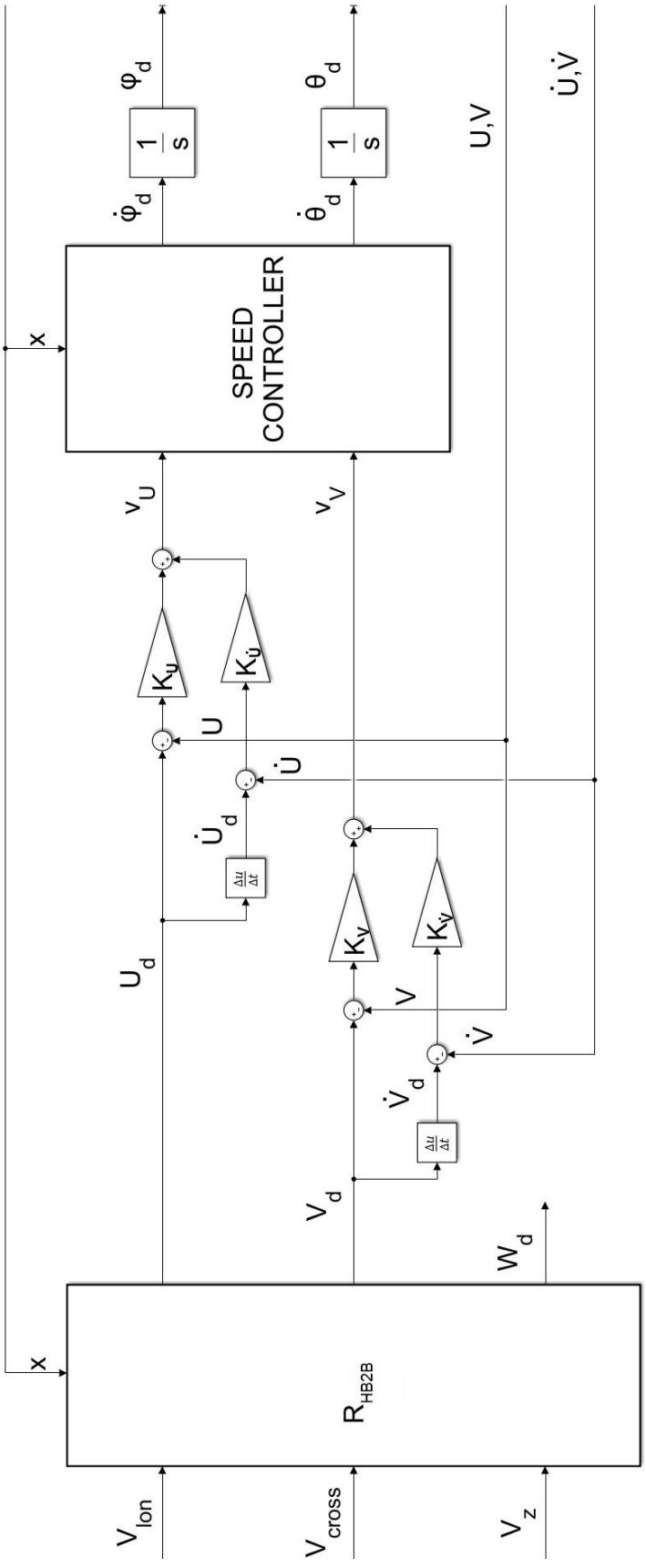

Figure 5.11: Sketch of slower controller.

Taking $\boldsymbol{h}$ as output to control:

$$\boldsymbol{h} = \begin{bmatrix} U \\ V \end{bmatrix} \tag{5.19}$$

the corresponding relative degree is $\{r_U, r_V\} = \{2, 2\}$.

The fictitious input signal used to linearize the model is v_{speed}:

$$v_{speed} = \begin{bmatrix} v_U \\ v_V \end{bmatrix} = \begin{bmatrix} K_U e_U + K_{\dot{U}} \dot{e}_U \\ K_V e_U + K_{\dot{V}} \dot{e}_V \end{bmatrix} = \begin{bmatrix} K_U \cdot (U_d - U) + K_{\dot{U}} \cdot \left(\dot{U}_d - \dot{U}\right) \\ K_V \cdot (V_d - V) + K_{\dot{V}} \cdot \left(\dot{V}_d - \dot{V}\right) \end{bmatrix} \tag{5.20}$$

The feedback gains, determined using pole-placement method, are:

$$\begin{bmatrix} K_U \\ K_{\dot{U}} \\ K_V \\ K_{\dot{V}} \end{bmatrix} = \begin{bmatrix} 0.3 \\ 3 \\ 0.3 \\ 3 \end{bmatrix} \tag{5.21}$$

As anticipated in Chapter 3 the controller must be developed in order to have as inputs the velocities in the horizontal-body reference system: V_{lon}, V_{cross} and V_z.

Having said that, the corresponding schematic representation of the controller is shown in Fig. 5.11.

5.5.1 Slower circuit simulation results

Even for the slower controller, some simulation test have been created.

The system was initialized in hovering condition and was excited by different tracking signals V_{lon}, V_{cross} and V_z.

For each simulation only one input channel at a time was excited by a non-zero signal. For V_{lon} and V_{cross} the input signal was a square wave with amplitude 20 m/s, mean-value 0 m/s and frequency $0.0\overline{3}$ Hz. For V_z the input signal was a square wave with amplitude 13 m/s, mean-value -3.5 m/s and frequency $0.0\overline{3}$ Hz.

For each input channel, rate-limiters, with rising and falling rate of $3\,m/s^2$,were used to avoid instability problems.

Time responses to a tracking signal V_{lon} are shown in Fig. 5.12-5.14.

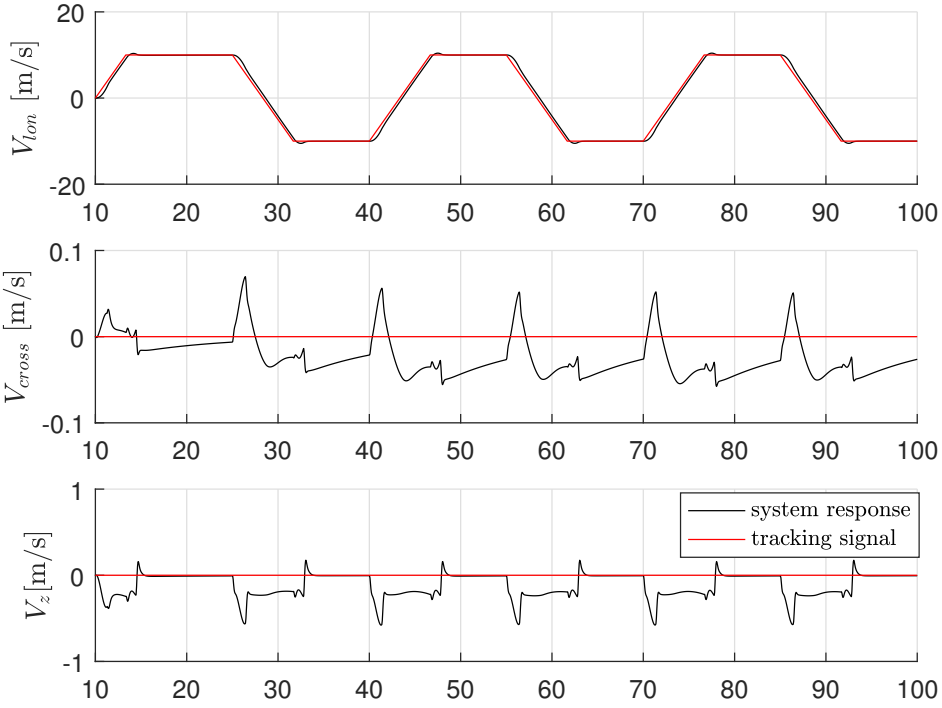

Figure 5.12: Speed response to a tracking signal V_{lon}.

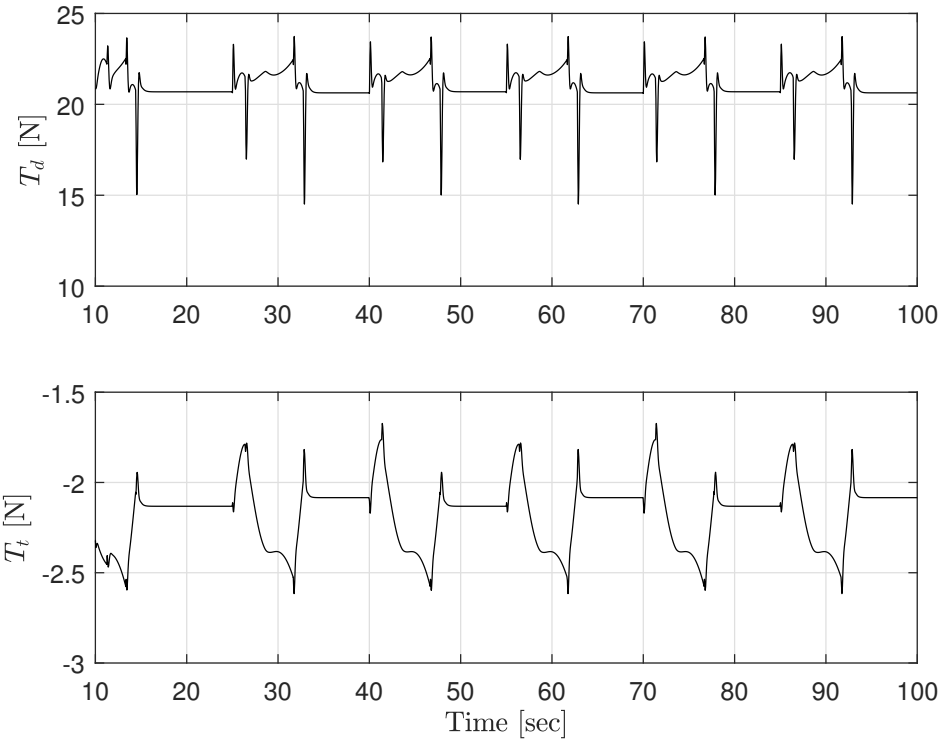

Figure 5.13: Thrust commands response to a tracking signal V_{lon}.

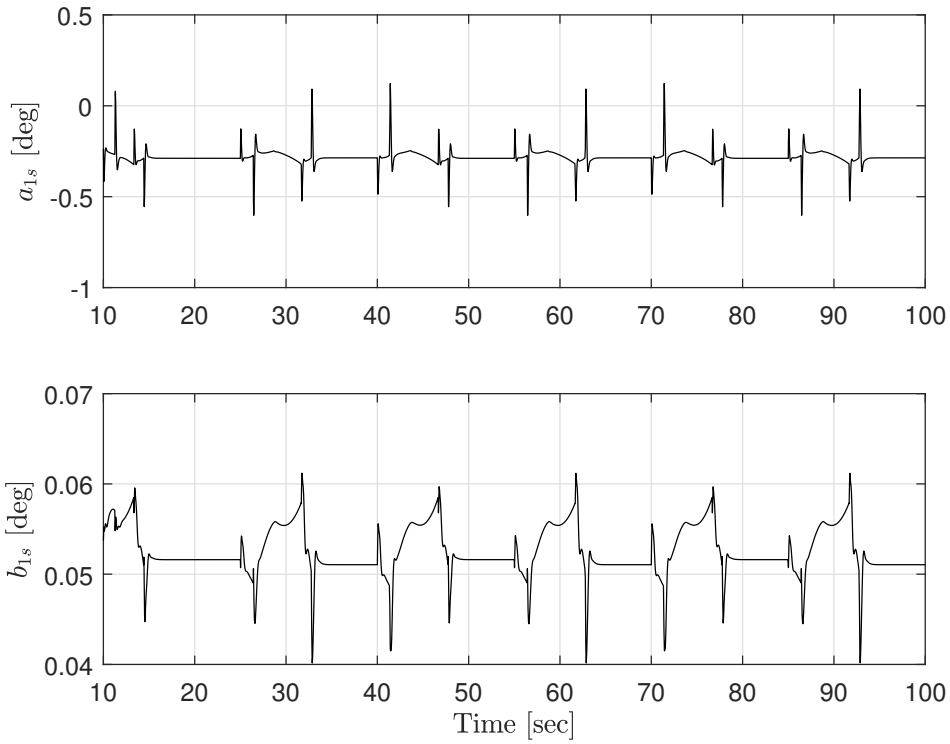

Figure 5.14: Flapping coefficients response to a tracking signal V_{lon}.

The other simulation results are shown in Appendix B.3.

The system act as an high damped second order system with maximum value of overshot of 10 per cent and asymptotic error almost zero; the coupling effects are very small so the zero signals are followed pretty well.

5.6 Flapping and actuator's dynamics reintroduction

Now that the structure of the controller has been defined it is necessary to reintroduce the part of the dynamic model that was neglected at first step.

In order to get a link between the required values of T_d, a_{1s}, b_{1s}, T_t and the corresponding values of θ_0, A_1, B_1, θ_t the command's effects have been considered instantaneous. According this approximation, the rotor and flybar dynamic model was inverted taking into consideration only the zero-order dynamic equations and neglecting every transient response.

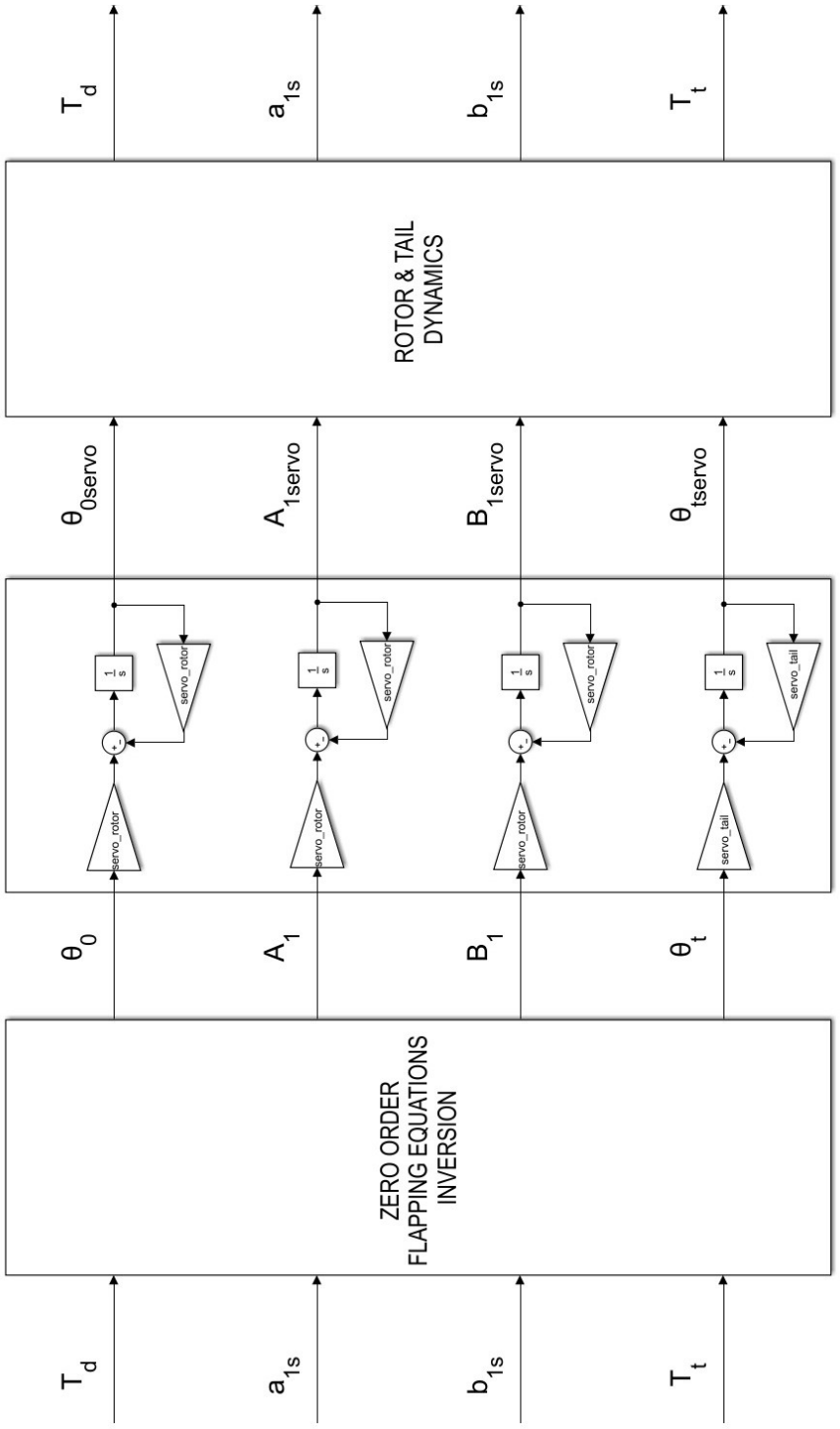

Figure 5.15: Sketch of reintroduced dynamics.

Mathematically, it is necessary to invert the Eqs. 5.22-5.24:

$$T_d = f(\theta_0, U, V, W) \tag{5.22}$$

$$\boldsymbol{K}\begin{bmatrix} a_{1s} \\ b_{1s} \end{bmatrix} = \boldsymbol{f}_{comm}\begin{bmatrix} A_{1corr} \\ B_{1corr} \end{bmatrix} + \boldsymbol{f}_{ang}\begin{bmatrix} p_w \\ q_w \\ \dot{p}_w \\ \dot{q}_w \end{bmatrix} + \boldsymbol{f}_{\lambda}\begin{bmatrix} \lambda \\ \lambda_i \end{bmatrix} \tag{5.23}$$

$$T_t = f(\theta_t, V, \mu, p, q) \tag{5.24}$$

Finally the actuator's dynamics has also been introduced, as shown in Fig. 5.15.

As can be seen the actuators have a dynamic of the first order with:

$$\begin{cases} servo_{rotor} = 33 \\ servo_{tail} = 50 \end{cases} \tag{5.25}$$

Furthermore the gains of the controller have been reformulated:

$$\begin{bmatrix} K_p \\ K_q \\ K_r \\ K_W \\ K_\phi \\ K_\theta \\ K_\psi \\ K_U \\ K_{\dot{U}} \\ K_V \\ K_{\dot{V}} \end{bmatrix} = \begin{bmatrix} 30 \\ 30 \\ 20 \\ 10 \\ 25 \\ 15 \\ 10 \\ 1 \\ 1.5 \\ 0.3 \\ 1.5 \end{bmatrix} \tag{5.26}$$

5.6.1 Complete model simulation results

The complete model has been tested with the same simulation tests used in section 5.5.1.

Time responses to a tracking signal V_{lon} are shown in Fig. 5.16-5.18.

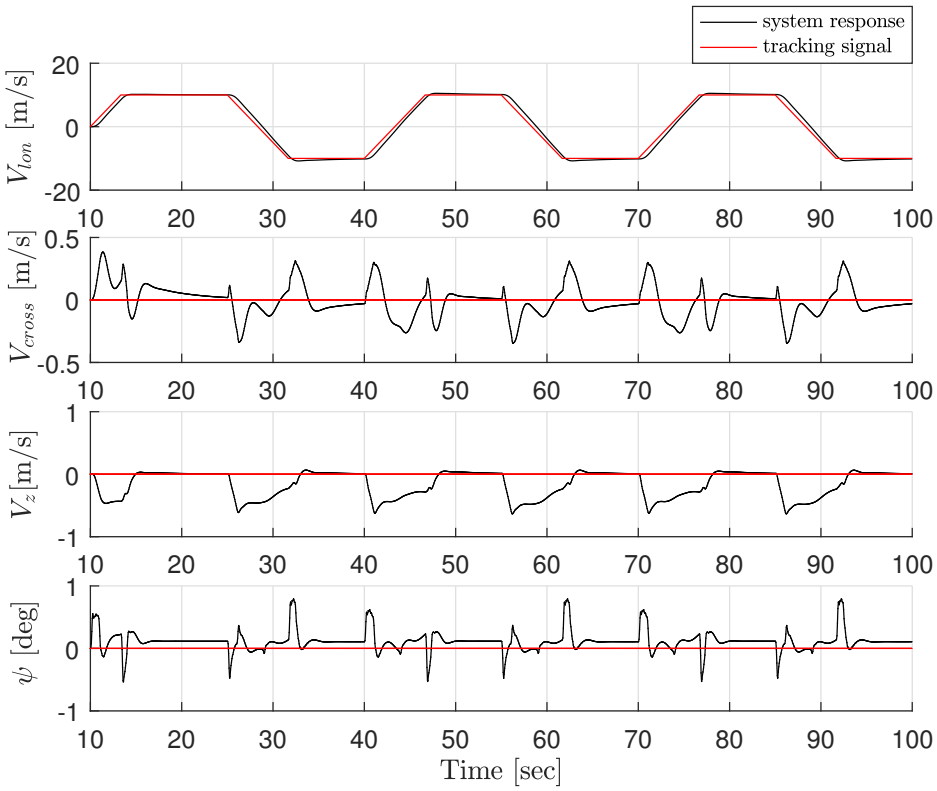

Figure 5.16: Speed response to a tracking signal in V_{lon}.

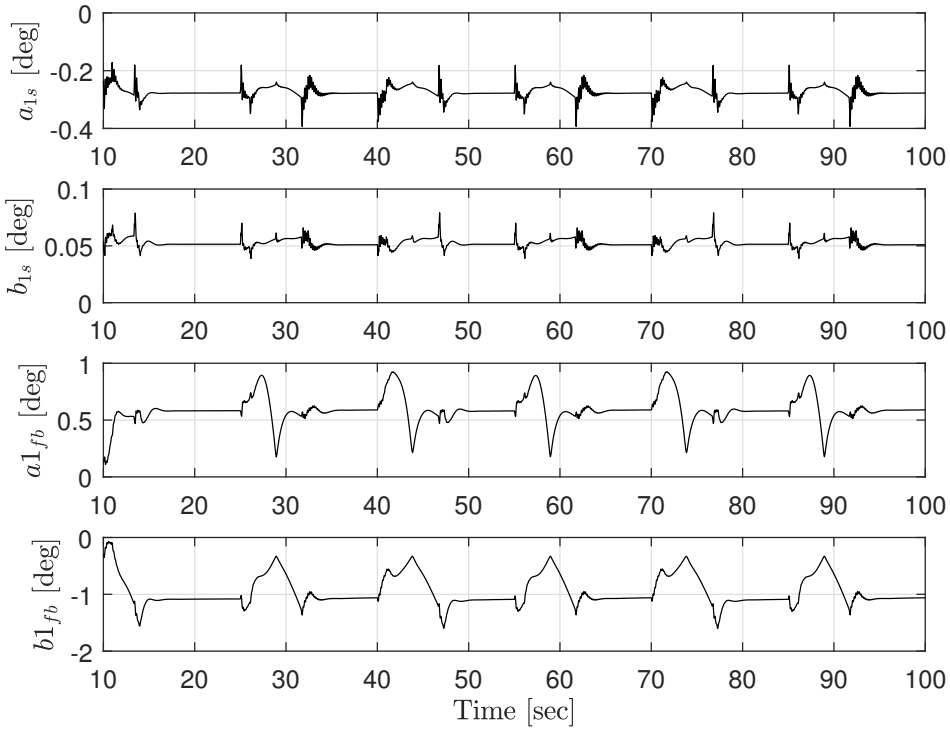

Figure 5.17: Flapping coefficients response to a tracking signal V_{lon}.

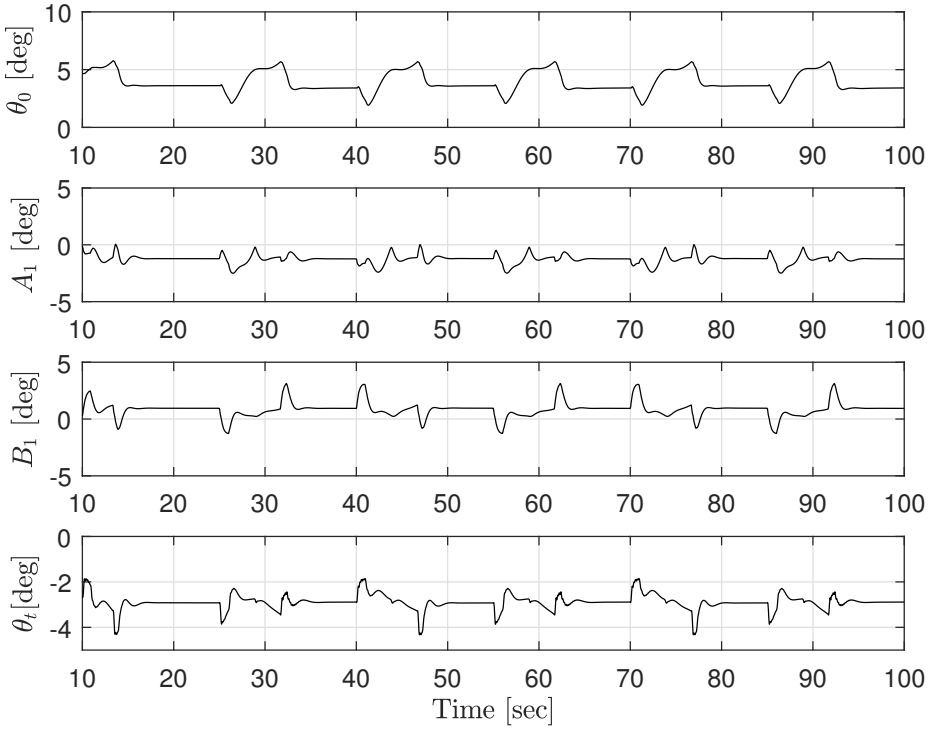

Figure 5.18: Pitching coefficients response to a tracking signal V_{lon}.

The other simulation results are shown in Appendix B.4.

The system acts as an high damped second order system with maximum value of overshot of 15 per cent and asymptotic error almost zero; in this case the coupling effects, between lateral and longitudinal dynamics, and between flapping and rigid body dynamics, are stronger so the zero-signals tracking is less accurate.

5.7 Validation simulation

In order to test the effective capability of the controller the dynamic model was excited by a realistic command sequence.

As can be seen, although we have asked values of velocity at the limit of the allowable operating range of the machine, collective and cyclic pitch angles do not have any saturation.

In Fig. 5.19-5.21 are shown the response to this command sequence.

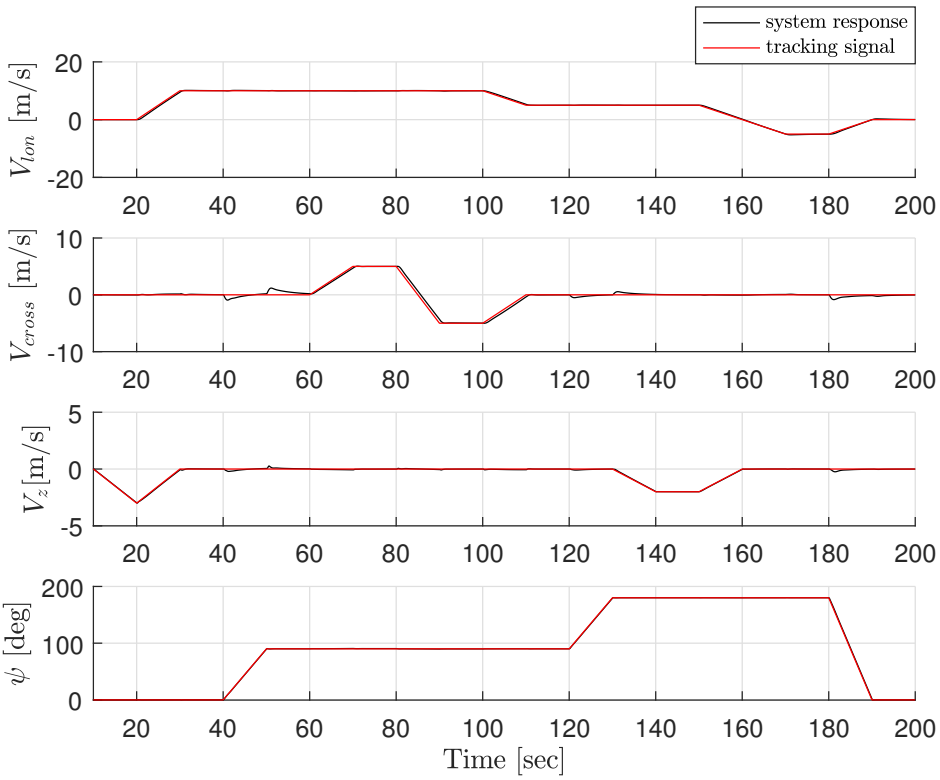

Figure 5.19: Speed response to the tracking signal.

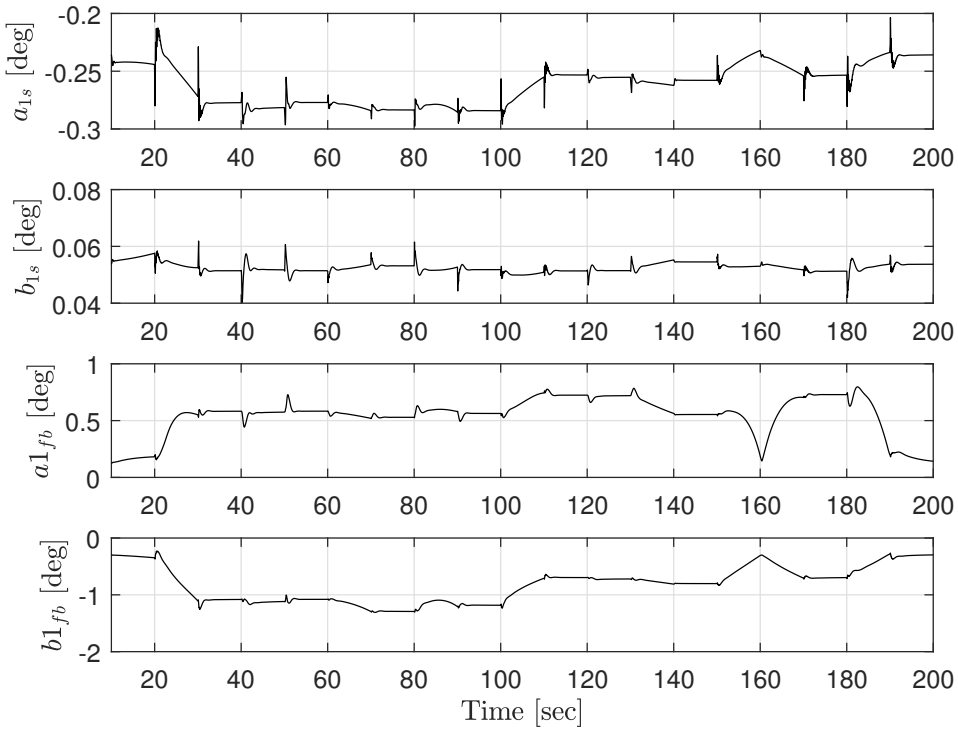

Figure 5.20: Flapping coefficients response to the tracking signal.

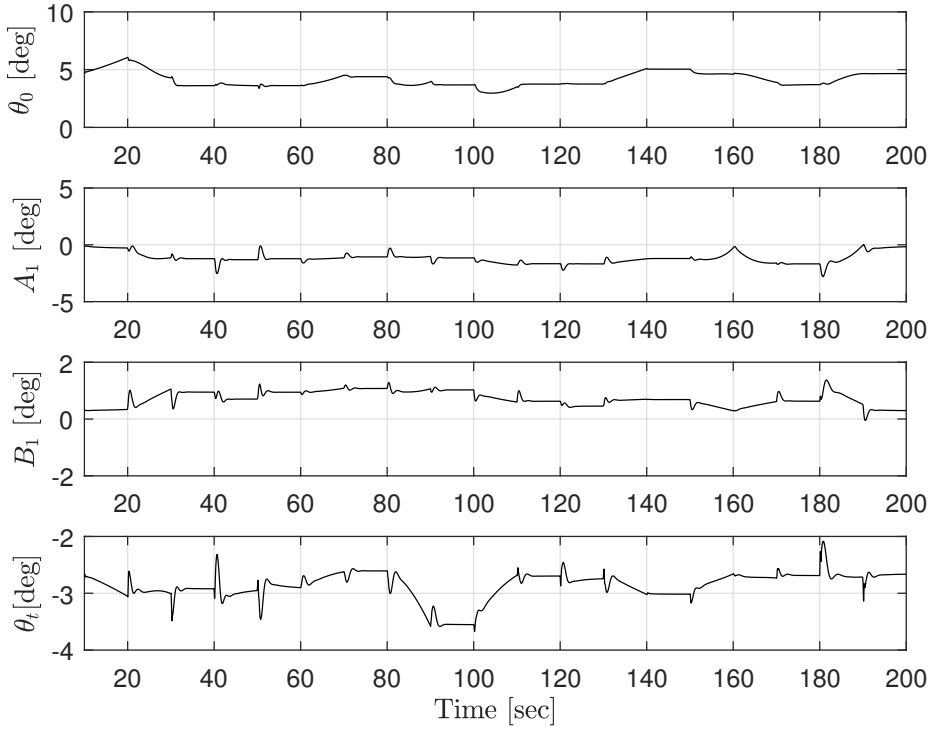

Figure 5.21: Pitching coefficients response to the tracking signal.

5.8 Hovering Controller

The state equations of Hovering controller can be expressed as follows:

$$\begin{bmatrix} \dot{x} \\ \dot{y} \\ \dot{z} \end{bmatrix} = \begin{bmatrix} 0 \\ 0 \\ 0 \end{bmatrix} + \boldsymbol{R}_{BV} \begin{bmatrix} U \\ V \\ W \end{bmatrix} \tag{5.27}$$

where:

$$\boldsymbol{R}_{BV} = \begin{bmatrix} \cos\theta\cos\psi & \sin\phi\sin\theta\cos\psi - \cos\phi\sin\psi & \cos\phi\sin\theta\cos\psi + \sin\phi\sin\psi \\ \cos\theta\sin\psi & \sin\phi\sin\theta\sin\psi + \cos\phi\cos\psi & \cos\phi\sin\theta\sin\psi - \sin\phi\cos\psi \\ \sin\theta & -\sin\phi\cos\theta & -\cos\phi\cos\theta \end{bmatrix} \tag{5.28}$$

The minus sign in the last row of the rotation matrix is due to the fact that the z axis points upwards.

Taking $\boldsymbol{h}$ as output to control:

$$\boldsymbol{h} = \begin{bmatrix} x \\ y \\ z \end{bmatrix} \tag{5.29}$$

the corresponding relative degree is $\{r_x, r_y, r_z\} = \{1, 1, 1\}$.

The fictitious input signal used to linearize the model is v_{pos}:

$$v_{pos} = \begin{bmatrix} v_x \\ v_y \\ v_z \end{bmatrix} = \begin{bmatrix} K_x e_x \\ K_y e_y \\ K_z e_z \end{bmatrix} = \begin{bmatrix} K_x \cdot (x_d - x) \\ K_y \cdot (y_d - y) \\ K_z \cdot (z_d - z) \end{bmatrix} \tag{5.30}$$

The feedback gains, determined using pole-placement method, are :

$$\begin{bmatrix} K_x \\ K_y \\ K_z \end{bmatrix} = \begin{bmatrix} 0.5 \\ 0.5 \\ 3 \end{bmatrix} \tag{5.31}$$

A schematic representation of the controller is shown in Fig. 5.22.

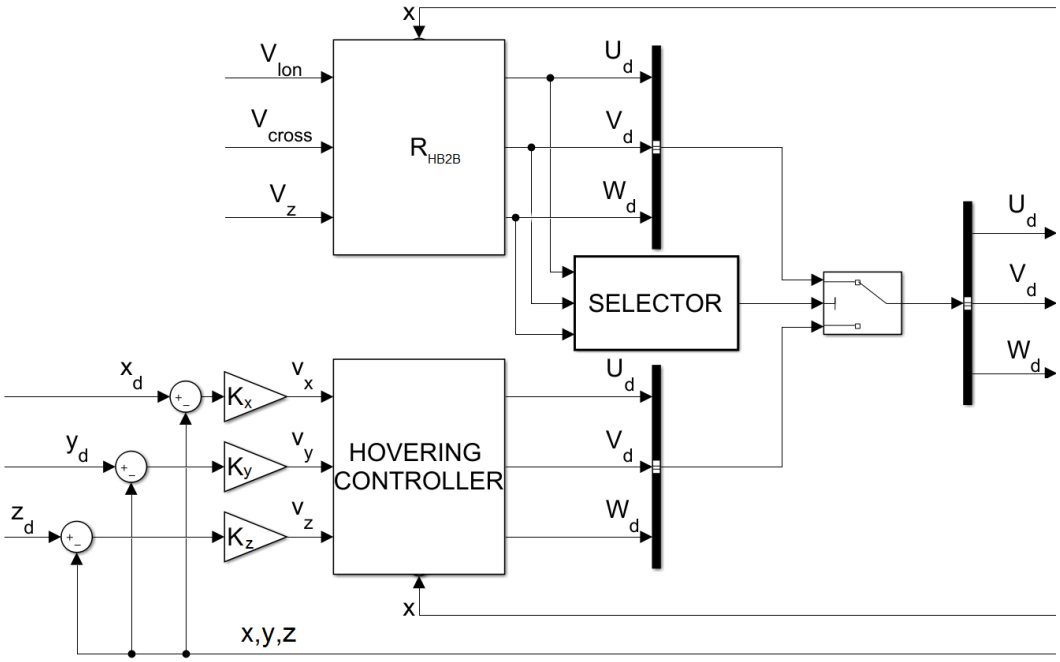

Figure 5.22: Sketch of hovering controller.

If there are not velocity inputs the controller switches automatically in hovering mode and it retains the helicopter position countering any external input.

5.8.1 Hovering controller simulation results

In order to test the controller capabilities, the helicopter has to keep the zero position while it is perturbed by an external gust in V_{lon} and V_{cross}.

The results of this simulation are shown in Fig. 5.23-5.25.

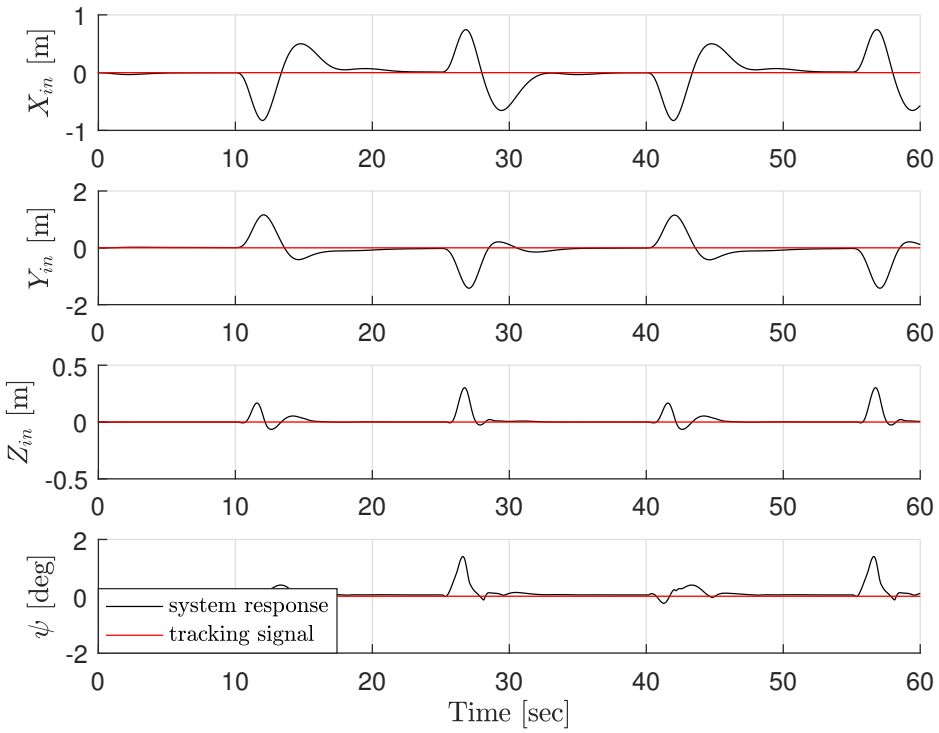

Figure 5.23: Position and ψ.

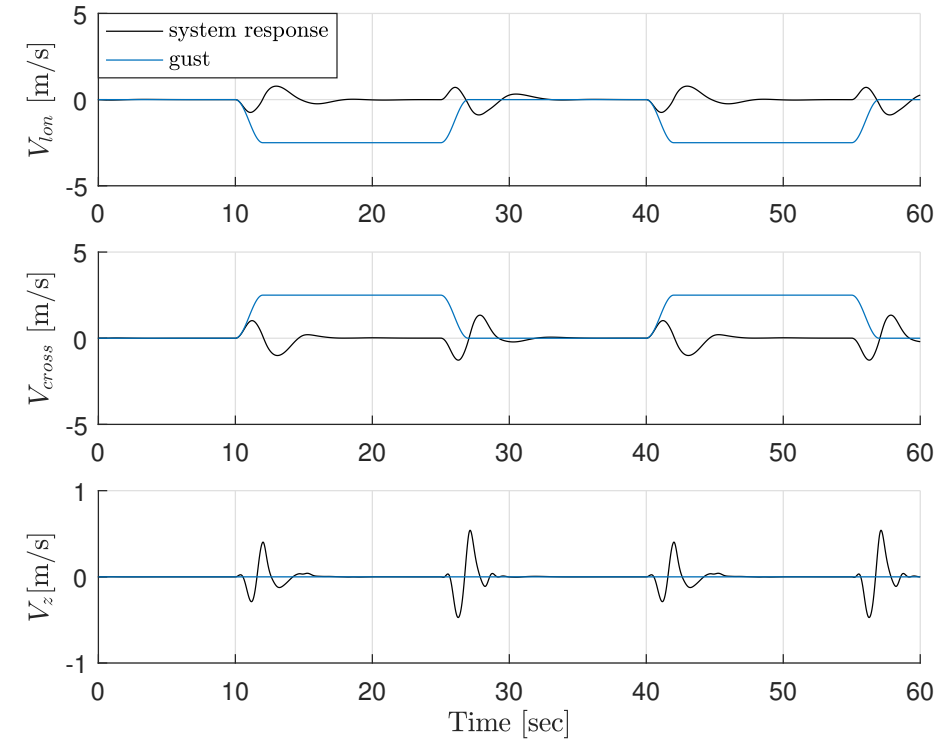

Figure 5.24: Velocities.

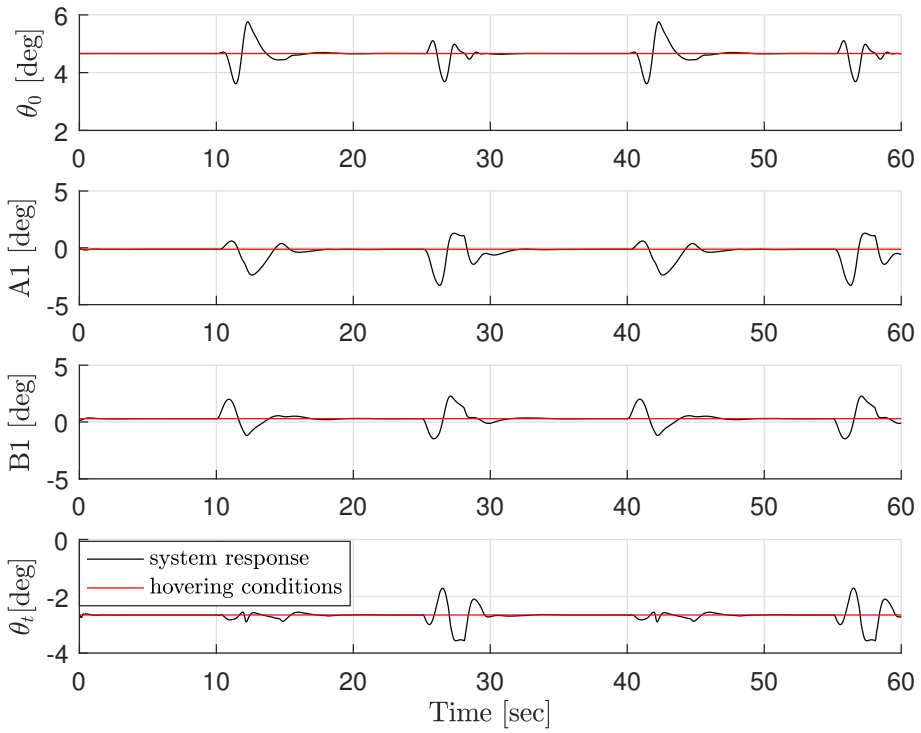

Figure 5.25: Command coefficients.

As can be seen the setting time, considering a threshold of $\pm 0.1\,\mathrm{m}$ around reference position, is less then 10 s.

In section B.5 is shown the response to a vertical gust.

Furthermore in Appendix C it is shown an analysis on the robustness of the controller.

As can be seen from the simulation results the controller is very robust in the following of speed references and the hovering maintenance. Only the estimation of the asymptotic value of ψ is affected by an observable error that can be removed introducing an integral effect on the ψ controller.

Conclusions and future works

The key point of this work has been the development of a controller for the automatic flight, based on a feedback linearization procedure.

The work on the search for trim and the following phase of linearization it was very useful for the understanding of the helicopter dynamics and for the realization of the cascade controller.Its main results were:

- there is a good agreement, concerning the trim, between the non-linear model, developed by our team, and the model coming from literature [2];
- following the application of a command, there is a fast divergence between the response of the linearized system and the non linear one;
- the helicopter dynamic behavior can be divided in different frequency ranges;
- there is an high level of coupling between the longitudinal dynamics and the lateral dynamics;
- there is an high level of coupling between the rigid body dynamics and the lateral dynamics;
- back position of the centre of gravity, relative to the shaft, compromises the controllability of the helicopter using control laws based on the linearized system.

According to these results a control method based on the feedback linearization is a good choice for a number of reasons. Compared to a conventional linearization procedure the feedback linearization is more versatile because it is not necessary to study the control laws around trim conditions but controller suits all flight conditions. The lateral and the longitudinal dynamics can be controlled simultaneously. Furthermore it is not necessary the rebalancing of the helicopter weight.

The application of the input-output exact feedback linearization procedure has not led to satisfactory results due to the generation of a set of unobservable states that prevented the stabilization of the system. Therefore it was necessary to use a procedure of feedback linearization based on a time scale separation approximation.

This procedure, called dynamic inversion linearization, has allowed us to build a controller in cascade, acting separately on the fast, middle and low frequencies.

The implementation of this controller has provided good resuts: the responses to a tracking signal in velocities and yaw angle ψ show a short settling time, a little value of maximum overshoot (max. 20 per cent), an high level of damping and an asymptotic error almost zero, both for high and little values of the tracking signal.

The good results given from this work can be increased in the environment of this research, so the future developments will be:

- implementation of the controller in the FCC and validation of its capabilities trough flight tests;
- development of the control laws for the takeoff and landing phases to allow to the T-Rex to perform autonomous missions entirely and not only for the cruise phase.

The last step will be the substitution of the pilot whit a FMS that carries out the mission in autonomous mode.

Part III

Appendix

Appendix A

Blade and Flybar flapping equation

A.1 Introduction

The following analysis (made with the aid a previous thesis [1]), has been made to obtain a differential equation for blade flapping simulation. The analysis includes a study of the steady-state flapping response with respect to control inputs.
The flapping equation of motion was derived explicitly for a two-blade rotor, with hinge offset e, blade Lock number γ and stiffness of the flapping hinge K_β.

To develop analytic expressions, the following simplification and assumptions have been used:

- Rotor blade is rigid in bending and torsion, with no twist (see Fig. A.1); it can be considered a symmetric body (the shape of the airfoils give a negligible contribute to centrifugal moments of inertia), so its inertia tensor is a diagonal matrix;
- Drag coefficient δ and lift coefficient a of airfoil are independent of local blade angle of attack (mean values have been considered);
- Both the flapping angle and the inflow angle were assumed to be small (i.e. low ratio T/A and high blade aspect ratio) and this analysis uses simple Glauert theory;
- Lead-lag motion negligible: lead-lag dynamics, which is the result of Coriolis forces induced by flapping motion, produce smaller forces on the hub than flapping motion, and they will be ignored.
- The effects of the helicopter dynamic on the blade flapping were limited to those due to the angular accelerations $\dot{p}$ and $\dot{q}$, the angular rates p and q, z-axis acceleration $\dot{w}$ and translation velocities u and v;
- The reversed flow region was ignored, as the compressibility and stall effects;
- The inflow was assumed to vary according the Glauert theory:

$$v_i = v_{i0} \cdot (1 + K_{iv} x \cos\psi) \tag{A.1}$$

- Inflow dynamic was used according to Pitt-Peters model [9]: effects on flapping dynamics are negligible and computational effort is high, so it will not be considered any more;
- The *tip loss factor* was assumed to be 1; *root-cutout effect* is neglected;

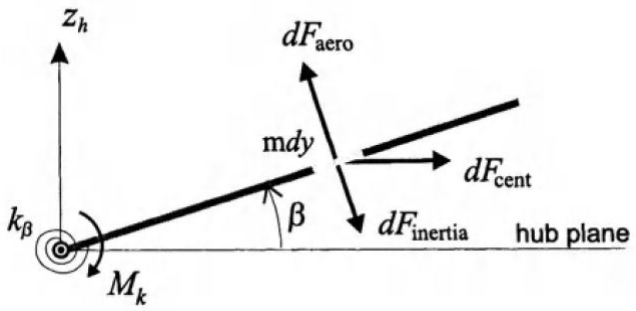

Figure A.1: Blade simplified representation.

Because of these assumptions, the results of this analysis are valid only in a limited range of conditions; however it can be demonstrated that these results are usually valid for rotorcraft simulation up to an advance ratio μ of 0.2.

A.2 Derivation of flapping equation

Referring to local blade reference system, the angular velocity of the blade during motion can be expressed as:

$$\boldsymbol{\Omega} = \boldsymbol{R}_{hb2loc} \begin{bmatrix} p \\ q \\ r + \Omega \end{bmatrix} + \begin{bmatrix} -\dot{\theta}_{bl} \\ -\dot{\beta} \\ 0 \end{bmatrix} \tag{A.2}$$

where:

$$\boldsymbol{R}_{hb2loc} = \begin{bmatrix} R_{11} & R_{12} & R_{13} \\ R_{21} & R_{22} & R_{23} \\ R_{31} & R_{32} & R_{33} \end{bmatrix} \tag{A.3}$$

where:

$$\begin{aligned}
R_{11} &= -\cos\psi\cos\beta \\
R_{12} &= -\sin\psi\cos\beta \\
R_{13} &= -\sin\beta \\
R_{21} &= -\sin\beta\sin\theta_{bl}\cos\psi - \cos\theta_{bl}\sin\psi \\
R_{22} &= -\sin\beta\sin\theta_{bl}\sin\psi + \cos\theta_{bl}\cos\psi \\
R_{23} &= \cos\beta\sin\theta_{bl} \\
R_{31} &= \sin\beta\cos\theta_{bl}\cos\psi - \sin\theta_{bl}\sin\psi \\
R_{32} &= \sin\beta\cos\theta_{bl}\sin\psi + \sin\theta_{bl}\cos\psi \\
R_{33} &= -\cos\beta\cos\theta_{bl}
\end{aligned}$$

The absolute angular momentum is:

$$\boldsymbol{K}_O = \begin{bmatrix} A & 0 & 0 \\ 0 & B & 0 \\ 0 & 0 & C \end{bmatrix} \left[-\boldsymbol{\Omega}\right] - m_{bl}\boldsymbol{OG} \times \boldsymbol{v}_O \tag{A.4}$$

The Euler's equations for blade dynamics are, generally:

$$\dot{\boldsymbol{K}}_O = \boldsymbol{M}_O + \boldsymbol{\Psi}_O + \boldsymbol{Q} \times \boldsymbol{v}_O \tag{A.5}$$

Extracting the component according the j-axis, supposing that angles are small and neglecting second order terms, we obtain the differential equation for blade flapping:

$$\begin{aligned} \ddot{\beta} + \left[\frac{K_\beta}{B} + \Omega^2\left(1 + \frac{m_{bl}x_g eR}{B}\right)\right]\beta = -\dot{p}\sin\psi + \dot{q}\cos\psi + \\ - 2\Omega(q\sin\psi + p\cos\psi)\cdot\left(1 + \frac{m_{bl}x_g eR}{B}\right) + \\ + \frac{m_{bl}x_g}{B}(\dot{w} - uq + pv - g) + \boldsymbol{M}_A/B \cdot \boldsymbol{j} \end{aligned} \tag{A.6}$$

Before being able to calculate the forces and moments on the blade, it is necessary to know the velocity components of the air relative to the blade. The blade will be assumed to be a rigid beam with an elastic flapping hinge, and only simplified theories about induced velocity and airfoil characteristic will be used. For the calculation of the aerodynamic moment, it is sufficient to assume that the flapping hinge offset e is zero. The only velocity component affected by the flapping hinge offset is that due to blade flapping, but, since e is only 4% of the blade radius, the error is negligible. Henceforth, refer to an auxiliary hub-plane reference system $\tau'_{HP}(x'_{HP}, y'_{HP}, z'_{HP})$, wherein axis z'_{HP} is coincide with z_{HP} and plane $x'_{HP} - y'_{HP}$ contains the helicopter velocity vector $\boldsymbol{V}$. Neglecting the spanwise component of air velocity, it is usual to denote as U_T the velocity component that is tangential to axis x'_{HP}, positive when blows from front to back, and U_P the component along axis z'_{HP}, positive when blows from wing underside to the upper surface (Fig. A.2):

$$U_T = \Omega r + V\cos\alpha_{HP}\sin\psi \tag{A.7}$$

$$U_P = V\sin\alpha_{HP} - V\cos\alpha_{HP}\beta\cos\psi - r\dot{\beta} - v_i - p_w \cdot r\sin\psi + q_w \cdot r\cos\psi \tag{A.8}$$

where:

$$V = \sqrt{u^2 + v^2 + w^2} \tag{A.9}$$

$$p_w = p\cos\beta_w + q\sin\beta_w \tag{A.10}$$

$$q_w = -p\sin\beta_w + q\cos\beta_w \tag{A.11}$$

Defining:

$$\lambda' = (V\sin\alpha_{HP} - v_i)/\Omega R \tag{A.12}$$

$$\mu = (V\cos\alpha_{HP})/\Omega R \tag{A.13}$$

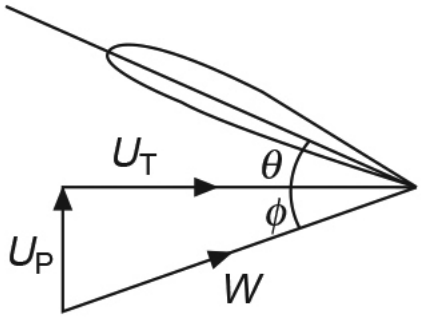

Figure A.2: Velocity components at a blade section.

$$u_T = U_T/\Omega R \tag{A.14}$$

and

$$u_P = U_P/\Omega R \quad , \tag{A.15}$$

equation(A.7) and equation(A.8) can be rewritten as:

$$u_T = x + \mu \sin\psi \tag{A.16}$$

$$u_P = \lambda - \mu\beta\cos\psi - x\frac{d\beta}{d\psi} - \frac{v_i}{\Omega R} + \frac{q_w}{\Omega}x\cos\psi - \frac{p_w}{\Omega}x\sin\psi \tag{A.17}$$

The induced velocity v_i is assumed to vary accordingly Glauert's formula,

$$v_i = v_{i0}\cdot(1 + K_{iv}x\cos\psi) \tag{A.18}$$

where v_{i0} is the induced velocity at the rotor center (disk actuator theory), $x = r/R$ and K_{iv} is the induced velocity coefficient, according to Payne (1959, [10] and [11]):

$$K_{iv} = \frac{4}{3}\frac{\mu/\lambda}{1.2 + \mu/\lambda} \tag{A.19}$$

In this, we assume that the expression (A.18) holds equally for the auxiliary hub plane as for the plane it actually applies to, which most nearly corresponds to the tip path plane. The blade pitch changes according the equation (A.20):

$$\theta = \theta_0 - A_1\cos\psi - B_1\sin\psi \tag{A.20}$$

The aerodynamic flapping moment dM_A about the hinge due to elementary lift (the moment due to airfoil drag is assumed to be negligible) is:

$$dM_A = \frac{1}{2}\rho a U_T^2\left(\theta + \frac{U_P}{U_T}\right)crdr \tag{A.21}$$

Substituting expressions for velocities, integrating and neglecting the terms containing e^3, e^4 and higher order, we obtain:

$$\begin{aligned} dM_A =& \frac{1}{2}\rho ac\Omega^2R^4\Bigg\{\left[\theta\mu^2\sin^2\psi + \mu\sin\psi\left(\lambda - \frac{v_i}{\Omega R} - \mu\beta\cos\psi\right)\right]x + \\ &+ \left[2\mu\sin\psi\theta + \mu\sin\psi\left(-\frac{d\beta}{d\psi} - \frac{p_w\sin\psi}{\Omega} + \frac{q_w\cos\psi}{\Omega}\right) + \lambda + \right. \\ &\left. - \frac{v_i}{\Omega R} - \mu\beta\cos\psi\right]x^2 + \left[\theta - \frac{d\beta}{d\psi} - \frac{p_w\sin\psi}{\Omega} + \frac{q_w\cos\psi}{\Omega}\right]x^3\Bigg\} \end{aligned} \tag{A.22}$$

Integrating and neglecting the terms of third and higher order the result is:

$$\begin{aligned} M_A =& \frac{1}{2}\rho a c \Omega^2 R^4 \Bigg\{ \mu \sin\psi \left[\theta \mu \sin\psi + \lambda - \lambda_{i0} - \mu\beta\cos\psi \right] \left(\frac{1}{2} - e + \frac{e^2}{2} \right) + \\ &+ \left[\mu \sin\psi \left(2\theta - \frac{d\beta}{d\psi} - \frac{p_w \sin\psi}{\Omega} + \frac{q_w \cos\psi}{\Omega} - \lambda_{i0} \cos\psi k_{iv} \right) + \right. \\ &\left. + \lambda - \lambda_{i0} - \mu\beta\cos\psi \right] \left(\frac{1}{3} + e^2 - e \right) + \left[\theta - \frac{d\beta}{d\psi} - \frac{p_w \sin\psi}{\Omega} + \right. \\ &\left. + \frac{q_w \cos\psi}{\Omega} - \lambda_{i0}\cos\psi k_{iv} \right] \left(\frac{1}{4} - e + \frac{3}{2}e^2 \right) \Bigg\} \end{aligned} \tag{A.23}$$

The aerodynamic moment M_A depends on the aero-mechanical parameters of the helicopter blade, as expected. Rearranging Eq. (A.6) and (A.23) one can obtain the differential equation of blade flapping and write it in a non dimensional form using the following expressions:

$$\ddot{\beta} = \frac{d^2\beta}{dt^2} = \Omega^2 \frac{d^2\beta}{d\psi^2} = \Omega^2 \cdot \bar{\bar{\beta}} \tag{A.24}$$

$$\dot{\beta} = \frac{d\beta}{dt} = \Omega \frac{d\beta}{d\psi} = \Omega \cdot \bar{\beta} \tag{A.25}$$

The result becomes:

$$\begin{aligned} &\bar{\bar{\beta}} + \frac{\gamma}{2}\left[\frac{1}{4} - e + \frac{3e^2}{2} + \left(\frac{1}{3} - e + e^2 \right) \mu \sin\psi \right] \bar{\beta} + \\ &+ \left\{ P^2 + \frac{\gamma}{2} \left[\frac{1}{3} + e^2 - e + \left(\frac{1}{2} - e + \frac{e^2}{2} \right) \mu \sin\psi \right] \right\} \beta = \\ &- \frac{\dot{p}_w}{\Omega^2}\sin\psi + \frac{\dot{q}_w}{\Omega^2}\cos\psi - 2\left(\frac{q_w}{\Omega}\sin\psi + \frac{p_w}{\Omega}\cos\psi \right) \left(1 + \frac{m_{bl} x_g e R}{B} \right) + \\ &+ \frac{m_{bl} x_g}{B\Omega^2}(\dot{w} - u q_w + p_w v - g) + \frac{\gamma}{2} \Bigg\{ \left[\frac{1}{4} - e + \frac{3e^2}{2} + \right. \\ &\left. + \mu \sin\psi \left(\frac{2}{3} + 2e^2 - 2e + \frac{1}{2}\mu \sin\psi \left(1 - 2e + e^2 \right) \right) \right] \theta + \\ &+ \lambda \left[\frac{1}{3} + e^2 - e + \mu \sin\psi \left(\frac{1}{2} - e + \frac{e^2}{2} \right) \right] - \lambda_{i0} \Bigg[\mu \sin\psi \left(\frac{1}{2} + \frac{e^2}{2} - e \right) + \\ &+ \frac{1}{3} + e^2 - e + \mu \sin\psi \cos\psi k_{iv} \left(\frac{1}{3} + e^2 - e \right) + \\ &+ \cos\psi k_{iv} \left(\frac{1}{4} - e + \frac{3e^2}{2} \right) \Bigg] + \\ &+ \left(\frac{-p_w \sin\psi + q_w \cos\psi}{\Omega} \right) \left[\mu \sin\psi \left(\frac{1}{3} + e^2 - e \right) + \frac{1}{4} - e + \frac{3e^2}{2} \right] \Bigg\} \end{aligned} \tag{A.26}$$

Equation(A.26) is a linear equation with periodic coefficients and there is not a solution in closed form. Moreover, it is valid only for the advancing region, since in the reverse flow area the lift and flapping moment are incorrectly evaluated: this is a negligible error, however.

A.3 Tip-path plane dynamics

A.3.1 Derivation of matrix-form equations

To obtain a simplified and more practical form of the equation for numerical simulation, the flapping is approximated by the first-harmonic terms with time varying coefficients, as in Eq. (A.27)

$$\beta(t) = a_0(t) - a_{1s}(t)\cos\psi - b_{1s}(t)\sin\psi \tag{A.27}$$

where $a_0(t)$, $a_{1s}(t)$ e $b_{1s}(t)$ are the blade flapping coefficients [12].

Remembering (A.20) and substituting in (A.26) can be obtained an equation in $\sin\psi$ and $\cos\psi$: developing these terms and considering only the first order harmonics the tip-path plane dynamic equation results:

$$\ddot{\boldsymbol{a}} + \Omega\ \boldsymbol{D}\ \dot{\boldsymbol{a}} + \Omega^2\ \boldsymbol{K}\ \boldsymbol{a} = \boldsymbol{f} \tag{A.28}$$

where $\boldsymbol{a}$ is the blade flapping state matrix, $\boldsymbol{D}$ is the damping matrix (A.30), $\boldsymbol{K}$ is the stiffness matrix (A.31) and $\boldsymbol{f}$ are the forcing terms (A.32), (A.33), (A.34) and (A.35).

$$\begin{bmatrix} \ddot{a}_0 \\ \ddot{a}_{1s} \\ \ddot{b}_{1s} \end{bmatrix} + \Omega \boldsymbol{D} \begin{bmatrix} \dot{a}_0 \\ \dot{a}_{1s} \\ \dot{b}_{1s} \end{bmatrix} + \Omega^2 \boldsymbol{K} \begin{bmatrix} a_0 \\ a_{1s} \\ b_{1s} \end{bmatrix} = \Omega^2 \boldsymbol{f}_{comm} \begin{bmatrix} \theta_0 \\ A_{1corr} \\ B_{1corr} \end{bmatrix} + \Omega^2 \boldsymbol{f}_{ang} \begin{bmatrix} p_w \\ q_w \\ \dot{p}_w \\ \dot{q}_w \end{bmatrix} + \Omega^2 \boldsymbol{f}_{\lambda} \begin{bmatrix} \lambda \\ \lambda_i \end{bmatrix} + \boldsymbol{f}_{misc} \tag{A.29}$$

where:

$$\boldsymbol{D} = \begin{bmatrix} \frac{\gamma}{2}\left(\frac{1}{4} - e + \frac{3e^2}{2}\right) & 0 & -\frac{\gamma}{4}\mu\left(\frac{1}{3} - e + e^2\right) \\ 0 & \frac{\gamma}{2}\left(\frac{1}{4} - e + \frac{3e^2}{2}\right) & 2 \\ -\frac{\gamma}{2}\mu\left(\frac{1}{3} - e + e^2\right) & -2 & \frac{\gamma}{2}\left(\frac{1}{4} - e + \frac{3e^2}{2}\right) \end{bmatrix} \tag{A.30}$$

$$\boldsymbol{K} = \begin{bmatrix} P^2 & 0 & 0 & \frac{\gamma}{2}\left(\frac{1}{4} - e + \frac{3e^2}{2}\right) + \frac{\gamma}{8}\mu^2\left(\frac{1}{2} - e + \frac{e^2}{2}\right) \\ -\frac{\gamma}{2}\mu\left(\frac{1}{3} + e^2 - e\right) & P^2 - 1 & -\frac{\gamma}{2}\left(\frac{1}{4} - e + \frac{3e^2}{2}\right) + \frac{\gamma}{8}\mu^2\left(\frac{1}{2} - e + \frac{e^2}{2}\right) & P^2 - 1 \end{bmatrix} \tag{A.31}$$

$$\boldsymbol{f}_{comm} = \begin{bmatrix} \frac{\gamma}{2}\left(\frac{1}{4} - e + \frac{3e^2}{2}\right) + \frac{\gamma}{4}\mu^2\left(\frac{1}{2} - e + \frac{e^2}{2}\right) & 0 & 0 & -\frac{\gamma}{2}\mu\left(\frac{1}{3} + e^2 - e\right) \\ 0 & \frac{\gamma}{2}\left(\frac{1}{4} - e + \frac{3e^2}{2}\right) + \frac{\gamma}{8}\mu^2\left(\frac{1}{2} - e + \frac{e^2}{2}\right) & 0 & 0 \\ -\frac{\gamma}{2}\mu\left(\frac{2}{3} - 2e + 2e^2\right) & 0 & \frac{\gamma}{2}\left(\frac{1}{4} - e + \frac{3e^2}{2}\right) + \frac{3\gamma}{8}\mu^2\left(\frac{1}{2} - e + \frac{e^2}{2}\right) & 0 \end{bmatrix} \tag{A.32}$$

$$\boldsymbol{f}_{ang} = \begin{bmatrix} -\frac{\gamma}{4\Omega}\mu\left(\frac{1}{3} + e^2 - e\right) & 0 & 0 & 0 \\ \frac{2}{\Omega}\left(1 + \frac{m_{bl}x_g eR}{B}\right) & -\frac{\gamma}{2\Omega}\left(\frac{1}{4} - e + \frac{3e^2}{2}\right) & 0 & -\frac{1}{\Omega^2} \\ \frac{\gamma}{2\Omega}\left(\frac{1}{4} - e + \frac{3e^2}{2}\right) & \frac{2}{\Omega}\left(1 + \frac{m_{bl}x_g eR}{B}\right) & \frac{1}{\Omega^2} & 0 \end{bmatrix} \tag{A.33}$$

$$\boldsymbol{f}_\lambda = \begin{bmatrix} \frac{\gamma}{2}\left(\frac{1}{3}+e^2-e\right) & 0 & 0 \\ 0 & \frac{\gamma}{2}K_{iv}\left(\frac{1}{4}-e+\frac{3e^2}{2}\right) & 0 \\ -\frac{\gamma}{2}\mu\left(\frac{1}{2}-e+\frac{e^2}{2}\right) & 0 & 0 \end{bmatrix} \tag{A.34}$$

$$\boldsymbol{f}_{misc} = \begin{bmatrix} \frac{m_{bl}x_g}{B}\left(\dot{w}-uq+pv-g\right) \\ 0 \\ 0 \end{bmatrix} \tag{A.35}$$

where:

$$P^2 = 1 + \frac{K_\beta}{\Omega^2 B_{bl}} + \frac{m_{bl}eRx_g}{B_{bl}}$$

A.4 Flybar flapping equation

For the flybar a similar second order differential equation in matrix form can be obtained with the same approach.

$$\ddot{\boldsymbol{a}}_{fb} + \Omega \boldsymbol{D}_{fb} \dot{\boldsymbol{a}}_{fb} + \Omega^2 \boldsymbol{K}_{fb} \boldsymbol{a}_{fb} = \boldsymbol{f}_{fb} \tag{A.36}$$

where $\boldsymbol{a}_{fb}$ is the flybar flapping state matrix , $\boldsymbol{D}_{fb}$ is the damping matrix (A.38), $\boldsymbol{K}_{fb}$ is the stiffness matrix (A.39) and $\boldsymbol{f}_{fb}$ are the forcing terms ((A.40), (A.41) and (A.42)).

$$\begin{bmatrix} \ddot{a}_1^{fb} \\ \ddot{b}_1^{fb} \end{bmatrix} + \Omega \boldsymbol{D}_{fb} \begin{bmatrix} \dot{a}_1^{fb} \\ \dot{b}_1^{fb} \end{bmatrix} + \Omega^2 \boldsymbol{K}_{fb} \begin{bmatrix} a_1^{fb} \\ b_1^{fb} \end{bmatrix} = \Omega^2 \boldsymbol{f}_{comm} \begin{bmatrix} A_1 \\ B_1 \end{bmatrix} + \Omega^2 \cdot \boldsymbol{f}_{ang} \begin{bmatrix} p_w \\ q_w \\ \dot{p}_w \\ \dot{q}_w \end{bmatrix} + \Omega^2 \cdot \boldsymbol{f}_{\lambda} \begin{bmatrix} \lambda \\ \lambda_i \end{bmatrix} \tag{A.37}$$

$$\boldsymbol{D}_{fb} = \begin{bmatrix} \frac{\gamma}{4}\left(1 - e_{fb}^4\right) & 2 \\ -2 & \frac{\gamma}{4}\left(1 - e_{fb}^4\right) \end{bmatrix} \tag{A.38}$$

$$\boldsymbol{K}_{fb} = \begin{bmatrix} 0 & \frac{\gamma}{4}\left[1 - e_{fb}^4 - \frac{\mu^2}{2}\left(1 - e_{fb}^2\right)\right] \\ \frac{\gamma}{4}\left[-1 + e_{fb}^4 - \frac{\mu^2}{2}\left(1 - e_{fb}^2\right)\right] & 0 \end{bmatrix} \tag{A.39}$$

$$\boldsymbol{f}_{comm} = \begin{bmatrix} 0 & -\frac{\gamma}{2}\left[\frac{1 - e_{fb}^4}{2} + \frac{3}{4}\mu^2\left(1 - e_{fb}^2\right)\right] \\ \frac{\gamma}{2}\left[\frac{1 - e_{fb}^4}{2} + \frac{\mu^2}{4}\left(1 - e_{fb}^2\right)\right] & 0 \end{bmatrix} \tag{A.40}$$

$$\boldsymbol{f}_{ang} = \begin{bmatrix} -\frac{\gamma}{4\Omega}\left(1-e_{fb}^4\right) & -\frac{2}{\Omega} & -\frac{1}{\Omega^2} & 0 \\ \frac{2}{\Omega} & -\frac{\gamma}{4\Omega}\left(1-e_{fb}^4\right) & 0 & -\frac{1}{\Omega^2} \end{bmatrix} \tag{A.41}$$

$$\boldsymbol{f}_{\lambda} = \begin{bmatrix} \frac{\gamma}{2}\mu\left(1-e_{fb}^2\right) & 0 \\ 0 & \frac{\gamma}{4}K_{iv}\left(1-e_{fb}^4\right) \end{bmatrix} \tag{A.42}$$

Appendix B

Simulation results

In this Appendix are collected all the simulation results coming from chapter 5.

B.1 Inner circuit simulation results

In Fig. B.1-B.3 are shown the responses to a tracking signal q_d.

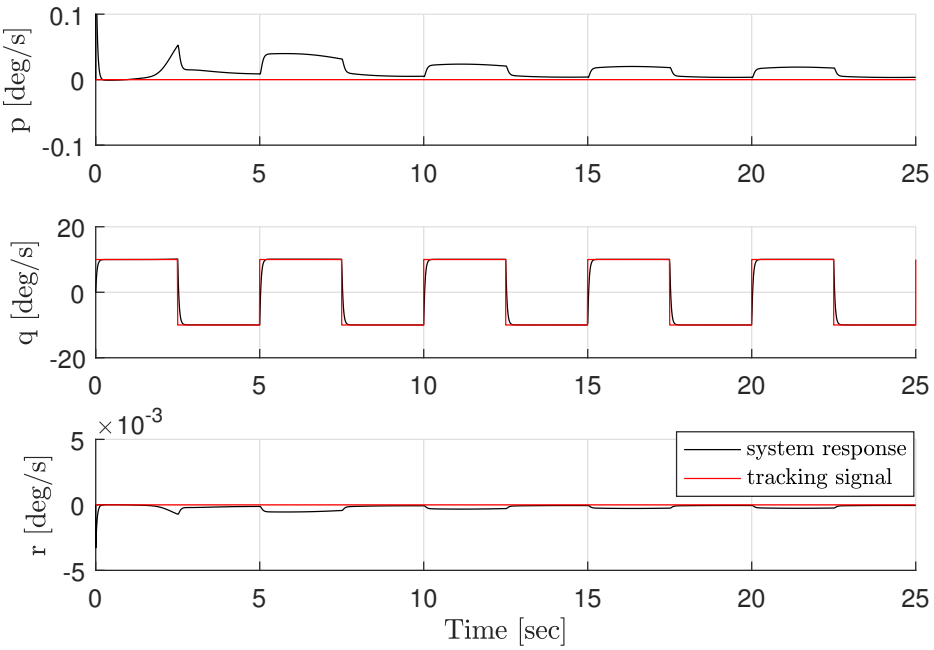

Figure B.1: Angular velocity response to a tracking signal q_d.

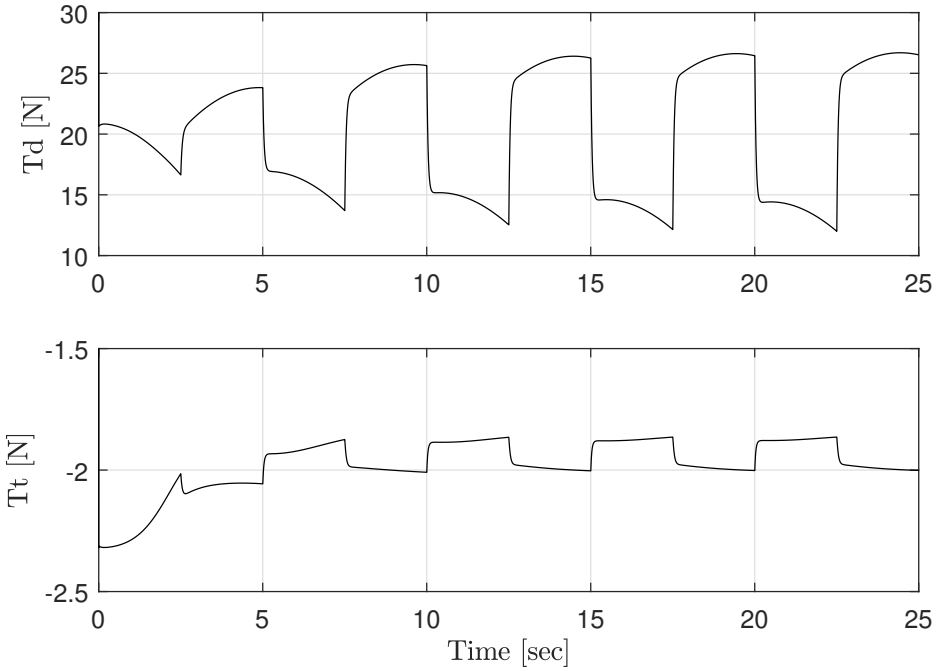

Figure B.2: Thrust commands response to a tracking signal q_d.

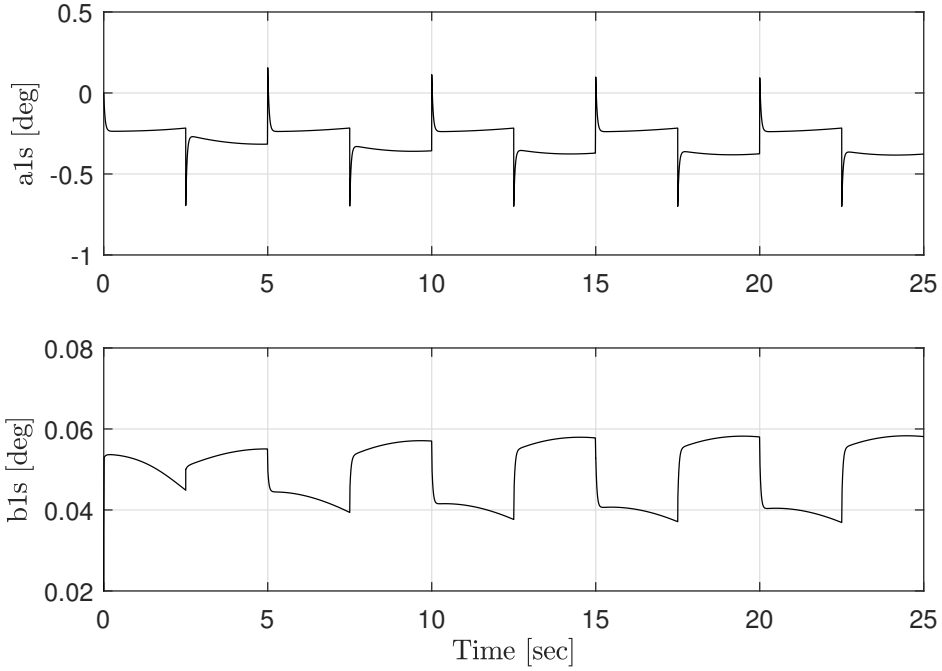

Figure B.3: Flapping coefficients response to a tracking signal q_d.

In Fig. B.4-B.6 are shown the responses to a tracking signal r_d.

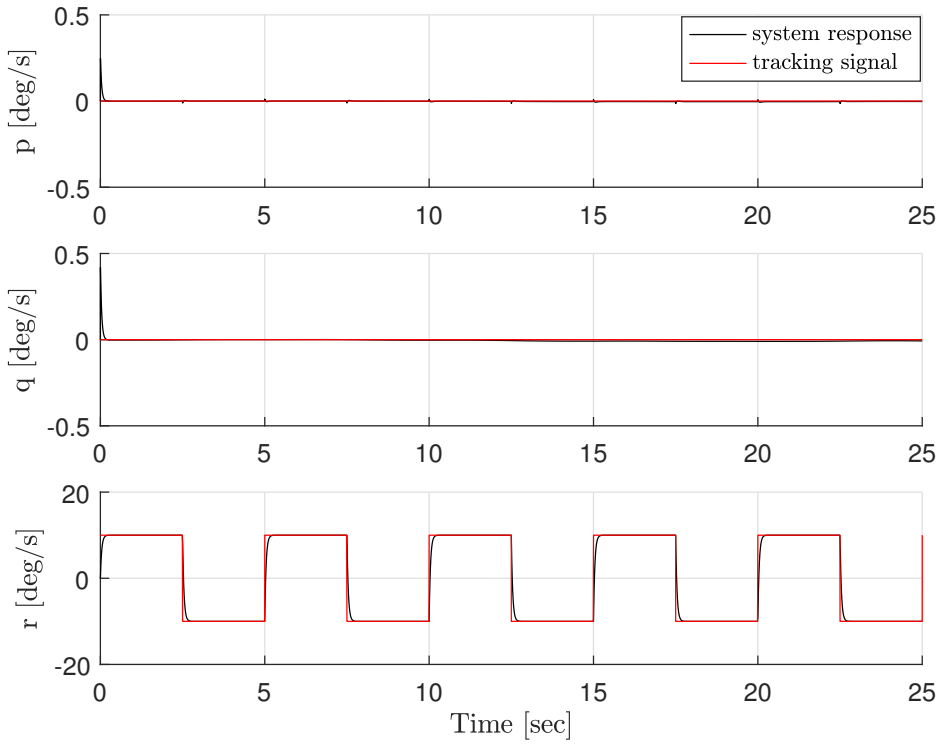

Figure B.4: Angular velocity response to a tracking signal r_d.

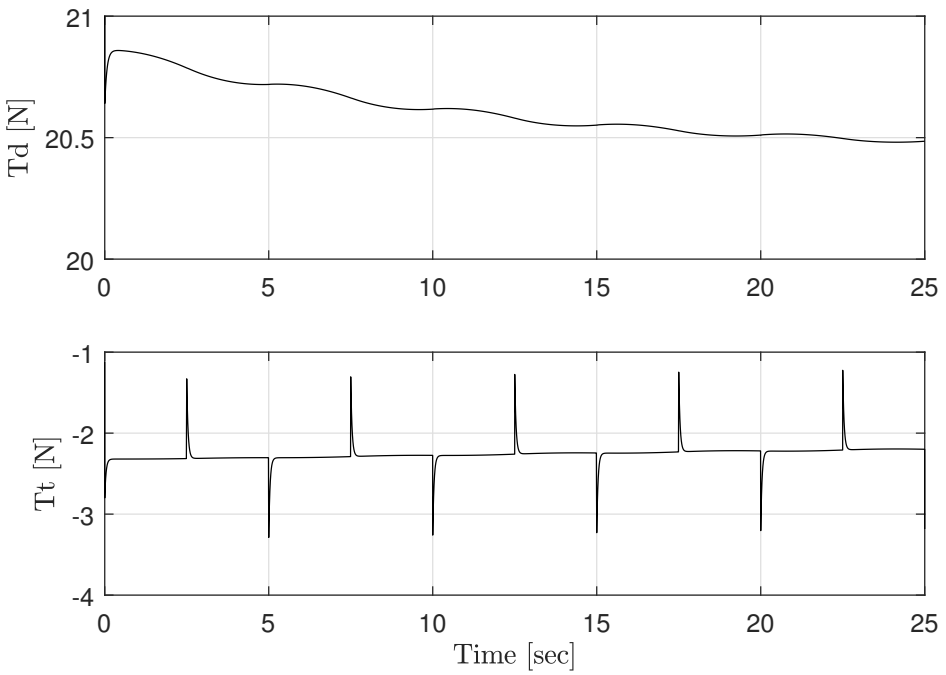

Figure B.5: Thrust commands response to a tracking signal r_d.

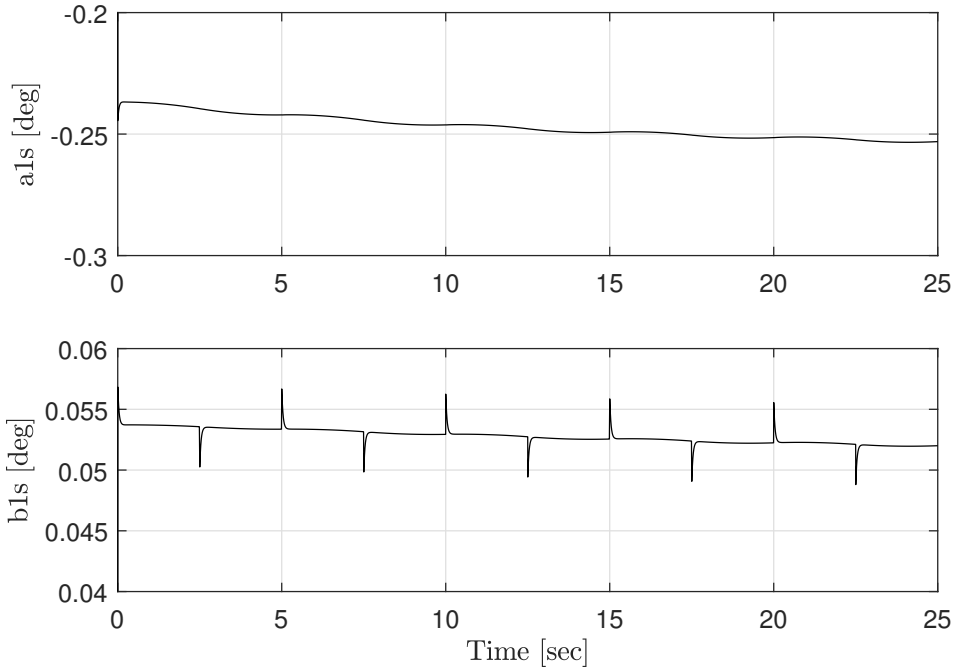

Figure B.6: Flapping coefficients response to a tracking signal r_d.

B.2 Slow circuit simulation results

In Fig. B.7-B.9 are shown the responses to a tracking signal θ_d.

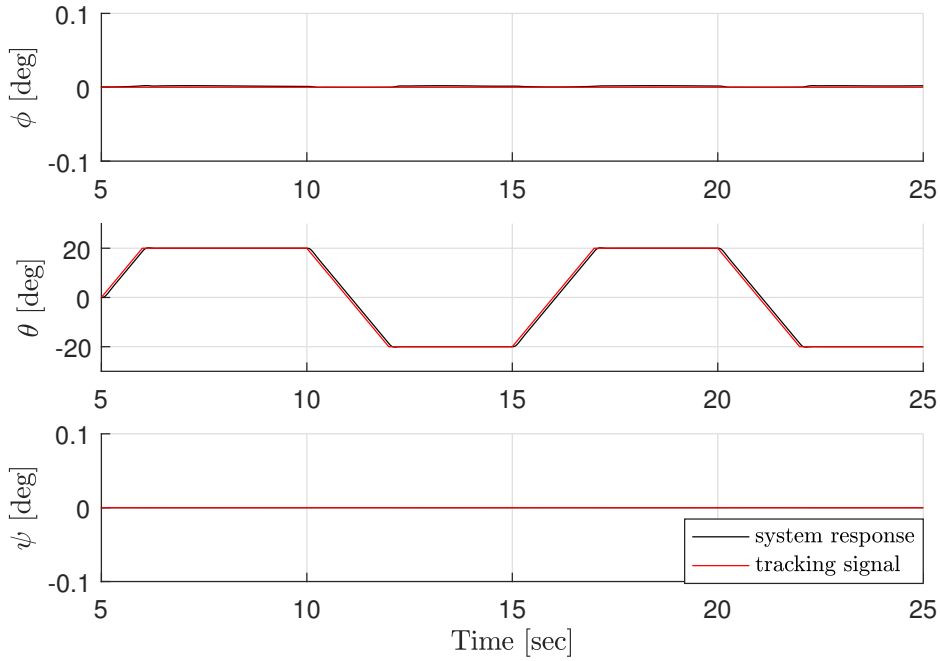

Figure B.7: Angular response to a tracking signal θ_d.

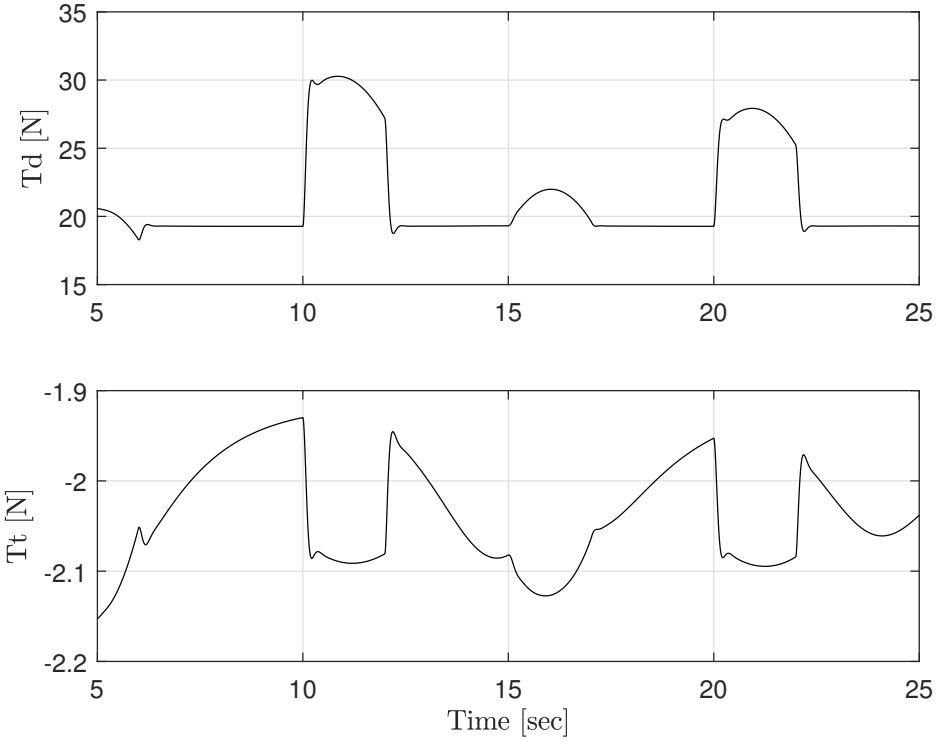

Figure B.8: Thrust commands response to a tracking signal θ_d.

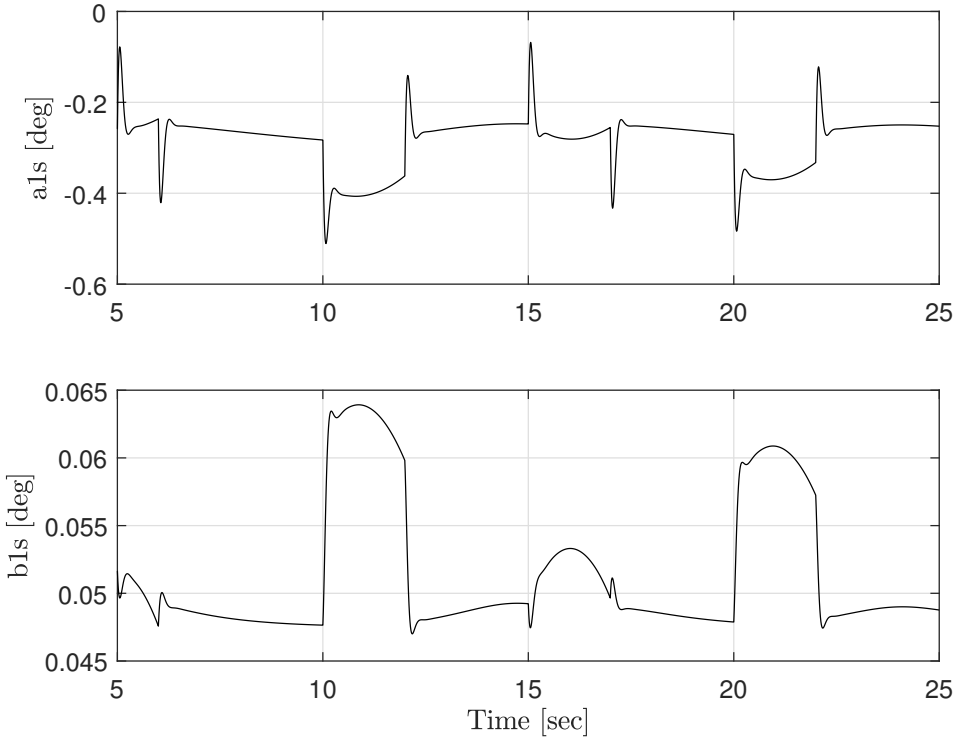

Figure B.9: Flapping coefficients response to a tracking signal θ_d.

In Fig. B.10-B.12 are shown the responses to a tracking signal ψ_d.

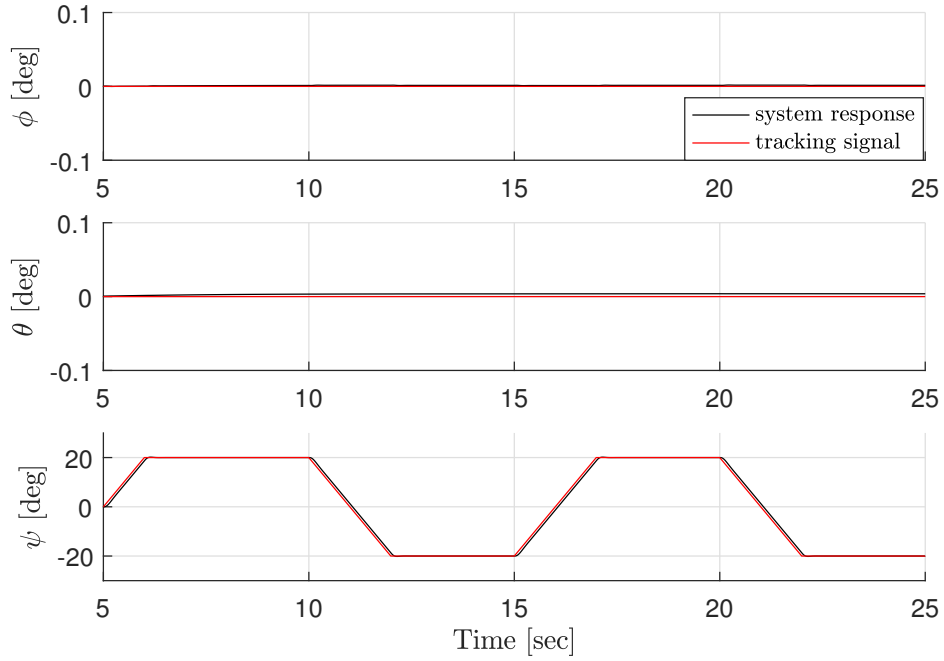

Figure B.10: Angular response to a tracking signal ψ_d.

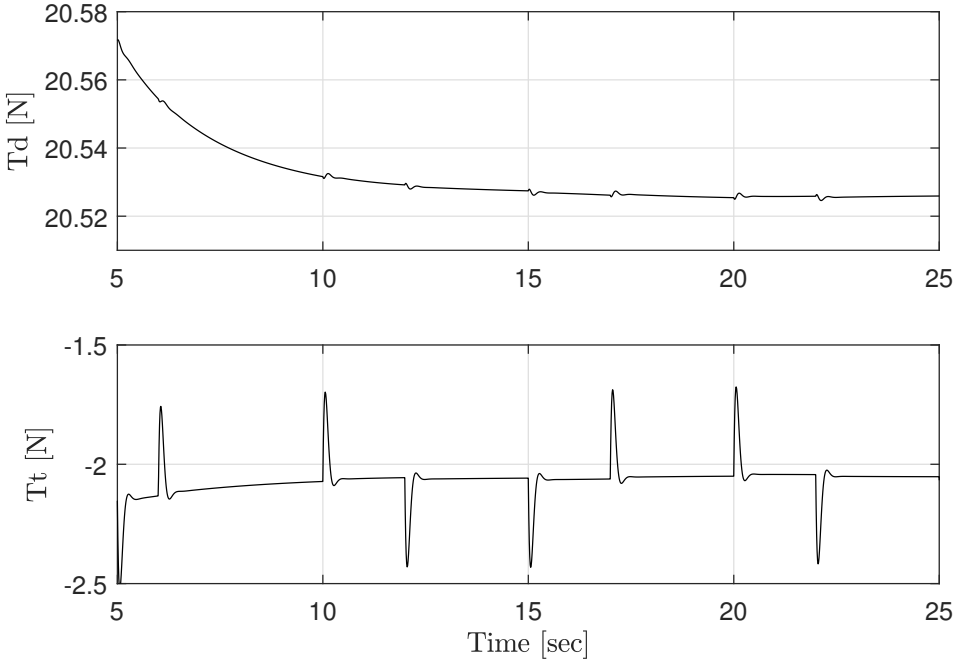

Figure B.11: Thrust commands response to a tracking signal ψ_d.

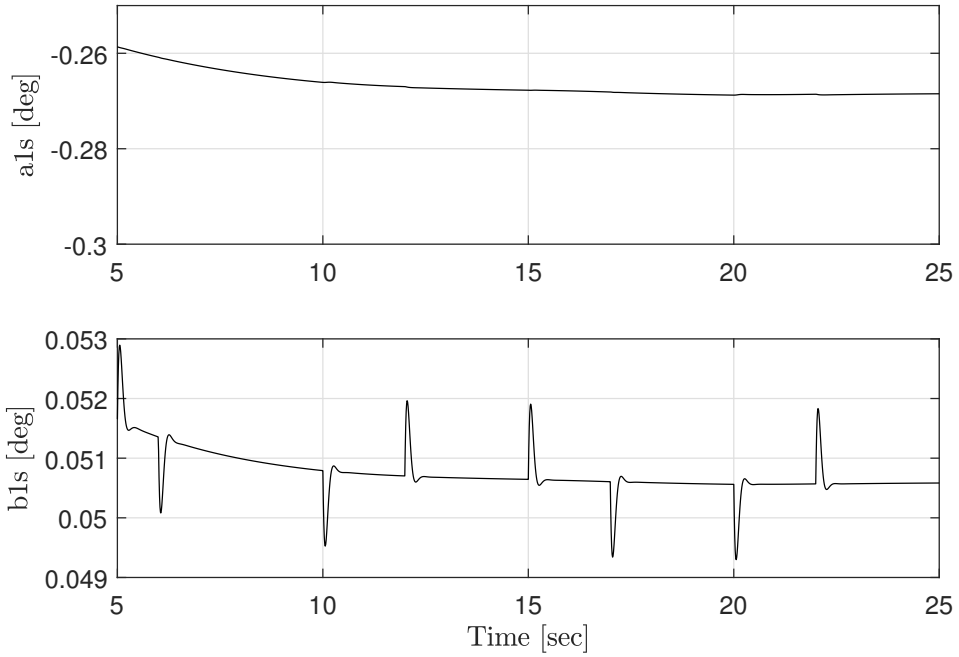

Figure B.12: Flapping coefficients response to a tracking signal ψ_d.

B.3 Slower circuit simulation results

In Fig. B.13-B.15 are shown the responses to a tracking signal V_{cross}.

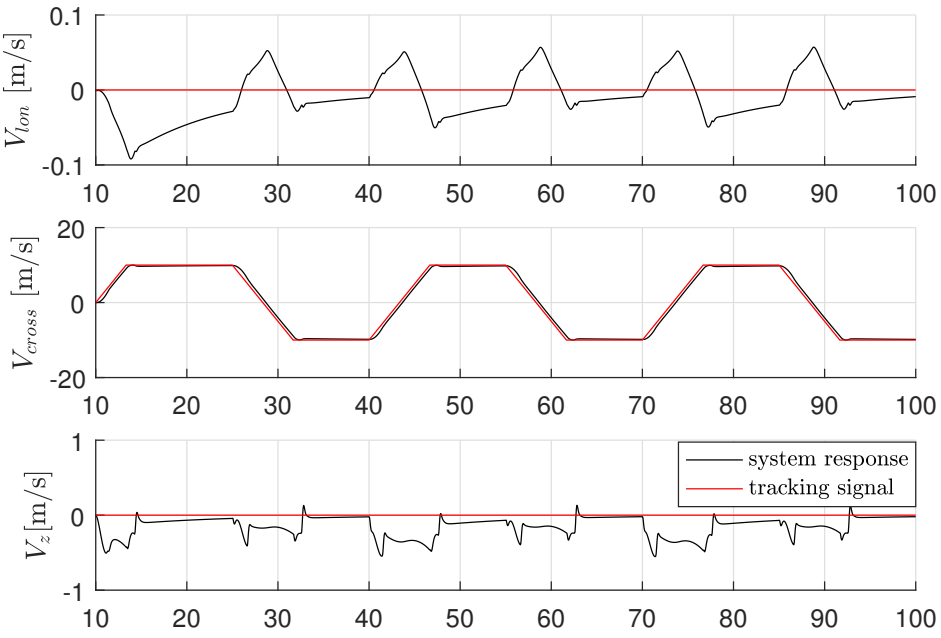

Figure B.13: Speed response to a tracking signal V_{cross}.

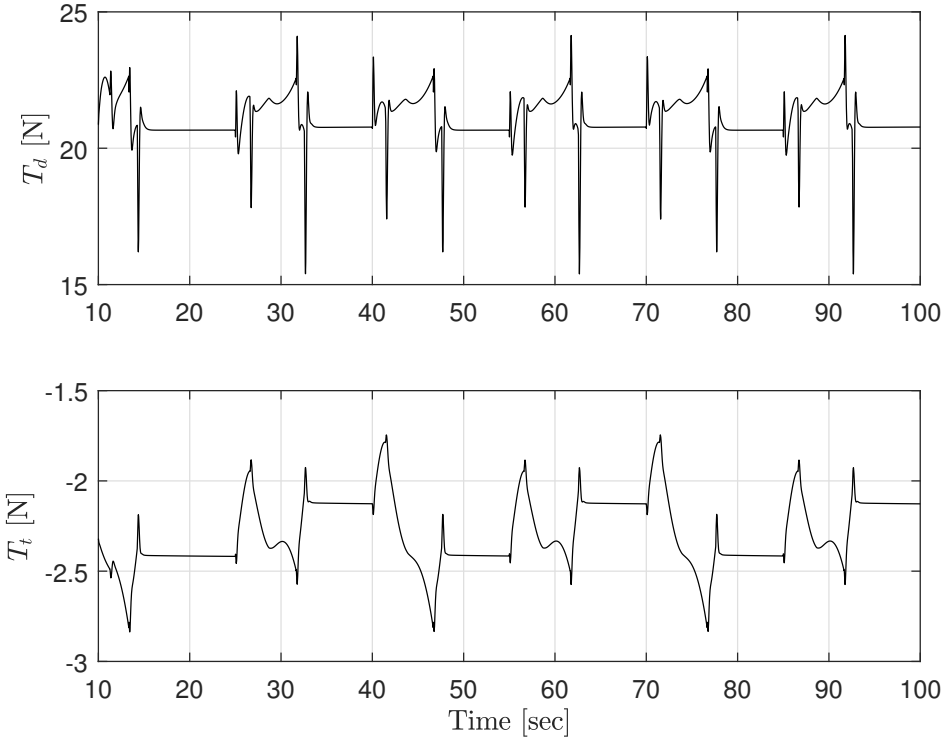

Figure B.14: Thrust commands response to a tracking signal V_{cross}.

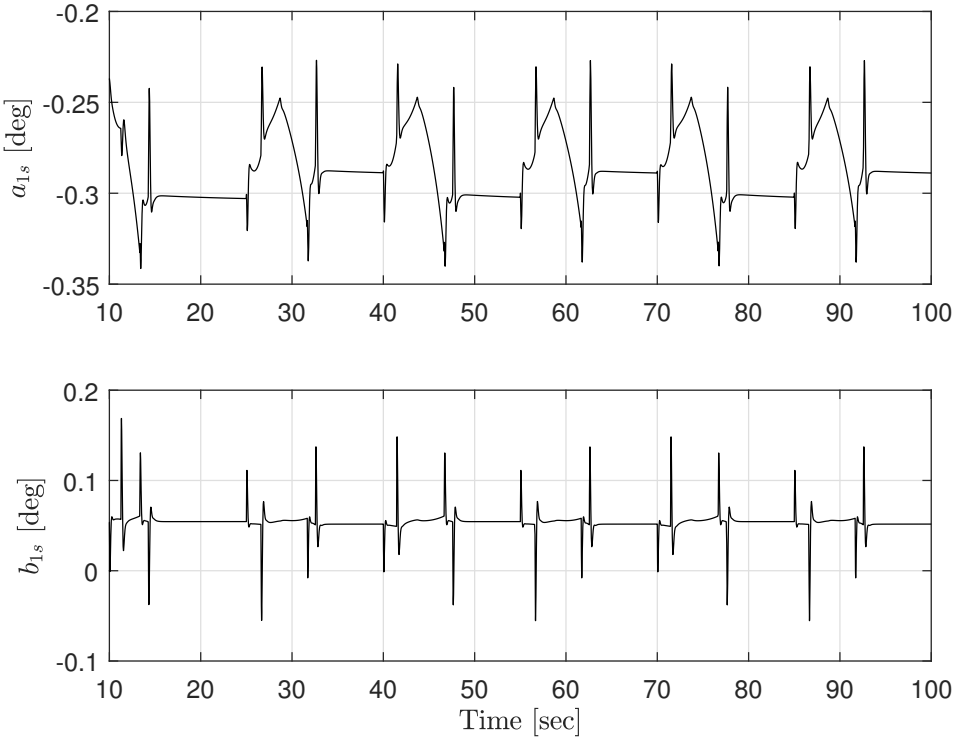

Figure B.15: Flapping coefficients response to a tracking signal V_{cross}.

In Fig. B.16-B.18 are shown the responses to a tracking signal V_z.

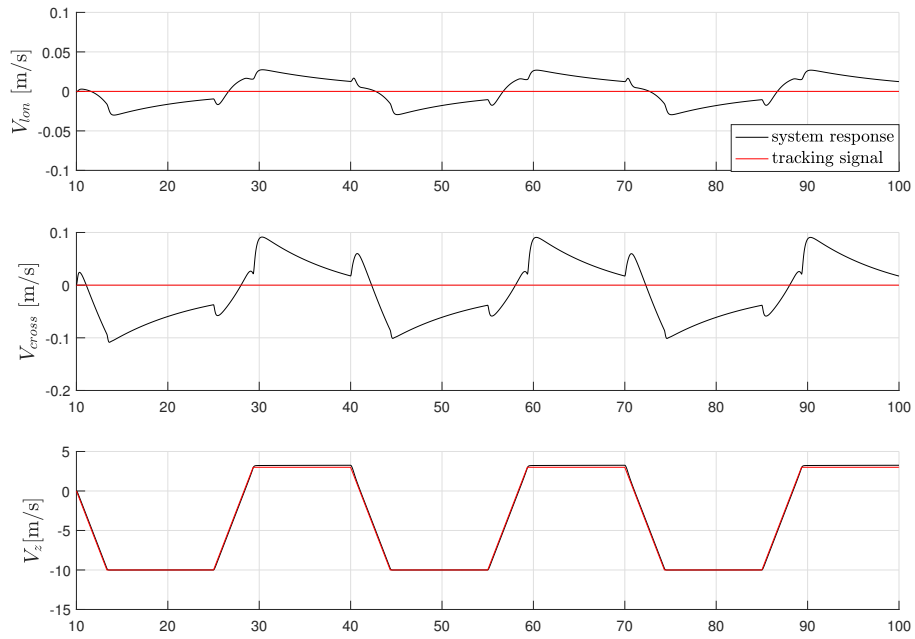

Figure B.16: Speed response to a tracking signal V_z.

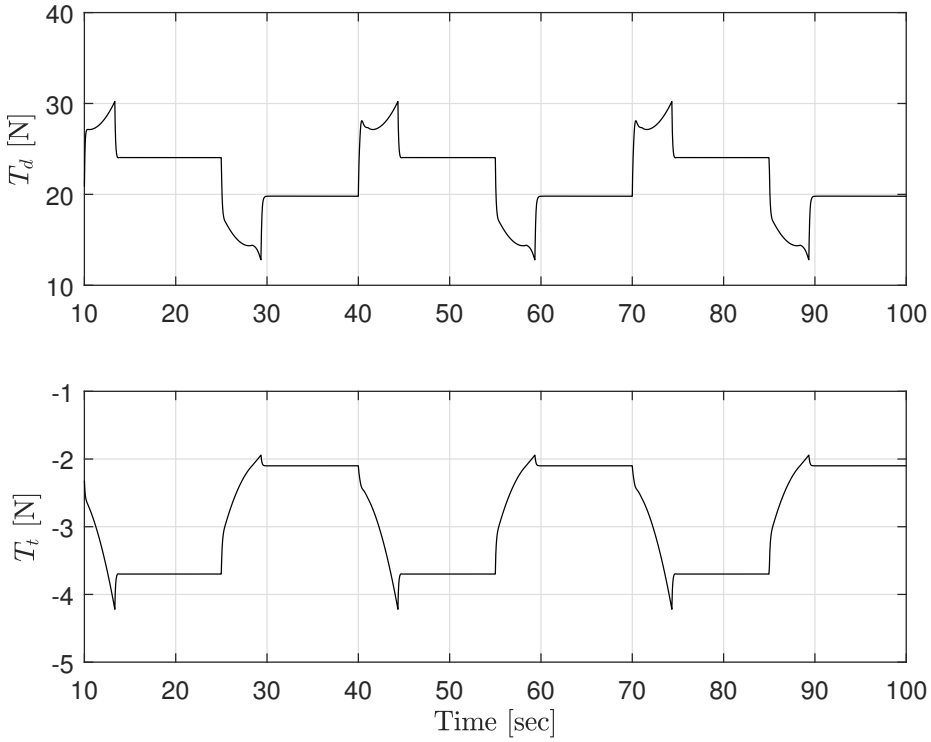

Figure B.17: Thrust commands response to a tracking signal V_z.

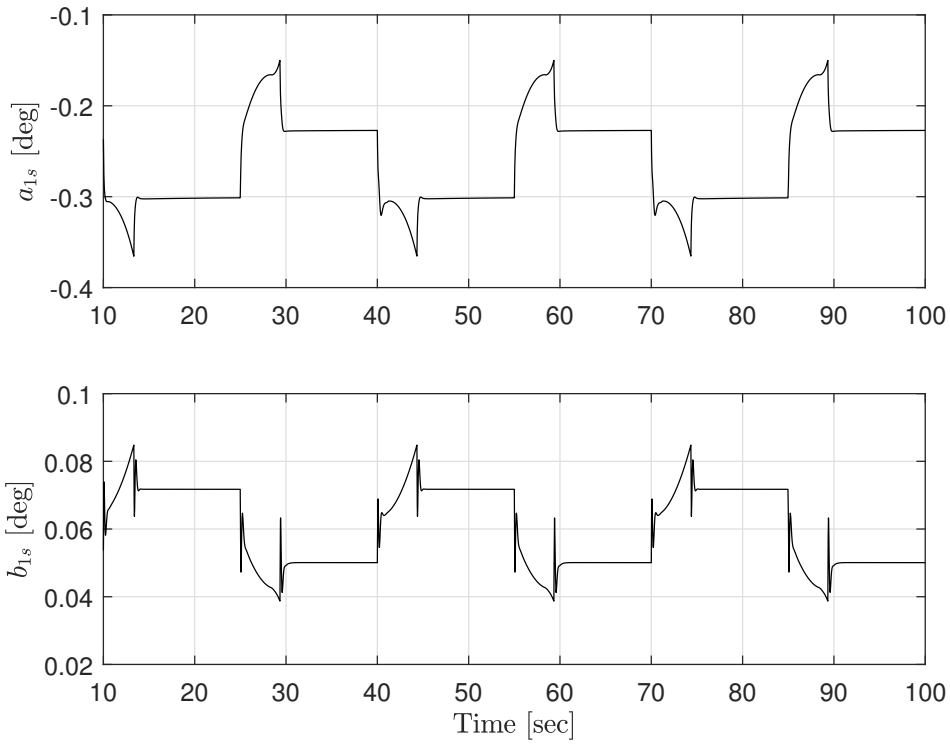

Figure B.18: Flapping coefficients response to a tracking signal V_z.

B.4 Complete model simulation results

In Fig. B.19-B.21 are shown the responses to a tracking signal in V_{cross}.

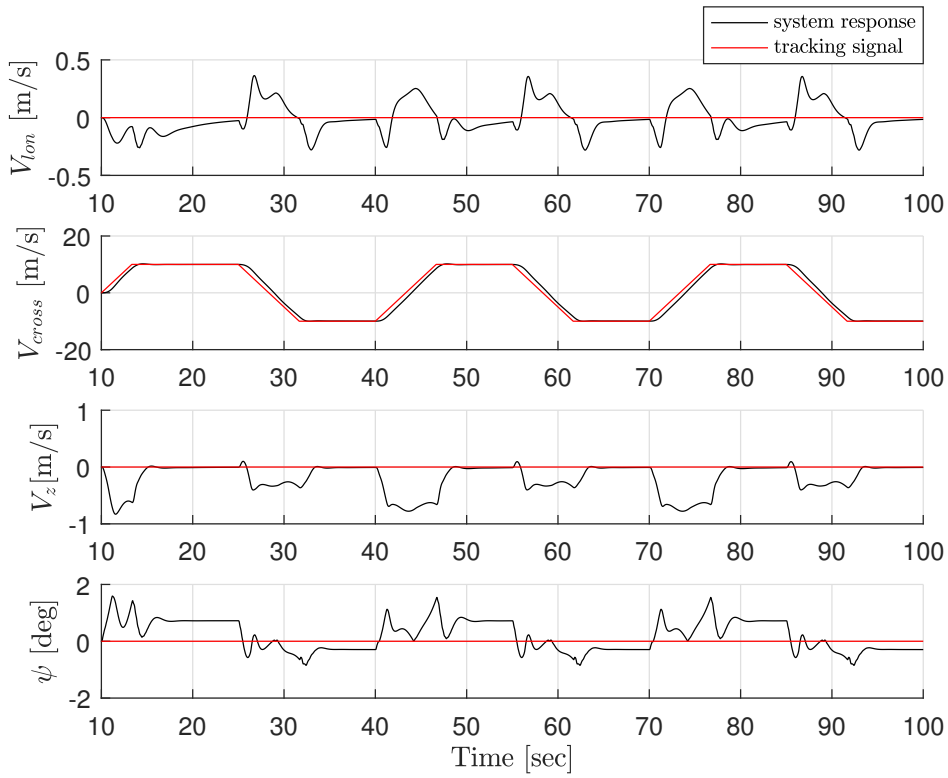

Figure B.19: Speed response to a tracking signal in V_{cross}.

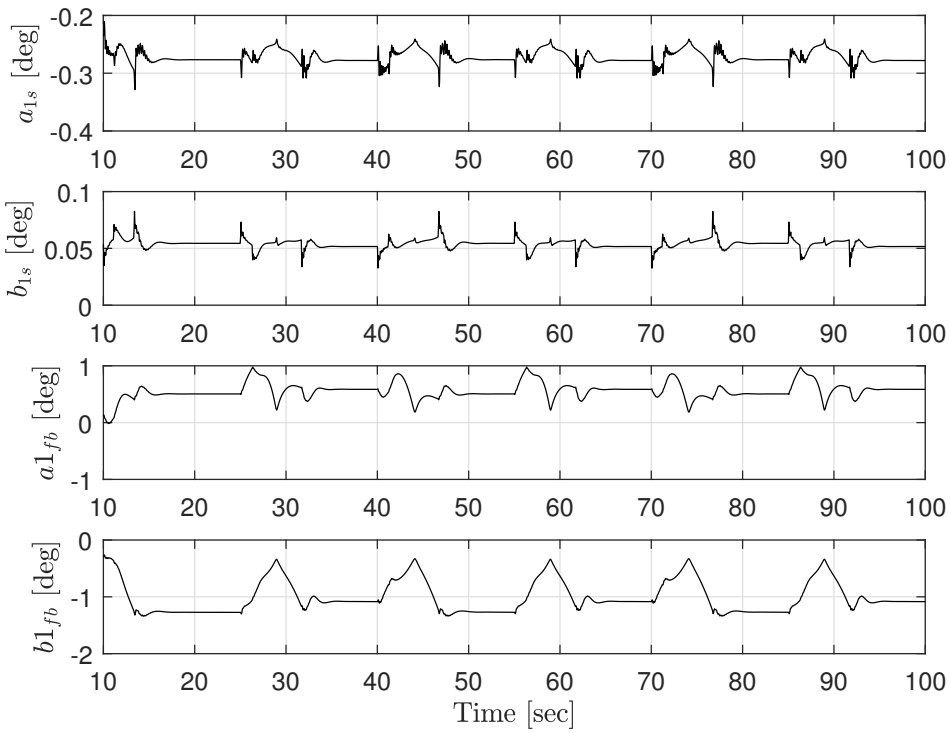

Figure B.20: Flapping coefficients response to a tracking signal V_{cross}.

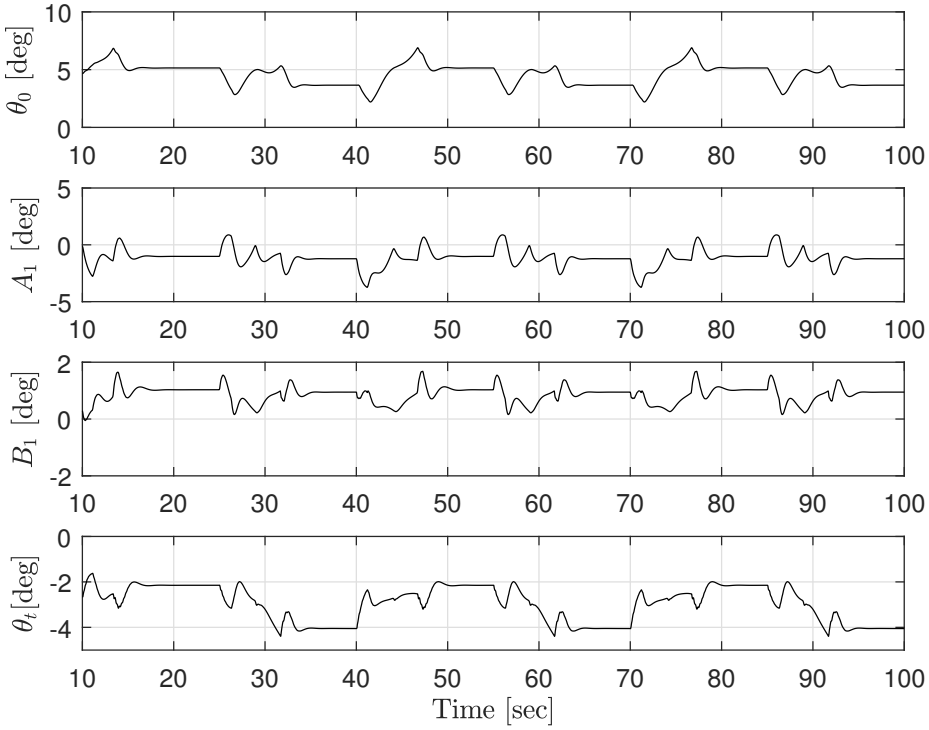

Figure B.21: Pitching coefficients response to a tracking signal V_{cross}.

In Fig. B.22-B.24 are shown the responses to a tracking signal in V_z.

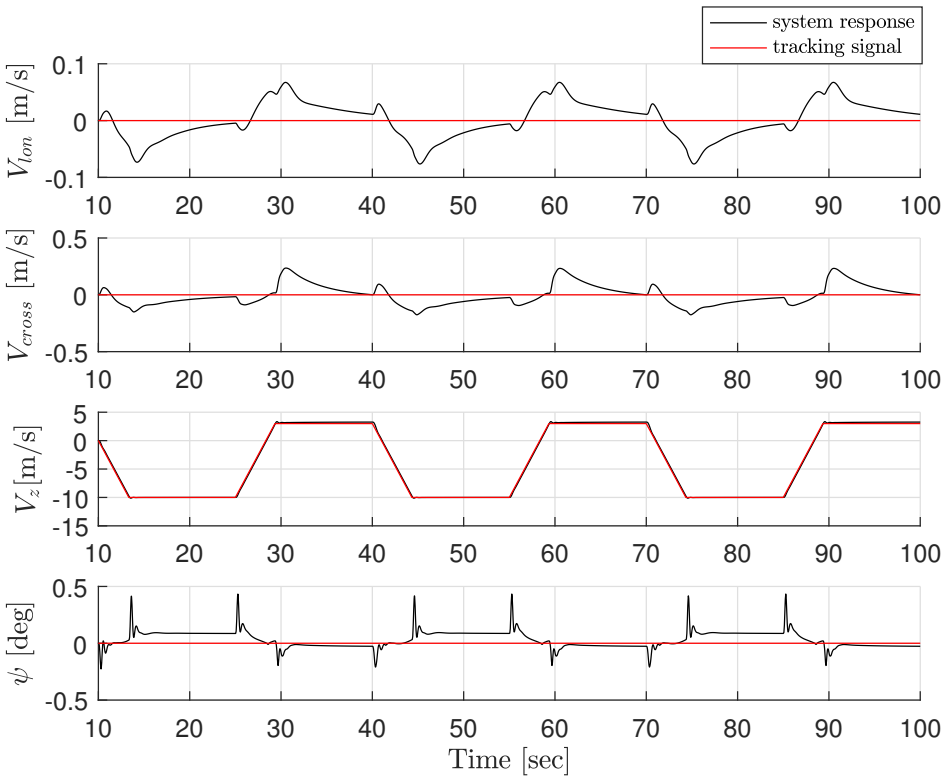

Figure B.22: Speed response to a tracking signal in V_z.

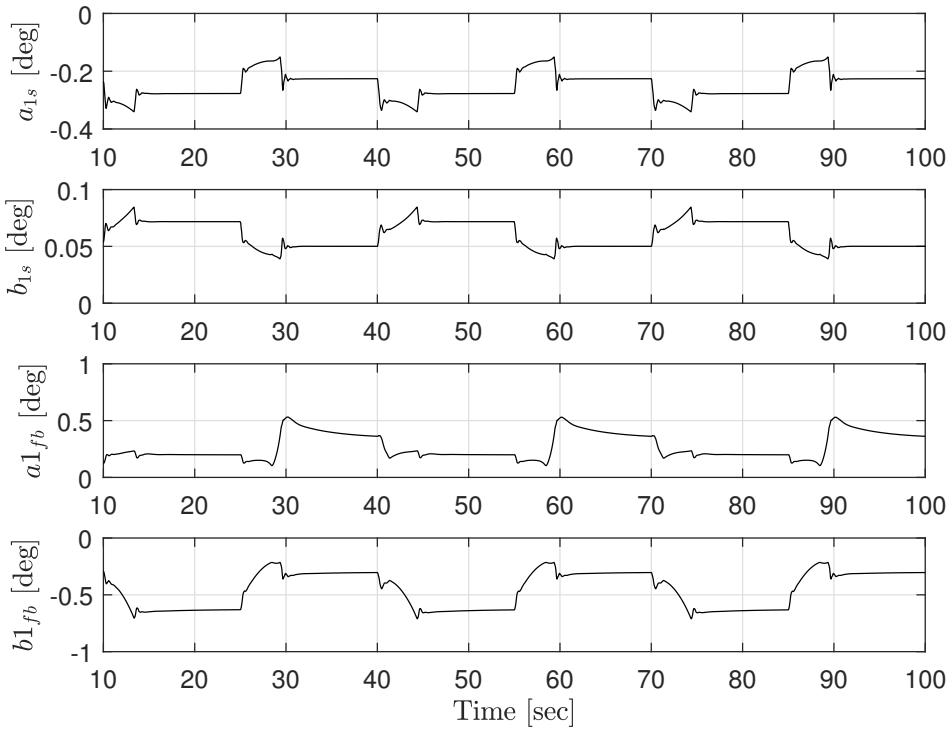

Figure B.23: Flapping coefficients response to a tracking signal V_z.

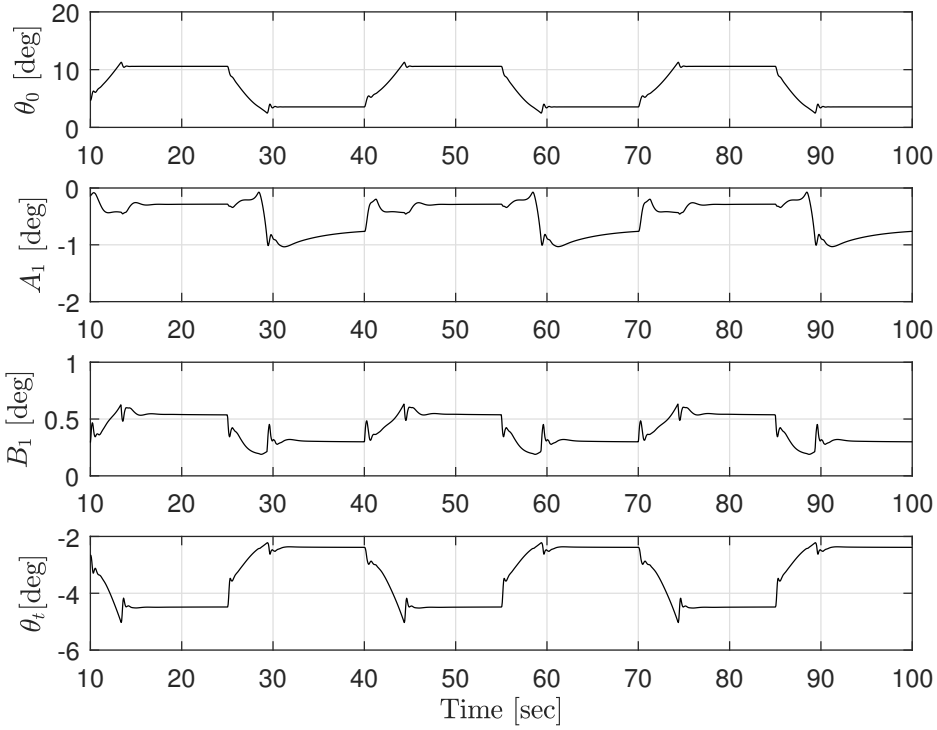

Figure B.24: Pitching coefficients response to a tracking signal V_z.

In Fig. B.25-B.27 are shown the responses to a tracking signal in ψ.

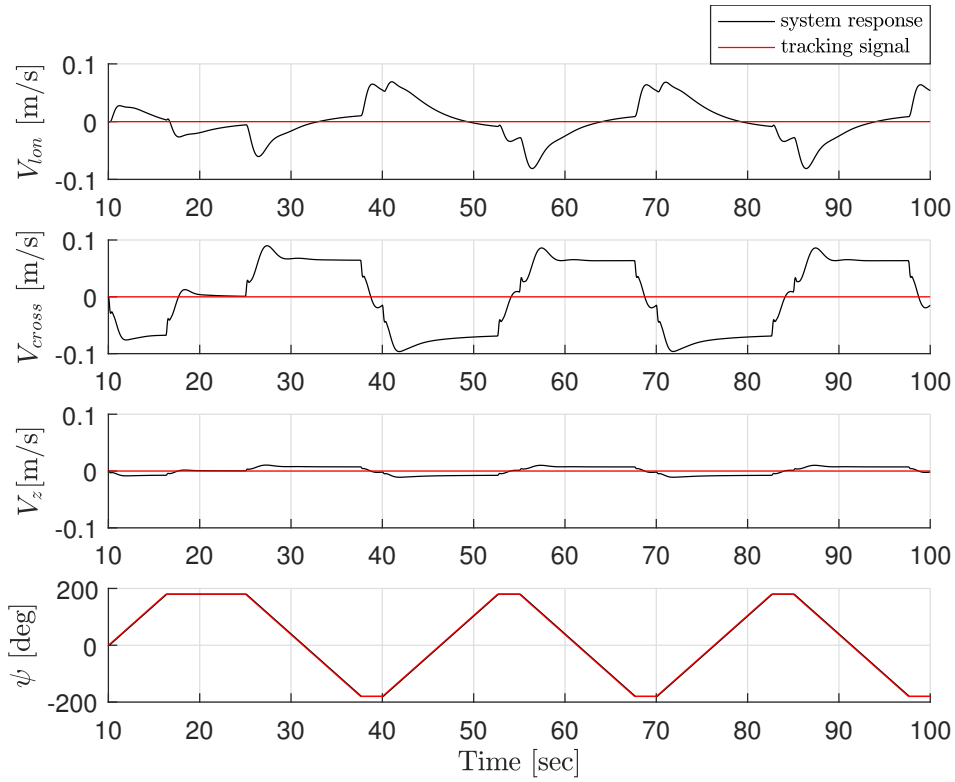

Figure B.25: Speed response to a tracking signal in ψ.

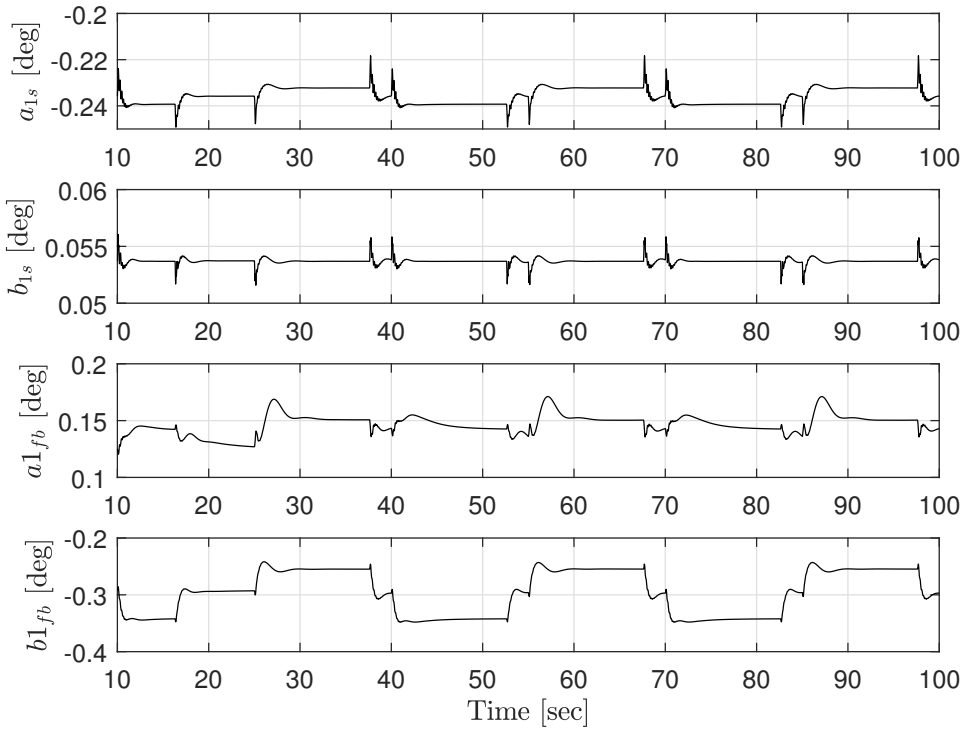

Figure B.26: Flapping coefficients response to a tracking signal ψ.

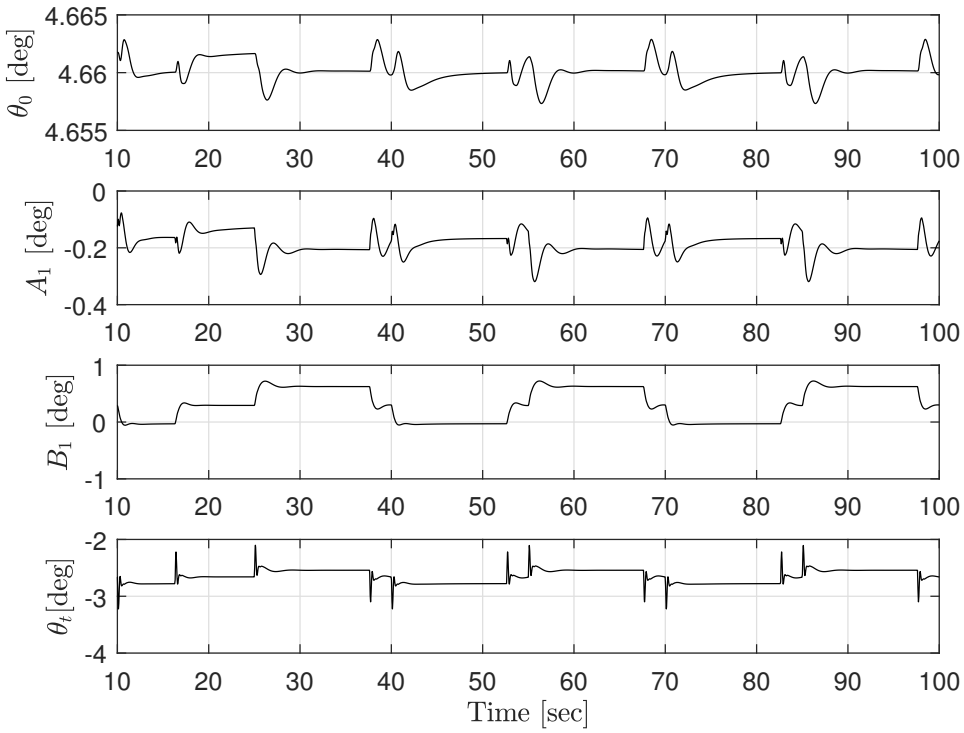

Figure B.27: Pitching coefficients response to tracking signal ψ.

B.5 Hovering simulation

The results to a vertical gust perturbation are shown in Fig. B.28-B.30.

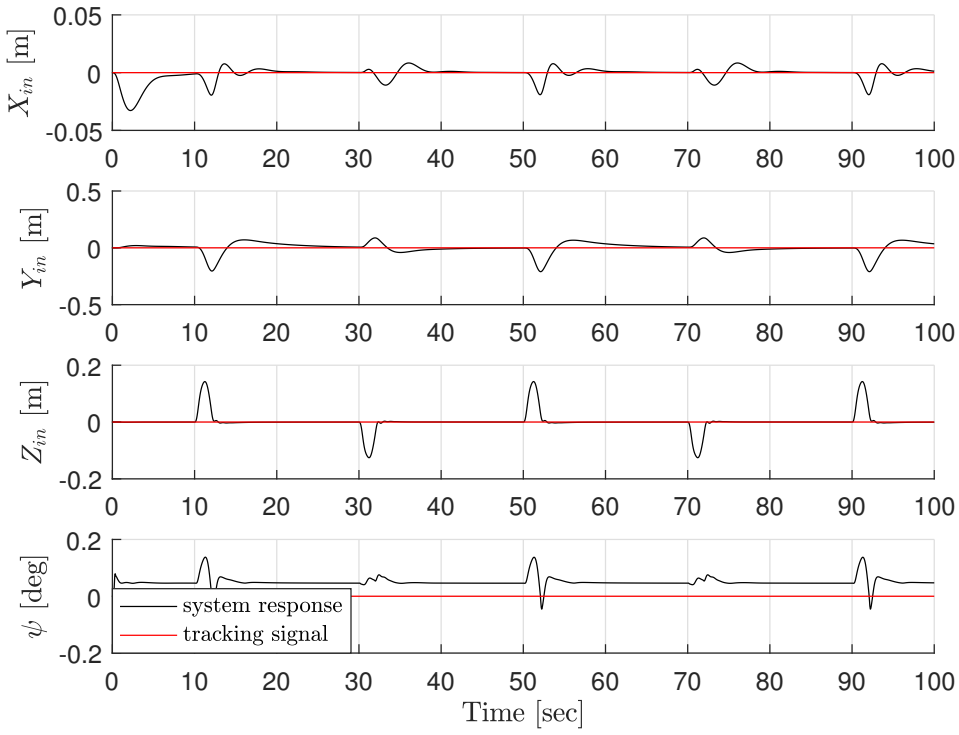

Figure B.28: Position and ψ.

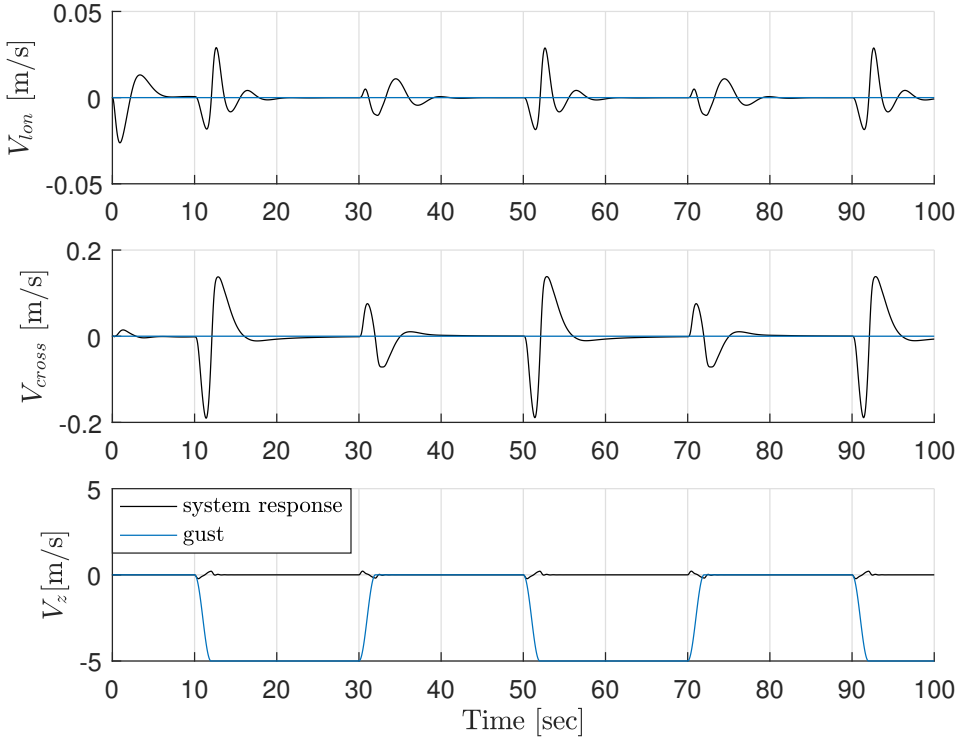

Figure B.29: Velocities.

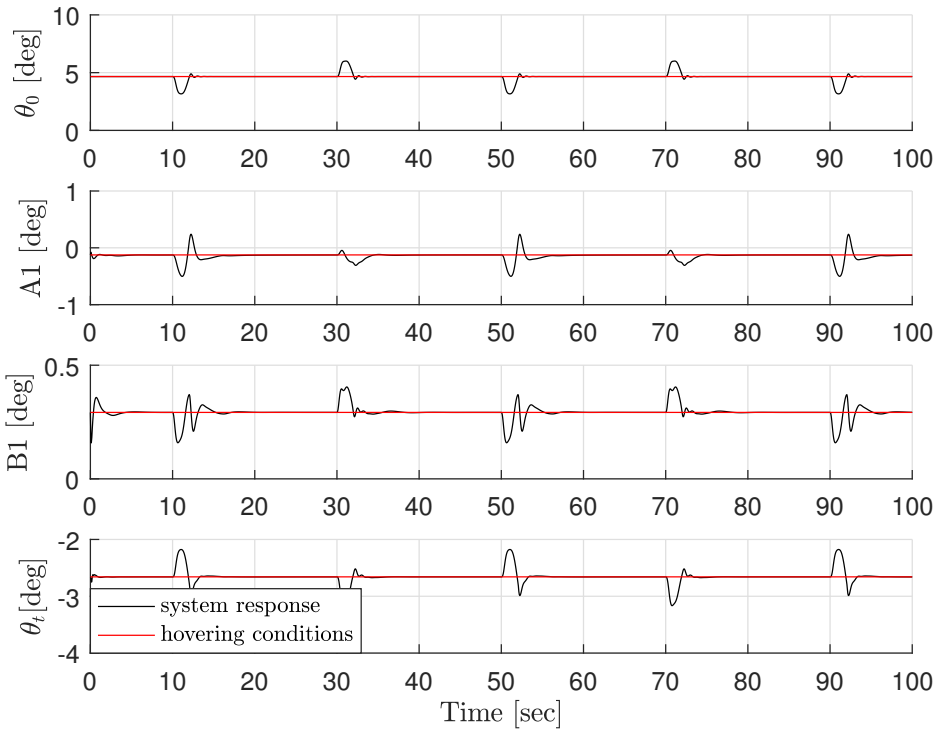

Figure B.30: Command coefficients.

Appendix C

Study of the robustness

In order to evaluate the robustness of the controller some modelling errors have been introduced during the simulation tests.

C.1 simulation test

Assuming a 20% error on the estimation of the c.g. and of the fuselage drag, some simulation tests have been used in order to evaluate the differences on the time response.

In Fig. C.1-C.4 are shown the response to a particular simulation.

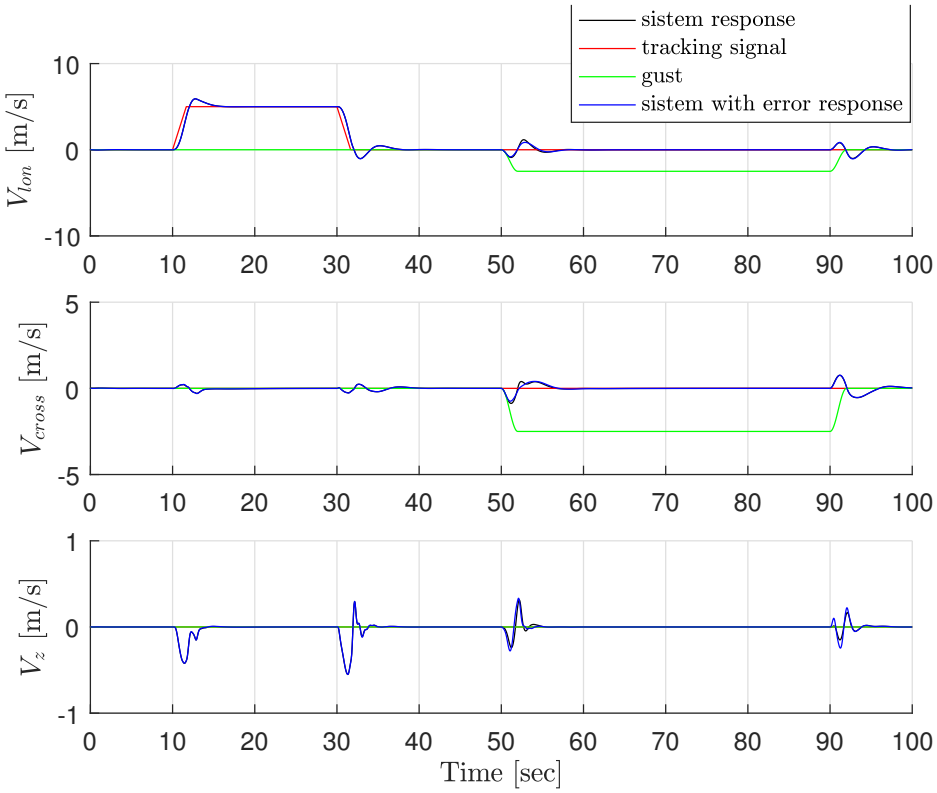

Figure C.1: Speed response.

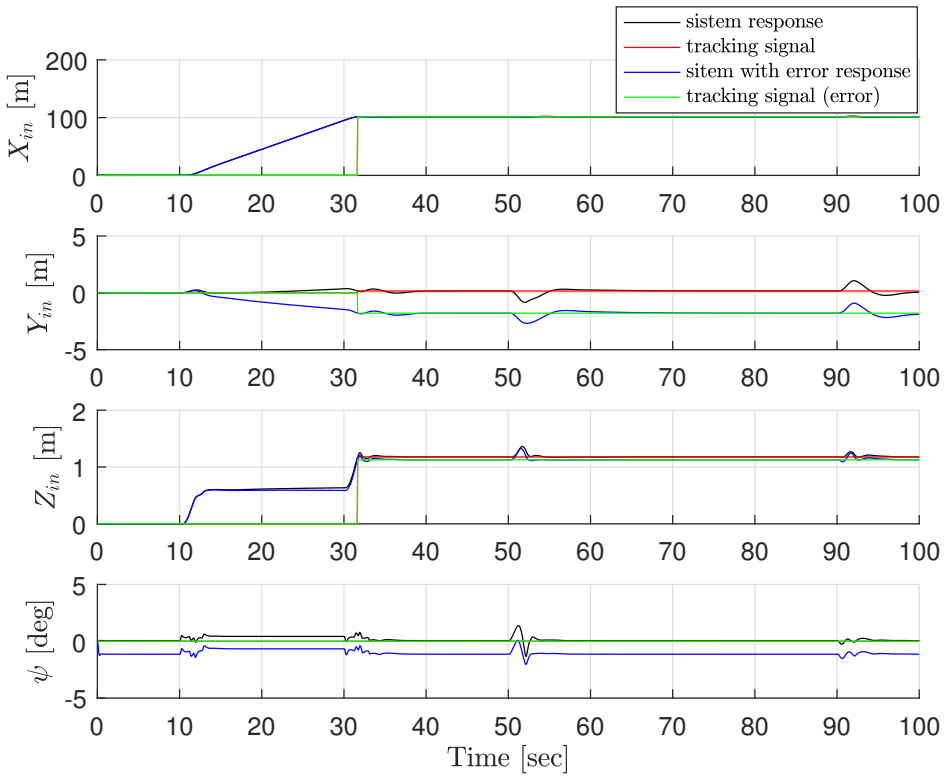

Figure C.2: Position response.

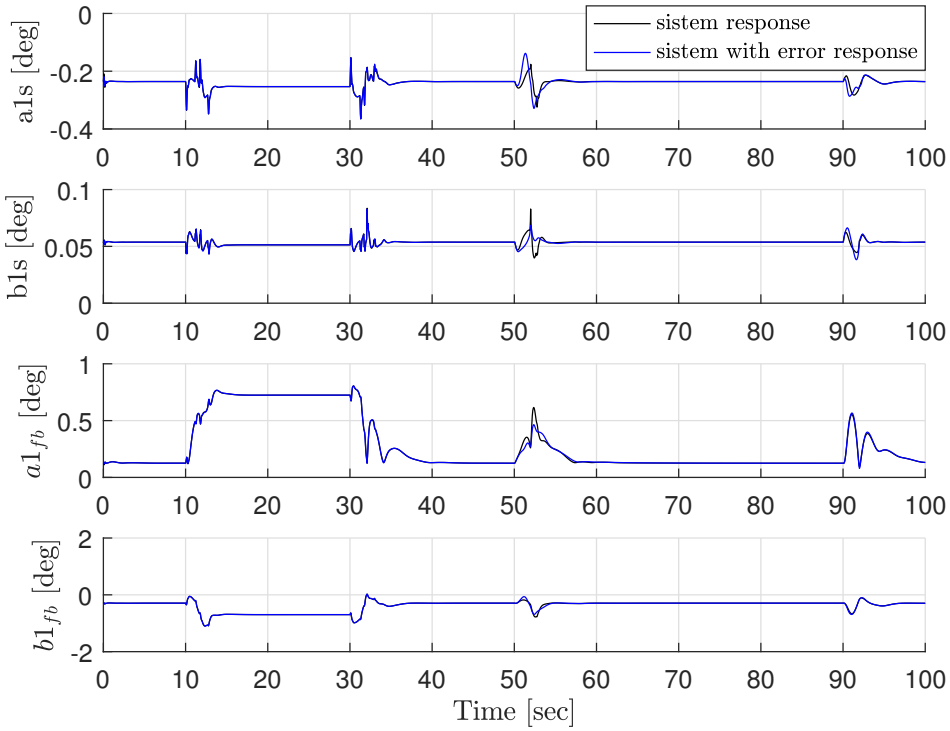

Figure C.3: Flapping coefficients response.

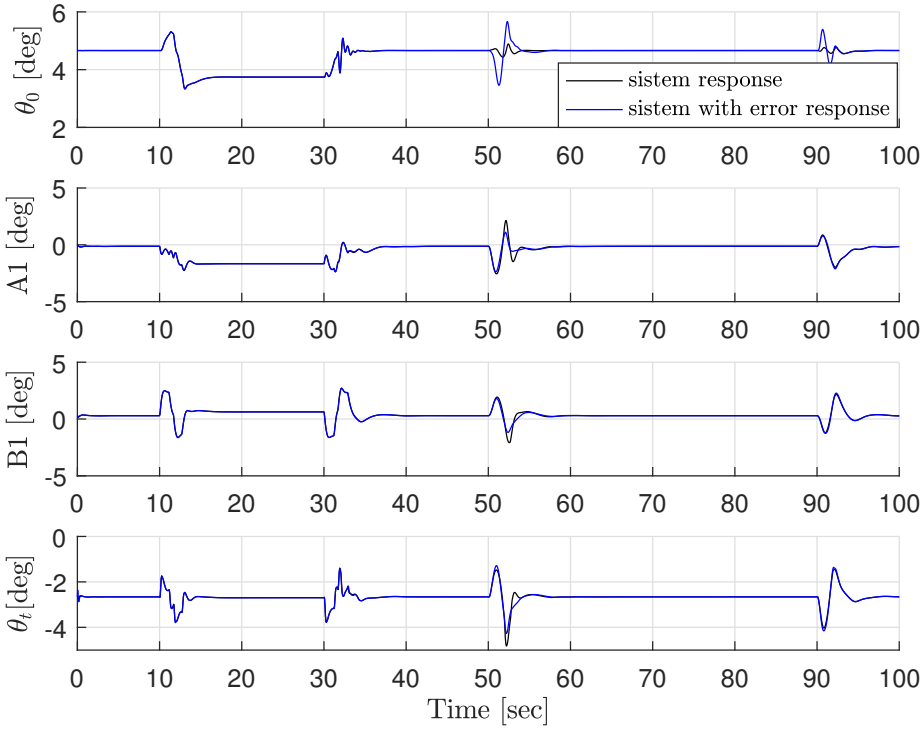

Figure C.4: Command coefficients response.

As can be seen from the simulation results the controller is very robust in the following of speed references and the hovering maintenance. Only the estimation of the asymptotic value of ψ is affected by an observable error that can be removed introducing an integral effect on the ψ controller.

Bibliography

[1] Pietro Rosata. "Identification of a small scale helicopter dynamic model". Master Thesis. Università di Pisa, 2015.

[2] A.R.S. Bramwell, George Done, and David Balmford. *Bramwell's Helicopter Dynamics*. 2nd ed. Butterworth-Heinemann, 2001.

[3] H. L. Price. *Rotor dynamics and helicopter stability*. Report. Aircraft Engineering, 1963.

[4] Johnson Wayne. *Helicopter theory*. Dover Publications, Inc., 1980.

[5] Alberto Isidori. *Nonlinear Control Systems*. 3rd ed. Springer-Verlag, 1995.

[6] T. John Koo, Yi Ma, and Shankar Sastry. *Nonlinear control of a helicopter based unmanned aerial vehicle model*. 2001. URL: `https://citeseer.ist.psu.edu/417459.html`.

[7] Roger Pettersen, Emir Mustafic, and Mads Fogh. "Nonlinear Control Approach to Helicopter Autonomy". Master Thesis. Aalborg University, 2005.

[8] S. Sieberling, Q. P. Chu, and J. A. Mulder. "Robust Flight Control Using Incremental Non-linear Dynamic Inversion and Angular Acceleration Prediction". In: *Journal of Guidance, Control, and Dynamics* 33.6 (Nov. 2010), pp. 1732–1742.

[9] Harry K. Heyson and S. Katzoff. *Induced velocities near a lifting rotor with nonuniform disk loading*. Report. NASA, 1957.

[10] J. Gordon Leishman. *Principles of helicopter aerodynamics*. Cambridge Aerospace Series, 2000.

[11] Robert Chen. *A Survey of Nonuniform Inflow Model for Rotorcraft Flight Dynamics and Control Application*. Report. NASA, 1989.

[12] Robert Chen. *Effects of primary rotor parameters on flapping dynamics*. Technical paper. NASA, 1980.

Ringraziamenti

Eccoci qui, finalmente l'agognato traguardo è giunto. Ma, come dicono anche in tv, quello che conta non è la destinazione, ma il viaggio. Ed è un viaggio che fai con un pulmino malandato, che cerchi di riempire con la gente a cui tieni di più, che ti faccia compagnia durante la strada e che ti aiuti a spingere quel catorcio quando rimani impantanato in mezzo al fango.

Adesso voglio ringraziare quelle persone che hanno avuto la voglia di salire su quel catorcio anche solo per un piccolo tratto di strada.

Ringrazio innanzitutto i miei genitori per essermi stati di supporto in tutti questi anni, per aver sempre creduto in me e, soprattutto, per avermi fatto semplicemente perfetto, "bello", "simpatico" e "intelligente".

Ringrazio le mie sorelle per volermi bene a discapito di tutti i miei difetti.

Ringrazio Francesco per essere stato sia una guida che un amico e tutti i ragazzi dell'ufficio per aver reso in periodo della tesi il più bello della mia carriera universitaria.

Ringrazio l'Halo Team per tutte le risate fatte insieme; che le vostre giornate possano sempre iniziare con un buongiornissimo.

Ringrazio tutti gli amici di Pisa per il tempo trascorso insieme tra cene, giochi, uscite (in verità non molte) e altre cene.

Infine voglio ringraziare Chiara per essere stata il mio punto fisso in tutti questi anni, per la forza con cui ci siamo sempre sostenuti e la capacità di saper rimanere sempre un po' bambini.

Ma questa non è mica la destinazione, accompagnatemi ancora per un altro po' di strada.